OAW
Austrian Academy
of Sciences

IBn
INSTITUTE OF BIOPHYSICS AND
NANOSYSTEMS RESEARCH

ANNUAL REPORT
2007

AUSTRIAN SAXS BEAMLINE AT elettra

Austrian Small Angle X-ray Scattering (SAXS) Beamline at ELETTRA

Annual Report 2007

Compiled by the SAXS-Group:

- for IBN: B. Sartori, M. Rappolt & H. Amenitsch
- for ELETTRA: S. Bernstorff

Cover-pictures taken from I. Shyjumon et al., S.K. Gosh et al. and P. Falcaro et al. (see pages 57, 85 and 112, respectively)

Table of Contents

Preface

Peter Laggner
Director
Institute of Biophysics and Nanosystems Research
Austrian Academy of Sciences

The Austrian SAXS beamline is both, an intensely and broadly utilized research facility as well as a hot foundry for technological innovation. The combination of the two is the competitive strength of our research infrastructure unit in the international scenario. The user operation has been smoothly supported by our beamline staff as well as by the logistical and technical backup through Sincrotrone Trieste. Clearly, the financial support to users through the FEL-I3 scheme within FP6 of the European Union is of big help. The storage ring upgrade by the new booster will increase the efficiency even further, particularly for SAXS, where the beam performance and stability at high level are a key element. As a consequence, one needs now to seriously consider also an upgrade of the SAXS-beamline, and the planning for an extension of the optical length has been started. This should come into effect in 2008 and will open new possibilities: higher resolution, microfocus potential, installation of larger sample environments. The cross-over between different analytical techniques has been explored: simultaneous IR-spectroscopy and SAXS or deep X-ray lithography and SAXS projects have been initiated with great success. Within our part in the SAXIER project of FP6, the exploitation of microfluidics, gas-phase scattering and nanoanalytics has also been initiated and here, too, very promising highlights were obtained. This is a strongly booming field, and this was reflected by the success of the International Workshop on Microfluidics and Nanoanalytics at the IBN in Graz. The old and new challenge in the whole game, however, are X-ray detectors, which are still lagging back with time and space resolution.

While all these scientific and technological efforts are a good basis for strengthening the role of the station as one of the world-leaders in the field, it will be increasingly difficult to ensure the financial basis for growing and successful activity. While FP6 with its I3-scheme has provided a strong boost to the field, the cuts foreseen with FP7 are threatening. And national sources, while stable over the years, do not seem to come easy, either. The natural way to cope with this prospect, is a strategy swing to technology exploitation with industry. This requires some fresh thinking and adapted institutional instruments. Moves in this direction have been made but they will not excuse national or European authorities from their responsibility for research infrastructure facilities such as ours.

Peter Laggner

Alfonso Franciosi
Director, ELETTRA Laboratory
Chief Executive Officer, Sincrotrone Trieste S.C.p.A.

We are pleased to welcome the publication of the 2007 Annual Report of the SAXS Beamline of the Austrian Academy of Sciences. The year 2007 has seen the progression of the effort to relaunch the Elettra Laboratory activities and to develop the upgrading projects of the Elettra light source. Several of these machine upgrade projects have been successfully completed in 2007, including construction of the Booster full-energy injector, upgrade of the RF plant, installation of a Global Orbit Feedback. Full-energy injecton has already been achieved at the time of this writing and top-up operation is scheduled for the end of 2008.

We have mapped a strategy - in collaboration with our key partners and users - to take maximum advantage of the upgraded Elettra storage ring with top-up operating mode. Important steps included the successful workshop “New Frontiers in Insertion Devices” (November 20-21, 2006) and "The Future of Elettra" series (May 21 and December 2-3, 2007). The scope of the workshops was to review insertion devices at the most advanced synchrotron radiation facilities worldwide, the prospects for top-up operation at Elettra, as well as the different undulator/wiggler beamlines at Elettra, including SAXS, and the related upgrade plans.

Several high performance beamlines were inaugurated at Elettra and/or opened to users, including the infrared microscopy and spectroscopy beamline SISSI in partnership with University of Rome "La Sapienza" and INFM-CNR, the high resolution photoemission beamline Bad-ELPH in partnership with University of Augsburg, the powder diffraction beamline MCX in partnership with University of Trento and the INSTM Consortium, the scanning and imaging microscopy beamline TWINMIC.

In addition, award of contracts by external public institutions made available significant resources for new development projects, such as the construction of a second structural biology beamline (and related support laboratories) and the upgrade of the SuperESCA and ESCAmicroscopy beamlines. Particularly relevant in 2007 was the award of a grant by the European Research Council (ERC) to the project for the construction of an inelastic scattering beamline for the FERMI source. The selection process by the ERC has been particularly strict: less than 3% of the submitted projects have been admitted to the funding.

As far as FERMI@Elettra is concerned, the design phase was concluded with success with the publication in February 2007 of the Conceptual Design Report (CDR), developed through scientific collaborations with Lawrence Berkeley National Laboratory, the Massachusetts Institute of Technology, INFN, and INFM, among others. The validity of the FERMI@Elettra project and the international collaborations have allowed us to be inserted into the European Roadmap developed by ESFRI (the European Strategy Forum on Research Infrastructures),

within the network of all FEL projects in Europe, supported by a funding from the EU for the constitution of an European consortium of complementary facilities (IRUVX).

The construction phase started off with the restructuring of the management team and the hiring in February 2007 of managers experienced in the execution of FEL light sources. An international engineering group with proven experience in the field has been retained to design all of the infrastructure of FERMI and manage the entire construction process. Since the Summer of 2007, feasibility studies have been carried out and development of the preliminary design has initiated. The photoinjector electron source project has been completed with the installation of the beam transport and diagnostics channel. Furthermore, the main components have been acquired from UCLA to perform the first tests on the beam in collaboration with MAX-Lab in Lund (Sweden), partner of the Elettra in the framework of the IRUVX Consortium.

The Booster project and the current upgrade of the beamlines will bring Elettra up to par with the most advanced competitors and will at the same time emphasize our experience accumulated in the international arena. The FERMI@Elettra project, the first and, at present, only sedeed FEL facility under construction worldwide, will relaunch our international presence and attract new and highly qualified international partners. These developments have been made possible by a loan from the European Investment Bank (EIB), which recognizes the importance of the project on a pan-European level. All this strengthens the trend towards an internationalization of Sincrotrone Trieste, the maaging company of Elettra, with the perspective of establishing institutional ties to long-term European programs.

The future of Elettra hinges on the support of our key partners, foremost among them the Austrian Academy of Sciences. The SAXS beamline is an essential facility for the users' community in the life sciences, materials chemistry and materials physics, because of the competence and dedication of the beamline management and staff. We at Sincrotrone Trieste look forward to increased collaboration with the Austrian Academy of Sciences in the exploration of the frontiers that the new upgraded Elettra and FERMI will open for us.

Alfonso Franciosi

The SAXS Group

HEAD OF PROJECT: Peter Laggner [1)]

e-mail: peter.laggner@oeaw.ac.at

SCIENTISTS: Heinz Amenitsch [1), 3)]

e-mail: amenitsch@elettra.trieste.it

Sigrid Bernstorff [2])

e-mail: bernstorff@elettra.trieste.it

Michael Rappolt [1), 3)]

e-mail: michael.rappolt@elettra.trieste.it

POST DOCS: Fernando Cacho [1), 3)]

e-mail: fernando.cacho@elettra.trieste.it

Shyjumon Ibrahimkutty [1, 3)]

e-mail: shyju.ibrahimkutty@elettra.trieste.it

Benedetta Marmiroli [1, 3)]

e-mail: benedetta.marmiroli@elettra.trieste.it

PhD STUDENT: Fabian Schmid [1), 3)]

e-mail: fabian.schmid@elettra.trieste.it

SCIENTIFIC ASSISTANT: Barbara Sartori [1, 3)]

e-mail: barbara.sartori@elettra.trieste.it

TECHNICIAN: Christian Morello [2)]

e-mail: christian.morello@elettra.trieste.it

1) Institute for Biophysics and Nanosystems Research, Austrian Academy of Sciences, Schmiedlstraße 6, 8042 Graz, Austria.
Tel 0043-316-4120 302
Fax 0043-316-4120 390

2) Sincrotrone Trieste, Strada Statale 14, km 163.5, 34012 Basovizza (TS), Italy.
Tel 0039-040-375 81
Fax 0039-040-938 0902

3) Institute for Biophysics and Nanosystems Research, Austrian Academy of Sciences
c/o Sincrotrone Trieste

The SAXS-Beamline in General

Small Angle X-ray Scattering has become a well known standard method to study the structure of various objects in the spatial range from 1 to 1000 Å, and therefore instruments capable to perform such experiments are installed at most of the synchrotron research centers. The high-flux SAXS beamline at ELETTRA is mainly intended for time-resolved studies on fast structural transitions in the sub-millisecond time region in solutions and partly ordered systems with a SAXS-resolution of 10 to 1400 Å in real-space.
The photon source is the 57-pole wiggler whose beam is shared and used simultaneously with a Macromolecular Crystallography beamline. The wiggler delivers a very intense radiation between 4 and 25 keV of which the SAXS-Beamline accepts 3 discrete energies, namely 5.4, 8 and 16 keV. The beamline optics consists of a flat double crystal monochromator and a double focusing toroidal mirror.
A versatile SAXS experimental station has been set-up, and an additional wide-angle X-ray scattering (WAXS) detector monitors simultaneously diffraction patterns in the range from 1 to 9 Å. The sample station is mounted move-able onto an optical table for optimising the sample detector distance with respect to SAXS resolution and sample size.
Besides the foreseen sample surrounding the users have the possibility to install their own specialised sample equipment. In the design phase, besides technical boundary conditions, user friendliness and reliability have been considered as important criteria.
The optimisation of the beamline with respect to high-flux and consequently high flux density, allows to perform the following experiments:

- Low Contrast Solution Scattering
- Grazing Incidence Surface Diffraction
- Micro-Spot Scanning
- X-ray Fluorescence Analysis
- Time-Resolved Studies ≥ 11 μs
- Simultaneously Performed Small- and Wide-Angle Measurements (SWAXS) on:
    - Gels
    - Liquid Crystals
    - (Bio) Polymers
    - Amorphous Materials
    - Muscles

Furthermore, using 5.4 and 16 keV energies, the beamline is widely applicable also to very thin, e.g. single muscle fibers, and optically thick (high Z) specimen, as often used in e.g., material science and solid state physics.

THE INSERTION DEVICE

The wiggler for the SAXS beamline consists of three 1.5 m long segments, each having 19 poles. The device can work with a minimum gap of 20 mm, which corresponds to K=20 at 2 GeV. The main parameters of the wiggler are:

- Critical Energy 4.1 keV
- Radiation Power 8.6 kW
- Flux 3.5×10^{14} ph/s/mrad/0.1%BW (at 400 mA)

The wiggler radiation cone has a horizontal width of 9 mrad. From this the SAXS-beamline accepts vertically 0.3 mrad, and horizontally +/-0.5 mrad at a 1.25 mrad off-axis position. The resulting source size for 8 keV photons is 3.9 x 0.26 mm^2 (horiz. x vert.).

THE OPTICS

The optics common with the diffraction beamline consists of:

- C-Filter and Beryllium window assembly to reduce the power load on the first optical elements by a factor of 2 and to separate the beamline vacuum from the storage ring.
- Beam defining slit chamber which allows to define the SAXS beam on three sides before the monochromator in order to reduce the straylight in the downstream beamline sections.

The SAXS beamline optics consists of:

- A double-crystal monochromator consisting of four individual chambers, in which three interchangeable asymmetric Si(111) crystal pairs are used to select one of three fixed energies. Each of the crystal pairs is optimised for the corresponding energy to accomplish a grazing angle of 2°. The energy resolution $\Delta E/E$ of the monochromator is in the range of 0.7 - 2.5 10^{-3}.
- A baffle chamber after the monochromator is used as an adjustable straylight fenditure.
- A segmented toroidal mirror focuses the light in horizontal and vertical direction with a 1/2.5 magnification onto the SAXS-detector.
- An aperture slit reduces the straylight after the monochromator and the toroidal mirror.
- A guard slit defines the illuminated region around the focal spot. The spot size on the detector is 1.6 mm horizontally and 0.6 mm vertically. The calculated flux at the sample is in the order of 10^{13} ph/s at 400 mA. For a maximum sample size of 5.4 x 1.8 mm^2 correspondingly a flux density of 10^{12} ph/s/mm^2 has been calculated.

SAMPLE STAGE

The multipurpose sample stage allows to perform fast time-resolved relaxation studies based on temperature- or pressure-jumps as well as stopped flow experiments. Shear jump relaxation experiments are planned. Specifically, T-jumps can be induced by an infra-red light pulse (2 ms) from an Erbium-Glass laser, raising the temperature about 20 °C in an aqueous sample volume of 10 µl. A hydrostatic pressure cell with a maximal accessible angular range of 30° for simultaneous SAXS and WAXS measurements is available. P-jumps are realised by switching fast valves between a low and a high pressure reservoir, increasing or decreasing the hydrostatic pressure in the range from 1 bar to 2.5 kbar within a few ms. A Differential Scanning Calorimeter (DSC) allows for DSC-scans simultaneously to SWAXS measurements. In an overview, the following sample manipulations are possible (further details, see page 32-38):

- Temperature Manipulations: Ramps, Jumps and Gradient Scans
- Pressure Manipulation: Scan and Jumps
- Stopped Flow Experiments
- SWAXS Measurements Applying Mechanical Stress
- Calorimetric measurements

Scientific Applications

Low Contrast Solution Scattering, Grazing Incidence Surface Diffraction, Micro-Spot Scanning, X-ray Fluorescence Analysis, Time-Resolved Studies ≥ 11 µs and Simultaneously Performed Small- and Wide-Angle Measurements (SWAXS) on:

Gels
Liquid Crystals
(Bio) Polymers
Amorphous Materials
Muscles

Source characteristics

Wiggler (NdFeB Hybrid):

Period	140 mm
No. full poles	57
Gap	20 mm
B_{max}	1.607 T
Critical Energy ε_c	4.27 keV
Power (9 mrad)	8.6 kW
Effective source size FWHM	3.9 x 0.26 mm^2(HxV)

Optics

Optical elements:	*Double crystal monochromator*:	*Mirror*:
	Si (111) asym. cut, water cooled.	two–segment,toroidal, Pt coated.
Distance from source:	18.4 m	26.5 m

Acceptance	1 mrad/0.3 mrad (HxV)
Energy (3 selectable)	5.4, 8, 16 keV (0.77, 1.54, 2.3 Å)
Energy resolution $\Delta E/E$	0.7-2.5 x 10^{-3}
Focal spot size FWHM	1.2 x 0.6 mm^2 (HxV)
Spot at Sample FWHM	5.4 x 1.8 mm^2(HxV)
Flux at sample	5 x 10^{12} ph s^{-1}(2 GeV, 200 mA, 8 keV)

Experimental apparatus

Resolution in real space: 10-1400 Å (small-angle), 1- 9 Å (wide-angle)

Sample stage: temperature manipulations: ramps, jumps and gradient scans, pressure manipulation: scan and jumps, stop flow experiments, SWAXS measurements applying mechanical stress, SWAXS measurements applying magnetic fields. In-line calorimetric measurements simultaneously with SWAXS.

Detectors: 1D gas-filled detectors for simultaneous small- and wide-angle (Gabriel type), 2D CCD-detector for small-angle, Vantec-1 detector (Bruker AXS).

Experiment control

Beamline control: Program-units written in LabView for Windows
1 D detector control: PC-card and software from Hecus X-ray Systems GmbH, Graz.
2 D detector control: Software from Photonic Science, Oxford.

CURRENT STATUS

The beamline has been built by the Institute for Biophysics and Nanosystems Research (IBN), Austrian Academy of Science in collaboration with staff members from Sincrotrone Trieste, and is in user operation since September 1996. The set-up of the beamline started at the beginning of January 1995 with the installation of the support structure. Until the end of 1995, the 8 keV single energy system had been realised. The upgrade to the full three energy system was finished in spring 1998. Time resolved experiments require fast X-ray detectors and data acquisition hard- and software. Depending on the desired resolution in time and in reciprocal space, on isotropic or anisotropic scattering of the sample, one-dimensional position sensitive (delay-line type) or two-dimensional CCD detectors are employed.

In August 2002 our new chemistry and X-ray laboratory went into operation. The chemistry unit serves mainly for sample preparation and analysis for both, in house research and external user groups, whereas the X-ray laboratory allows on-site testing of samples before moving on to the SR beamline (see page 31).

In conclusion, due to wide versatility of the beamline and the highly flexible sample stage, there are nearly no limits for the realisation of an experiment, and you are welcome by our team to propose any interesting and highlighting investigation for the benefit of material and life sciences.

Application for Beamtime at ELETTRA

1. Beamtime Policy at SAXS beamline

According to the agreement from March 2001 regarding the co-operation between the Austrian Academy of Sciences and Sincrotrone Trieste, at the Austrian SAXS-beamline the available beamtime of about 5000 hours/year is distributed as follows:

- 35% for Austrian Users, type: "CRG" (Collaborating Research Group)
- 35% for Users of Sincrotrone Trieste (General Users (GU))
- 30% is reserved for beamline maintenance and in-house research

In both user beamtime contingents also any industrial, proprietary and confidential research can be performed according to the "General User Policy" of Sincrotrone Trieste.

To apply for CRG and GU user beamtime proposals must be submitted according to the rules of Sincrotrone Trieste. The international review committee at ELETTRA will rank the proposals according to their scientific merit assessment. Based on this decision beamtime will be allocated according to the specific quotes for the beamtimes (CRG/GU) either for the following semester ("normal application") or for the next two years ("long term application"). However, at the moment no more than a maximum of 10% of the beamtime will be assigned to "long term" projects.

2. How to apply for beamtime

There are two deadlines each year for proposals, namely August 31st and February 28th. Accepted proposals will receive beamtime either in the then following first or second half year period, respectively. The Application Form must be completed on-line according to the following instructions.

ELETTRA USERS OFFICE

Strada Statale 14 - km 163.5
34012 Basovizza (Trieste), ITALY
Tel: +39 040 375 8628 - fax: + 39 040 375 8565
e-mail: useroffice@elettra.trieste.it

INSTRUCTIONS GIVEN BY THE USERS OFFICE

(see also http://www.elettra.trieste.it/UserOffice/)

1. Read carefully the General Guidelines.

2. Connect to the Virtual Unified Office: https://vuo.elettra.trieste.it/pls/vuo/guest.startup using your favorite browser with JavaScript enabled.

3. Select the Virtual Unified Office link.

4. When prompted, insert your ID and password. If you are a new user fill in the registration form with your data and choose your institution with the search button; in case your institution does not appear in the list, please contact useroffice@elettra.trieste.it giving all the details about it. When registered, you will receive an acknowledgment with your ID and password. You can change your password, if you wish. In case you forget your password, please don't register again but contact useroffice@elettra.trieste.it. At any moment you can select the help button and view more detailed instructions. By inserting your ID and password you will be able to continue.

5. Select the proposals button in the User functions group.

6. Select add and fill in on-line the proposal form. Please, type your proposal in English. Repeat this procedure for each proposal you intend to submit.

7. In case of continuation proposal: a) attach the experimental report of previous measurements; b) give your previous proposal number.

8. When finished, submit the proposal electronically, selecting the save button.

9. Print the proposal form together with each related safety form.

10. Sign the safety form(s).

11. Mail all signed safety form(s) as printed copy to the Users Office.

NOTE:

For technical questions related to proposals submission or other practical issues contact useroffice@elettra.trieste.it

For scientific questions related to the possibility of performing a given experiment contact bernstorff@elettra.trieste.it or amenitsch@elettra.trieste.it

List of Users and Institutes 2007

Australia

Monash University, Department of Parmaceutics, Victoria College of Pharmacy, Parkville VIC
BOYD Ben J.
DONG Aurelia Wenjing
DONG Charlie Yao-Da

School of Chemistry, University of Melbourne
JASIENIAK J.

Austria

Austrian Academy of Science, Institute of Biophysics and Nanosystems Research, Graz
AMENITSCH Heinz
BOULGAROPOULOS Beate
BRUENNER Franz
CACHO NERIN Fernando
DEUTSCH Günter
HODZIC Aden
HOEGER Birgit
IBRAHIMKUTTY Shyjumon
KRIECHBAUM Manfred
LAGGNER Peter
LOHNER Karl
LORENZUTTI Alexander
MARMIROLI Benedetta
PABST Georg
RAPPOLT Michael
SARTORI Barbara
SCHMID Fabian
SEVCSIK Eva
YAGHMUR Anan
ZWEYTICK Dagmar

Graz University of Technology Institute of Biomechanics, Center of Biomedical Engineering, Graz
HOLZAPFEL Gerd A.

Universität Wien, Institut für Materialphysik, Wien
University of Vienna, Institute of Materials Physics
KERBER Michael
SCHAFLER Erhard
WIECZOREK Arkadiusz
ZEHETBAUER Michael

Brazil

University of Sao Paulo, Institute of Physics, Sao Paulo
BARBOSA Leandro R. S.
ITRI R.

Croatia

Faculty of Sciences, Zagreb
SKOKO Željko

Institute for Physics, Zagreb
MILUN M.
KRAJNOVIC S.
SALAMON Krešimir

"Ruder Boskovic" Institute, Zagreb
BOGDANOVIC-RADOVIC I.
BULJAN Maya
DESNICA-FRANKOVIC Ida-Dunja
DESNICA Uroš V.
DUBČEK Pavo
GAJOVIČ Andreja
GRACIN Davo
MILE Ivanda
JURAIĆ Krunoslav
MUSIĆ Svetozar
PIVAC Branko
RADIĆ Nikola
RAKVIN B.
RISTIĆ Mira
SIKETIC Z.

University of Zagreb, Faculty of Electrical Engineering and Computing
Grozdanic D.

University of Zagreb, Faculty of Science, Department of Physics
DJERDJ I.

University of Zagreb, Faculty of Science, Institute of Mineralogy and Petrography
TOMASIC N.

Finland

Åbo Akademi University, Dept. of Physical Chemistry, Turku
LINDÉN Mika

France

Institut Charles Gerhardt de Montpellier, UMR 5253 CNRS/ENSCM/UM2/UM1, Matériaux Avancés pour la Catalyse et la Santé, MACS, Montpellier

BLANC Beatrice
REBOUL Julien

Université de Paris-sud XI, Faculté de Pharmacie, UMR CNRS, Chatênay-Malabry

PILI Barbara
BOURGAUX Claudie
COUVREUR P.
FAIVRE Vincent
KELLER Gerhard
OLLIVON Michel
PERRINE Pivette
VANESSA Allain

Université Pierre et Marie Curie, Chimie de la Matière Condensée, Paris

BACCILE Niki
BASS John
BOISSIÉRE Cédric
GROSSO David
KUEMMEL Monika

Université d' Orleans - Centre de Recherche sur la Matiére Divisée, Orleans

ERRE René
SINTUREL Christophe
VAYER Marylène

Germany

Research Center Rossendorf, Dresden

GRÖTZSCHNEL Rainer

University of Bremen, Institute of Solid State Physics

FALTA Jens
HILDEBRAND Radowan
SCHMIDT Thomas Jr.
SPECKMANN Moritz

University of Munich, Dept. of Chemistry and Biochemistry

BEIN T.
KEILBACH Andreas
KÖHN Ralf
ZÜRNER Andreas

Greece

National Hellenic Research Found - Dept. of Chemistry

MAVROMOUSTAKOS Thomas
ZOUMPOULAKIS Panagiotis

Hungary

Eötvös University, Department of General Physics, Budapest
IBÁRIK Gabor
NGÁR Tamas

India

Indian Institute of Science, Department of Physics, Bangalore
Sood A. K.

Indian Institute of Science, Solid State and Structural Chemistry Unit, Bangalore
NAG Angshuman
SANTRA Pralay
NAG Angshuman
SARMA Dipankar Das
VISWANATHA Ranjani

Indian Association for the Cultivation of Science, Department of Materials Science, Jadavpur, Kolkata
SEKHAR KARAN Niladri

Raman Research Institute, Bangalore
GHOSH S.K.
RADHAKRISHNAN A.V.
RAGHUNATHAN V.A.
SARANGI Bibhu Ranjan

Ireland

University College Cork (UCC), Dept. of Chemistry, Cork
ARNOLD Donna C.
HOLMES Justin D.
MORRIS Michael A.
O'CALLAGHAN John M.
PETKOV Nikolay

Italy

Associazione CIVEN, Nano Fabrication Facility, Marghera / Venice
FALCARO Paolo

I.N.F.M. - Laboratori Nazionali di Frascati
MARCELLI Augusto
PICCININI Massimo

INFM - CNR Laboratorio TASC, Trieste
BUSINARO Luca
GRENCI Gianluca

Sincrotrone Trieste, Trieste
BERNSTORFF Sigrid
MORELLO Christian

University Ca Foscari, Dep. of Physical Chemistry, Venizia-Mestre
SCOPECE Paolo (2007 with Innocenzi)

Università di Brescia - Dip. di Ing. Meccanica, Lab.di Chimica per le Tecnologie, BRESCIA
BONTEMPI Elza
ZANOLA Paolo

Universita di Cagliari, Dip. di Scienze Chimiche, Monserrato
CASULA Maria Francesca
MONDUZZI Maura

University of Camerino, Dep. of Molecular Cellular and Animal Biology, Genetic Immunization Laboratory
AMICI Augusto
MARCHINI Cristina
MONTANI Maura

University of Florence, Department of Chemistry, Sesto Fiorentino (FI)
MILANI Silvia

Università di Firenze, Dip. Scienze Fisiologiche, Firenze
University of Florence
BAGNI Maria Angela
BENELLI Giulia
CECCHI Giovanni
COLOMBINI Barbara
NOCELLA Marta

Università di Padova, Dip. di Biologia, Padova
VILLANOVA Laura

Università di Padova, Dep. of Mechanical Engineering, Padova
ANTONELLO Alessandro
BULLEN Craig
BUSO D.
MARTUCCI Alessandro

Università Politecnica delle Marche, Dipartimento di Scienze Applicate ai Sistemi Complessi, Ancona
MARIANI Paolo
ORTORE Maria Grazia
RENGHINI Chiara
SINIBALDI Raffaele
SPINOZZI Francesco

Università Politecnica delle Marche, Dipartimento di Fisica e Ingegneria dei Materiali e del Territorio, Ancona

ALBERTINI G.
GIRARDIN Emmanuelle

University of Rome “La Sapienza”, Department of Chemistry

CAMINITI Ruggero
CARACCIOLO Giulio
POZZI Daniela

University of Rome “La Sapienza”, Chemistry Department, and IMC-CNR

MANCINI Giovanna
LUCIANI Paola

Università di Sassari, Laboratorio di Scienza dei Materiali e Nanotecnologie, Alghero

COSTACURTA Stefano
FIGUS Cristiana
INNOCENZI Plinio
KIDCHOB Tongjit
MALFATTI Luca
TAKAHASHI Masahide

Japan

Aida Nanospace Project, Exploratory Research for Advanced Technology Agency, National Museum for Emerging Science and Innovation, Tokyo

FUKUSHIMA T.
JIN W.

Slovenia

Josef Stefan Institute, Ljubljana

STERN Igor
JENKO KOKALJ Sasa

National Institute of Chemistry, Ljubljana

BITENC Marko
CRNJAK OREL Zorica
PODBRŠČEK Peter

University of Ljubljana, Department of Mathematics and Mechanics

OREL Bojan

Spain

Center of biophysical studies, Dept. Bioquímica i Biología Molecular, Universitat Autònoma de Barcelona

TEIXEIRA Cilâine Veronica

Chemical and Environmental Research Institute of Barcelona (IIQAB-CSIC)
BARBOSA BARROS Lucyanna
DE LA MAZA A.
LÓPEZ SERRANO Olga

United Kingdom

University Laboratory of Physiology, Oxford
ASHLEY Christopher Charles
GRIFFITHS Peter John

List of Performed Experiments

2007 (first half year)

Proposal	Proposer	Institution	Country	Title	Research Area
2006462	CECCHI Giovanni	Università di Firenze, Dip. di Scienze Fisiologiche	Italy	The origin of spacing changes in the M3 reflection of skeletal muscle upon activation	Life Sciences
2006463	SEVCSIK Eva	Austrian Academy of Sciences (AAS), Institute of Biophysics and Nanosystem Research (IBN), Graz	Austria	Effect of the human antimicrobial peptide LL-37 on bacterial model membranes	Life Sciences
2006574	DESNICA Uros	Ruder Bošković Insitute, Zagreb	Croatia	Formation of three-dimensional Ge quantum dot superlattices	Materials Science
2006582	SCHAFLER Erhard	Universität Wien, Inst. für Materialphysik	Austria	Investigation of stacking faults in severely plastically deformed metals by in-Situ Synchrotron WAXS, Part I: Face Centered Cubic Metals	Materials Science
2006590	CARACCIOLO Giulio	Università di Roma La Sapienza, Dip. di Chimica	Italy	Interaction between lipid/DNA complexes and anionic liposomes intended as model systems of cellular membranes	Life Sciences
2006607	GROSSO David	Université Paris 6, Chimie de la Matiere Condensee	France	Morphological characterization of Mesoporous-Nano-Patterns	Chemistry
2006655	INNOCENZI Plinio	Universitá di Sassari	Italy	Study and development of new lithographic techniques in rewritable mesostructured films	Chemistry
2006670	TEIXEIRA Cilaine Veronica	Center of biophysical studies, Dept. Bioquímica i Biología Molecular, Universitat Autònoma de Barcelona	Spain	In-situ synchrotron SAXS study of the formation of self-assembled carbon nanotubes and influence of rapid temperature jumps on the nanotubes stability	Chemistry
2006698	MARMIROLI Benedetta	AAS, IBN, Graz	Austria	Microsecond resolved observation of protein unfolding by rapid mixing methods and SAXS	Materials Science
2006708	IBRAHIMKUTTY Shyjumon	AAS, IBN, Graz	Austria	In-situ Gas phase study of metal nanoclusters using a gas aggregation source	Materials Science
2006757	SCHMID Fabian	AAS, IBN, Graz	Austria	2-dimensional Layer Specific Tensile Testing of Human Aorta	Life Sciences

2006765	YAGHMUR Anan	AAS, IBN, Graz	Austria	Rapid self-assembly and structural transitions of lipid-based nanostructures studied by combined time-resolved SAXS and stopped flow technique	Life Sciences
2005804	HOLMES Justin	University College Cork (UCC), Dept. of Chemistry	Ireland	In-situ, time-resolved GI-SAXS studies of the meso-structuring process of silica nano-filaments in confined environments under vacuum or varying relative humidity	Chemistry
2006824	KRIECHBAUM Manfred	AAS, IBN, Graz	Austria	Nanostructural mechanism of amyloid fibril formation of the protein stefin B (different variants) by SAXS	Life Sciences
2006840	GIRARDIN Emmanuelle	Università di Ancona, Dip. di Fisica ed Ingegneria dei Materiali e del Territorio	Italy	GISAXS study of metal nanoclusters-silica composite coatings	Materials Science
2006846	KOEHN Ralf	University of Munich, Dept. of Chemistry and Biochemistry	Germany	In-situ SAXS characterization of silica mesostructure formation in the confined space of anodic alumina membranes	Chemistry
2006863	AMENITSCH Heinz	AAS, IBN, Graz	Austria	SAXS-Study on cubic phase transitions of highly aligned phospholipids	Life Sciences
2005051 Long Term	FALTA Jens	Institute for Solid State Physics, University of Bremen	Germany	In-situ characterisation of self-assembled nanoparticle films under harsh conditions	Materials Science
In-house research	BERNSTORFF Sigrid & MARIANI Paolo	Sincrotrone Trieste & Universitá Politecnica delle Marche, Ancona	Italy	The influence of concentration and pH on the bovine serum albumin structure	Life Sciences
In-house research	BERNSTORFF Sigrid & GRACIN Davor	Sincrotrone Trieste & Ruder Bošković Insitute, Zagreb	Italy & Croatia	SAXS investigation of SnOx structures	Materials Science
In-house research	AMENITSCH Heinz & SARMA Dipankar Das	AAS, IBN, Graz & Indian Institute of Science, Department of Organic Chemistry, Bangalore	Italy & India	Study of the growth of CdSe nanocrystals: with SAXS	Chemistry
In-house research	BERNSTORFF Sigrid & PIVAC Branko	Sincrotrone Trieste & Ruder Bošković Insitute, Zagreb	Italy & Croatia	Si nanoclusters production in SiO2/SiO multilayers: a search for selforganization in 3D	Materials Science
In-house research	AMENITSCH Heinz & SINTUREL Christophe	AAS, IBN, Graz & Université d Orleans, Centre de Recherche sur la Matiére Divisée	Italy & France	In-situ SWAXS study of self-assembled PE-PEO block copolymer in liquid precursor of unsaturated polyester thermoset	Materials Science

In-house research	BERNSTORFF Sigrid & RADIC Nikola	Sincrotrone Trieste & Ruder Bošković Insitute, Zagreb	Italy & Croatia	Study of thin films of a completely immiscible Ag-W system	Materials Science
In-house research	AMENITSCH Heinz & OLLIVON Michel	AAS, IBN, Graz & C.N.R.S., Universite de Paris Sud	Italy & France	Emulsifiers structures at subzero temperature and/or at oil-water interface	Life Sciences
Test	CRNJAK OREL Zorica	National Institute of Chemistry, Ljubljana	Slovenia	Nucleation and growth of monodispersed metal oxide particles in their nano to submicrometer size range	Chemistry
Test	BONTEMPI Elza	INSTM and Laboratorio di Chimica per le Tecnologie, Università di Brescia	Italy	Distribution of particles in a matrix of gum	Materials Science

2007 (second half year)

Proposal	Proposer	Institution	Country	Title	Research Area
2007007	PABST Georg	AAS, IBN, Graz	Austria	The role of membrane hydrocarbon chain composition in interactions with antihypertensive drugs	Life Sciences
2007022	MARTUCCI Alessandro	Dip. Ingegneria Meccanica (Settore Materiali), University of Padova	Italy	Early nucleation process of noble gold nanorods prepared by wet chemical methods	Materials Science
2007071	LOPEZ SERRANO Olga	Chemical and Environmental Research Institute of Barcelona	Spain	Study of bicellar systems containing ceramides using SAXS	Chemistry
2007116	SCHMID Fabian	AAS, IBN, Graz	Austria	2-dimensional Layer Specific Tensile Testing of Human Aorta	Life Sciences
2007147	SCHMIDT Thomas Jr	Institute for Solid State Physics, University of Bremen	Germany	Ordering of Ge quantum dots grown on faceted Si(113) studied by GISAXS	Materials Science
2007165	KRIECHBAUM Manfred	AAS, IBN, Graz	Austria	Self-assembled nanostructures of Monoelaidin-elaidic Acid and Monoelaidin-oleic systems: bulk vs. Aqueous Dispersions	Life Sciences
2007189	SARMA Dipankar Das	Indian Institute of Science, Department of Organic Chemistry, Bangalore	India	In-situ study of the growth of metal nanocrystals: gold, a case study	Chemistry
2007194	YAGHMUR Anan	AAS, IBN, Graz	Austria	Tuning curvature and stability of monoolein bilayers by short Surfactant-like designer peptides	Life Sciences

2007202	IBRAHIMKUTTY Shyjumon	AAS, IBN, Graz	Austria	In situ gas phase study of Si mesostructure by Evaporation Induced Self Assembly.	Materials Science
2007227	MARMIROLI Benedetta	AAS, IBN, Graz	Austria	Ultrafast Nucleation and Growth Study of Calcium Carbonate by SAXS	Materials Science
2007345	CRNJAK OREL Zorica	National Institute of Chemistry, Ljubljana	Slovenia	In situ study of nucleation and growth of metal oxide particles from nano to submicrometer size	Chemistry
2007367	BARBARA Pili	C.N.R.S., Universite de Paris Sud	France	Nanoparticles of squalenized anti-cancer drug	Life Sciences
In-house research	RAPPOLT Michael, AMENITSCH Heinz & BOYD Ben	AAS, IBN, Graz, & Monash University, Dept. of Parmaceutics, Victorian College of Pharmacy, Parkville	Austria & Australia	Formation and phase transitions in liquid crystalline dispersed particles using time resolved SAXS	Life Sciences
In-house research	PABST Georg & RAGHUNATHAN Velayudhan	AAS, IBN, Graz & Raman Research Institute, Bangalore	Austria & India	Structure of a novel sponge phase found in an ionic surfactant system	Life Sciences
In-house research	BERNSTORFF Sigrid & RADIC Nikola	Sincrotrone Trieste & Ruder Bošković Insitute, Zagreb	Italy & Croatia	Study of thin films of a completely immiscible Ag-W system	Materials Science
In-house research	BERNSTORFF Sigrid & PIVAC Branko	Sincrotrone Trieste & Ruder Bošković Insitute, Zagreb	Italy & Croatia	Structural characterization of thin amorphous Si films	Materials Science
Test	MONDUZZI Maura	Universita di Cagliari, Dip. di Scienze Chimiche, Monserrato	Italy	Characterization of the Internal Structure of Lipidic Nanoparticles	Life Sciences

User Statistics

1. Number of submitted proposals and assigned shifts from 1995 until December 2008

The Austrian SAXS-beamline at ELETTRA opened to users in September 1996. Since then many experiments have been performed related to the fields of life science, materials science, physics, biophysics, chemistry, medical science, technology and instrumentation.

From September 96 on users gained access to the SAXS-beamline on the basis of the proposals received for the periods shown in Fig. 1. The assignment of beamtime at this beamline is done separately for the group of "General Users" (GU) and the "Collaborating Research Group" (CRG), i.e., the Austrian users. Beamtime was assigned to the proposals of each group in the order of the rating received by the Scientific Committee, and up to the maximum number of shifts available to each group according to the contract between "The Austrian Academy of Sciences" and the "Sincrotrone Trieste". Until December 1997 up to 30 % of the beamtime was given to CRG, up to 55 % to GU, and 15% was reserved for maintenance purposes. From January 98 to June 2001 the quota for beamtime was up to 35 % for CRG, up to 50 % for GU, and again 15% reserved for maintenance purposes. From July 2001 on the two contingents for user proposals from CRG and GU receive up to 35% of the beamtime each. The remaining 30 % of beamtime are used for inhouse research projects as well as for maintenance purposes.

Figure 1 gives an overview of the numbers of received proposals, the numbers of requested and assigned shifts, as well as the percentage between assigned and requested shifts. Included in Fig.1 are also the same data for the period End 1995 - August 1996, during which some beamtime had been given already to users in order to perform first pilot- and test-experiments together with the beamline staff. These first experiments during the commissioning phase were not yet based on proposals, since the goal was mostly to evaluate and improve the performance of the beamline and the equipment of its experimental station. As can be seen in Fig.1, the request for beamtime at the SAXS-beamline increased continuously and strongly until the first half year of 1999 (also during the period Sept.-Dec. 1997, if one takes into account that this period was only 4 instead 6 month long, and that for this reason less proposals were submitted). Then, probably due to the high rejection rates, the number of submitted proposals decreased somewhat during 2001, which resulted in a better ratio of accepted / rejected proposals. This oscillating behaviour of beamtime request can also be seen for the period 2002 – 2008 where after higher numbers of submitted proposals slightly reduced request periods follow. The numbers for the second semester of 2007 and first of 2008 reflect also that, due to the long shut-down from 1.10.2007 to 3.03.2008 (for the booster installation) less proposals were submitted, and less beamtime was available.
In 2007, in total 73 proposals (15 from CRG, and 58 from GU) were submitted. From these 16 proposals (0 from CRG and 16 from GU) were submitted by "new" usergroups, i.e. groups which so far had never beamtime at the SAXS beamline. From these, 6 GU proposals were officially accepted.

Figure 1 (Next page). The statistical information about the beamtime periods since end of 1995 are given for the groups "CRG", and "GU" separately, as well as for both together ("Total"). Shown are, for all beamtime periods (from top to bottom):
● Number of received proposals, ● Number of requested shifts,
● Number of assigned shifts, and ● Relation between assigned and requested shifts

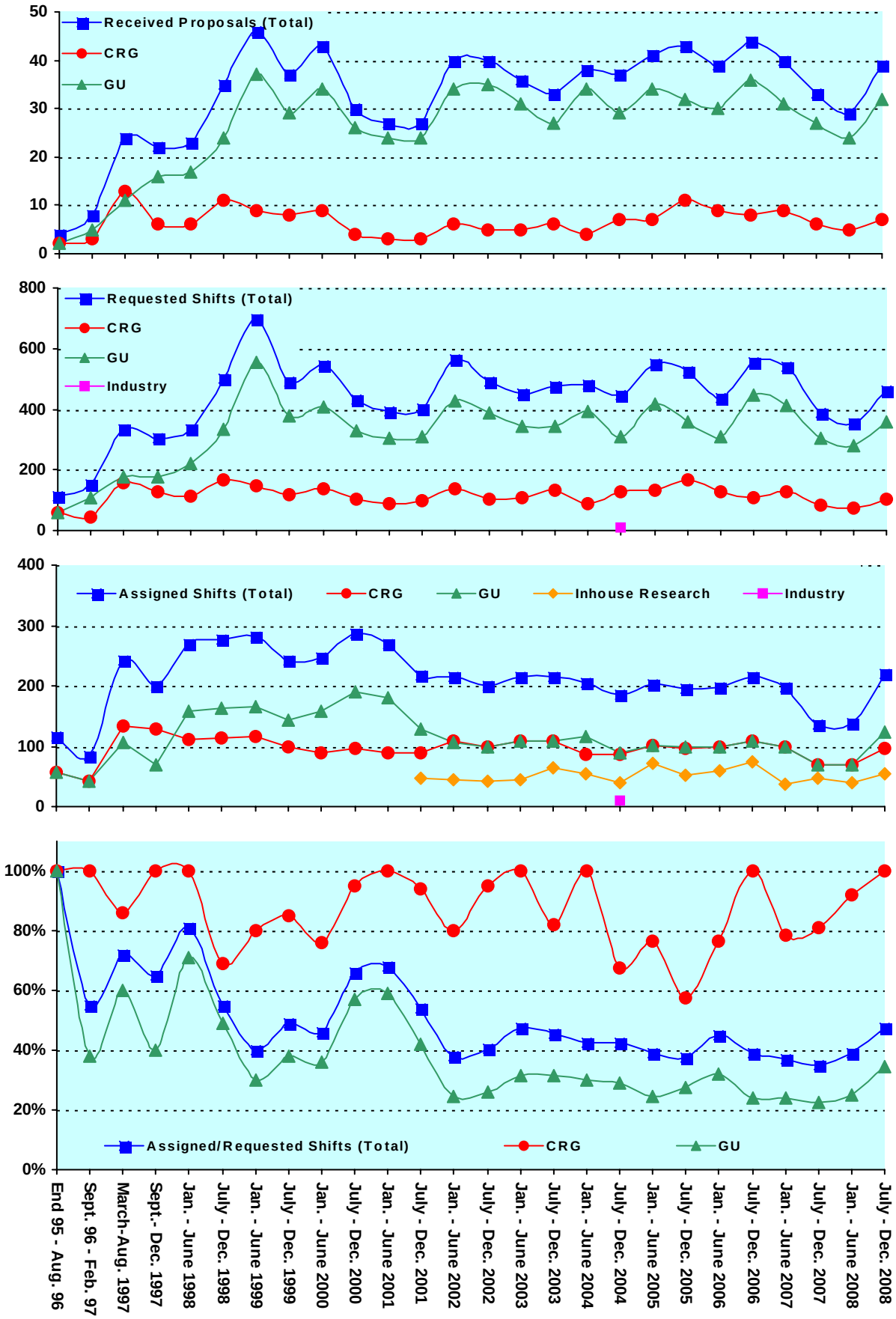
Received Proposals (Total)
CRG
GU
Requested Shifts (Total)
CRG
GU
Industry
Assigned Shifts (Total)
CRG
GU
Inhouse Research
Industry
Assigned/Requested Shifts (Total)
CRG
GU
End 95 - Aug. 96
Sept. 96 - Feb. 97
March-Aug. 1997
Sept.- Dec. 1997
Jan. - June 1998
July - Dec. 1998
Jan. - June 1999
July - Dec. 1999
Jan. - June 2000
July - Dec. 2000
Jan. - June 2001
July - Dec. 2001
Jan. - June 2002
July - Dec. 2002
Jan. - June 2003
July - Dec. 2003
Jan. - June 2004
July - Dec. 2004
Jan. - June 2005
July - Dec. 2005
Jan. - June 2006
July - Dec. 2006
Jan. - June 2007
July - Dec. 2007
Jan. - June 2008
July - Dec. 2008

2. Provenience of users

During 2007, 157 users from 50 institutes in 15 countries have performed experiments at the SAXS beamline. In Fig. 2 are shown both the provenience of these users, and of their respective institutes. Each user or institute was counted only once, even though many users performed experiments in both beamtime periods of 2007.

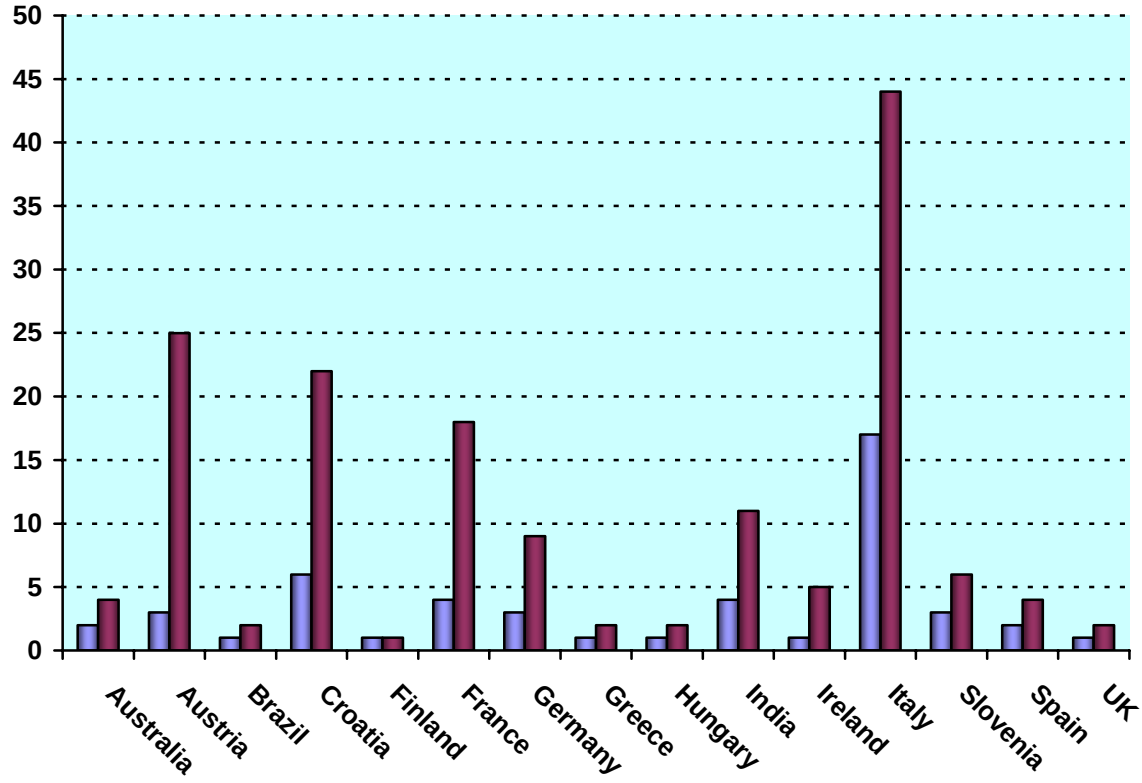

Figure 2. Provenience of users (dark grey) and of their corresponding institutes (light grey).

3. Documentation of experimental results

As could be expected, with the start of user-operation at the SAXS-beamline the number of contributions to conferences started to increase strongly. With a delay of one year - the average time needed for paper publications - also the number of publications increased accordingly, as can be seen in Fig. 3.

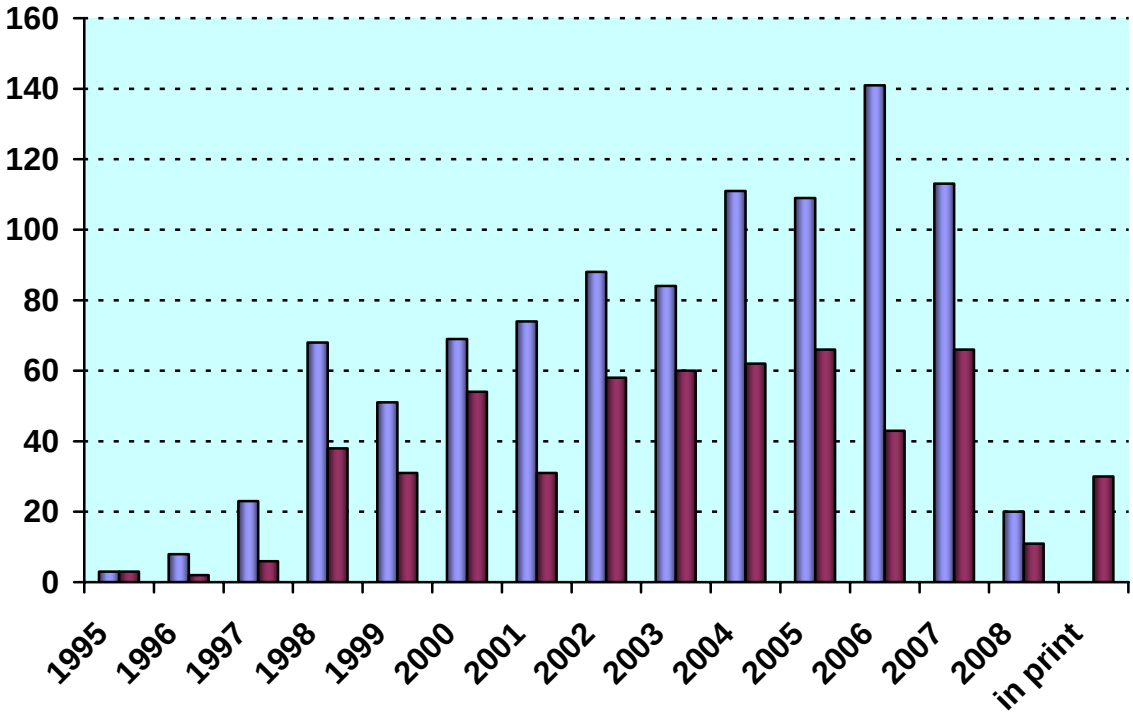

Figure 3. Number of conference contributions (light grey) and of refereed paper publications (dark grey) for the years 1995-2007. Also contributions, which have been published until June 2008 as well as those in print at that time are included.

In addition, from 1995 until June 2008, the following documentations based on instrumentation of the SAXS-beamline, or on data taken with it, have been produced.

Unrefereed publications:

Technical Reports on Instrumentation:	5
Contributions to Elettra Newsletters:	15
Contributions to Elettra Highlights:	29
Habil Thesis:	3
PhD Thesis:	63
Master Thesis :	28

Experimental Possibilities at the SAXS-beamline

1. LATEST DEVELOPMENTS

Image Plate Detector

In the beginning of September 2007, the SAXS group has acquired a Mar300 Image Plate detector (Figure 1). With a circular active area of 300mm in diameter, it is the largest-area detector available to users of the beamline, with a spatial resolution (pixel size) of 150µm.

This detector has two modes of operation (180mm or 300mm), depending on the desired active area, which result in image sizes of 1200x1200 and 2000x2000, respectively. They are stored in the mar image format (16 bit for compactness, with higher precision extensions for values out of range), and can be processed and converted using the Fit2D program [1].

The exposure time for the Image Plate is given in seconds, with typical values between 1 and 60. Readout time depends on the chosen active area (for 180mm mode, about 130 seconds; for 300mm mode, about 210 seconds), and therefore it is not suitable for samples where high time resolution is needed. On the other hand, weak scatterers benefit from the low-noise image for long exposure times, especially in the case of isotropic samples, where the signal quality can be improved through azimuthal integration. Typical applications are those that need a large Q-range with high dynamic range (typical values of 10^5), i.e. solution scattering from proteins and nanoparticles, temperature-step scans, slow processes like nanoparticle formation, mesophase formation, etc.

Figure 1: Mar300 Image plate.

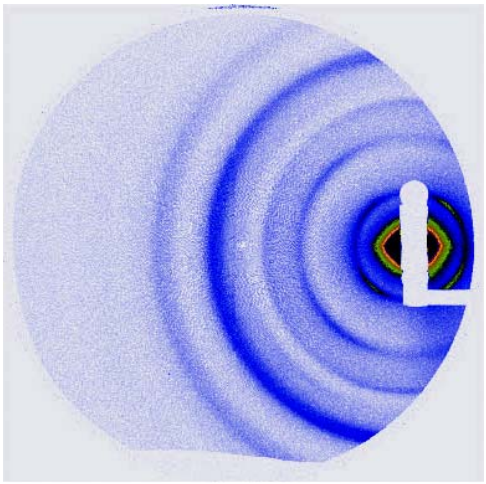

Figure 2: Scattering image of fiber-like structure of modified hexa-peri-hexabenzocoronene at 20°C (see users contibution, page 117)

The camera is controlled with an intuitive and easy to use interface, optimized for long image series. Exposure information, number of images in the series and other information is automatically written to a summary file after each image. Unfortunately at this time the detector cannot be triggered by an external trigger input. Similarly, controlling an additional (external) device or experiment can only be done by hardware wiring of the TTL shutter signal.

[1] A.P. Hammersley, "Fit2D: an introduction and overview", ESRF Internal Report, ESRF97HA02T, 1997

2. ACCESSIBLE SAXS AND WAXS RANGES

Simultaneous SAXS- and WAXS-measurements can be performed using a linear sensitive gas detector (Gabriel type, windows size 8 x 100 mm, active length 86.1 mm with a resolution of 0.135 mm/channel) for the WAXS-range, and either a second linear Gabriel type detector (windows size 10 x 150 mm, active length 134 mm with a resolution of 0.159 mm/channel), or the 2D CCD-system for the SAXS-range. A specially designed vacuum chamber (SWAXS-nose, see Annual Report of 1996/97, p. 32) allows to use both scattering areas below (for SAXS) and above (for WAXS) the direct beam, respectively.

Depending on the photon energy maximum SAXS resolutions of 2000 Å (5.4 keV), 1400 Å (8 keV) or 630 Å (16 keV) are available. The available possible WAXS-ranges are summarised in Table 1. The overall length of the SWAXS-nose in the horizontal direction, measured from the sample position, is 512 mm and the fixed sample to WAXS-detector distance is 324 mm. At the shortest SAXS camera-length an overlap in the d-spacings covered by the SAXS- and WAXS-detectors, respectively, is possible: then, the common regime lies around 9 Å.

Table 1. Possible d-spacing ranges in the WAXS-regime at the SAXS-beamline at ELETTRA. Since the WAXS-detector can be mounted at four different fixed positions on the SWAXS-nose (range 1-4), with the three possible energy choices (5.4, 8 and 16 keV) this results in 12 different d-spacing regimes. In italic the most common choice (8 keV, range 1) is highlighted. This range is suited for experiments, e.g., on lipid-systems and (bio)polymers.

Range	2θ [deg]	d-spacing (Å)		
		8 keV	5.4 keV	16 keV
1	9.4	*9.40*	14.03	4.27
	27.6	*3.23*	4.82	1.47
2	27.4	3.25	4.86	1.48
	45.6	1.99	2.97	0.90
3	45.4	2.00	2.98	0.91
	63.6	1.46	2.18	0.66
4	63.4	1.47	2.19	0.67
	81.6	1.18	1.76	0.54

3. CALIBRATION OF THE S-AXIS AND FLAT FIELD CORRECTION

At the SAXS beamline various standards are used for the angular (s-scale) calibration of the different detectors:

- Rat tail tendon for the SAXS detector - high resolution (rtt*.dat)
- Silver behenate for the SAXS detector – medium and low resolution (agbeh*.dat)
- Para-bromo benzoic acid for the WAXS detector – WAXS range 1 and 2 (pbromo*.dat)
- Combination of Cu, Al foils and Si powder for the WAXS detector – WAXS range 2 and higher

In Figure 2 a typical diffraction pattern of rat tail tendon is shown, depicting the diffraction orders (from the first to the 14th order) measured with a "high" resolution set-up (2.3 m) and the delay-line gas detector. The d-spacing is assumed to be 650 Å, but this value can vary depending on humidity up to 3%. Thus, the rat tail tendon is often used only to determine the position of the direct beam (zero order), while the absolute calibration is performed using the diffraction pattern of Silver behenate powder. Fig. 3 depicts a diffraction pattern of Silver behenate measured with "medium" resolution set-up (1.0 m) from the first to the 4th order (repeat spacing 58.4 Å) [1].

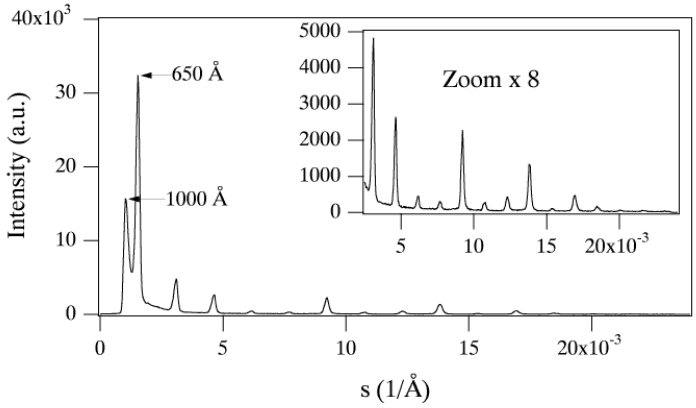

Figure 2. SAXS diffraction pattern of the collagen structure of rat tail tendon fibre at a distance of 2.3 m.

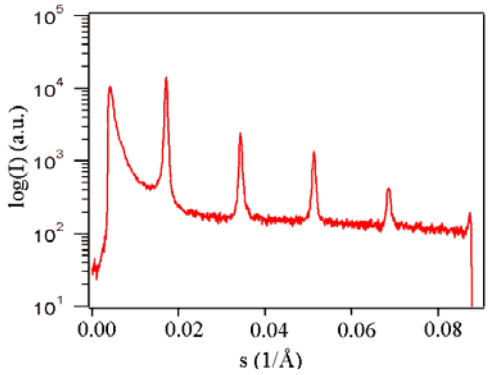

Figure 3. SAXS diffraction pattern of Ag behenate powder at a distance of 1.0 m

In Figure 4 a typical WAXS pattern of p-bromo benzoic acid is shown. The diffraction peaks are indexed according to the values given in Table 2, taken from [2].

Table 2. d-spacings and relative intensities of p-bromo benzoic acid according to [2].

d-spacing / Å	rel. intensity	d-spacing / Å	rel. intensity
14.72	18000	4.25	490
7.36	1200	3.96	2380
6.02	330	3.84	10300
5.67	980	3.74	26530
5.21	6550	3.68	1740
4.72	26000	3.47	760

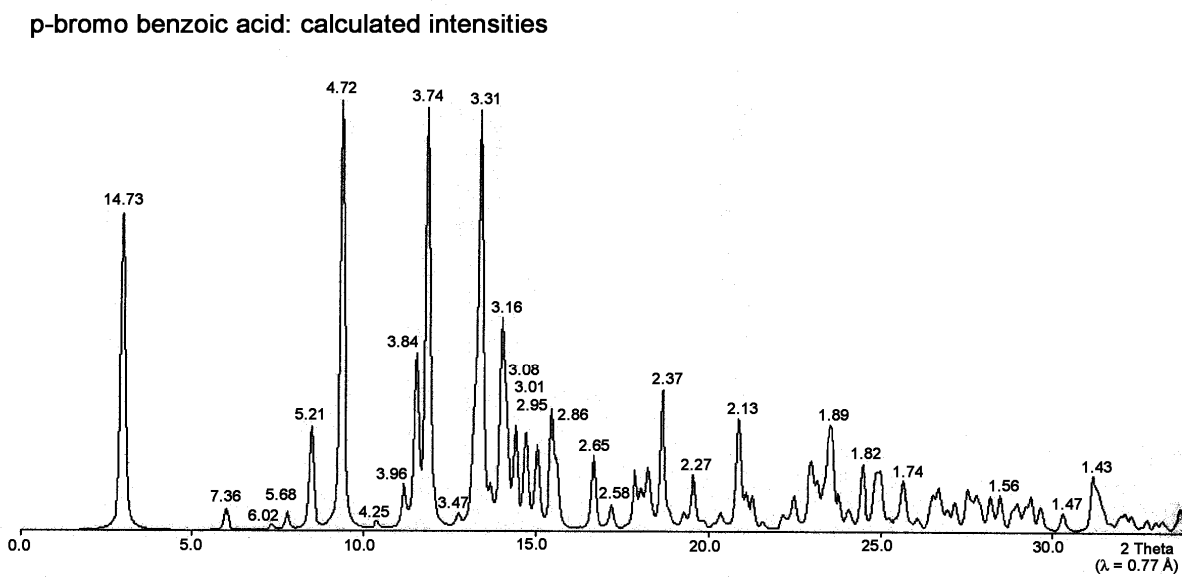

Figure 4. Calculated diffraction pattern of p-bromo benzoic acid. d-spacings are given in Å.

The s-scale for both, the SAXS and the WAXS range, can be obtained by linear regression, i.e., the linear relation between the kown s-values of the calibrant versus the measured peak positions has to be found.

A further correction is regarding the flat field response (efficiency) of the detectors. For this correction, the fluorescence light of various foils are used to illuminate the detectors rather homogeneously:

At 8 keV: iron foil (100 μm thick), fluorescence energy: 6.4 keV K_α, 7.1 keV K_β (effic*.dat)
At 16 keV: copper foil (> 100 μm thick), fluorescence energy: 8.028 keV $K_{\alpha 2}$, 8.048 keV $K_{\alpha 1}$, 8.905 keV K_β (effic*.dat)

The measured scattering pattern are corrected for the detector efficiency simply by dividing them by the fluorescence pattern. Note: The average of the detector efficiency data should be set to unity and a small threshold should be applied to avoid any division by zero.

[1] T.N. Blanton et. al., Powder Diffraction 10, (1995), 91
[2] K. Ohura, S. Kashino, M. Haisa, J. Bull. Chem. Soc. Jpn. 45, (1972), 2651

4. SITE LABORATORIES

In August 2002 our new chemistry and X-ray laboratory went into operation. The 70 m^2 big laboratory is divided in two parts, in which the bigger share of 43 m^2 is occupied by the chemistry lab. This unit serves mainly for sample preparation and analysis for both, in house research and external SAXS user groups. In the X-ray laboratory the set-up of a SWAX camera for simultaneous small and wide angle scattering has been completed (Hecus X-ray Systems, Graz, Austria: www.hecus.at), which allows on-site testing of samples before moving on to the SR beamline. The chemistry lab is meanwhile equipped with:

- micro centrifuge (max. 13200 rpm; model 5415D from Eppendorf , Hamburg, Germany)
- Chemical fume hood, equipped with a carbon filter for general organic solvents (model GS8000 from Strola, Italy)
- vacuum drying oven (min. pressure 1 mbar; max. T: 200 °C, precision +/- 0.4°C; Binder WTB, Tuttlingen. Germany)
- balance (min.-max.: 0.001 - 220g; model 770 from Kern & Sohn, Balingen, Germany)
- Magnetic stirrer with heating plate and thermometer, temp max 260°C
- vortex for microtubes (model MR 3001 and REAX; both from Heidolph, Schwabach, Germany)
- two water baths :
  - Unistat CC, freely programmable in the range from -30 to 100°C (Huber, Offenburg, Germany);
  - Lauda M3, available for heating only (Lauda-Könighofen, Germany)
- ultrasonic bath with water heater (VWR International, Milano, Italy)
- Ultrasonic processor equipped with a 3mm probe (Sonics VCX130, SY-LAB Geräte GmbH, Germany)
- HPLC pump, Pharmacia LKB; working range, 0,01-9,99 ml/min, 0,1-40MPa
- HPLC pump, Gilson 307; working range, 0,010- 5 ml/min, 0,1-60MPa
- three syringe pumps, low pressure; flow rate range, 1µl/hr – 2120 ml/hr
- three syringe pumps, high pressure: P max ~ 60 bar
- three high pressure infusion modules: P max ~ 690 bar

Further, four working benches (one with a water sink), two fridges (+ 4°C) and a separate freezer (- 20 °C), standard glassware, syringes and needles of different sizes, µ-pipettes (10 - 50 - 200 - 1000), as well as some standard chemical reagents (e.g., chloroform, ethanol, methanol); deionized water (milli-RO and ultrapure milli-Q water) is available.

Figure 6.
Typical lab activity: Barbara Sartori loads the centrifuge.

5. AVAILABLE SAMPLE MANIPULATIONS STAGES

1. General

Usually the sample is mounted onto the sample alignment stage which allows the user to place the sample into the beam with a precision of 5µm (resolution: 1µm). In Fig. 7 the ranges for vertical and horizontal alignment as well as the maximum dimensions of the sample holders are given. The maximum weight on the sample stage is limited to 10 kg. In case the envelope dimensions of a sophisticated sample station provided by the users are slightly larger than those given in Fig. 7, the user can ask the beamline responsible for a check up of his space requirements. If it does not fit at all to these specifications, user equipment can also be mounted directly onto the optical table, which allows much larger spatial dimensions.

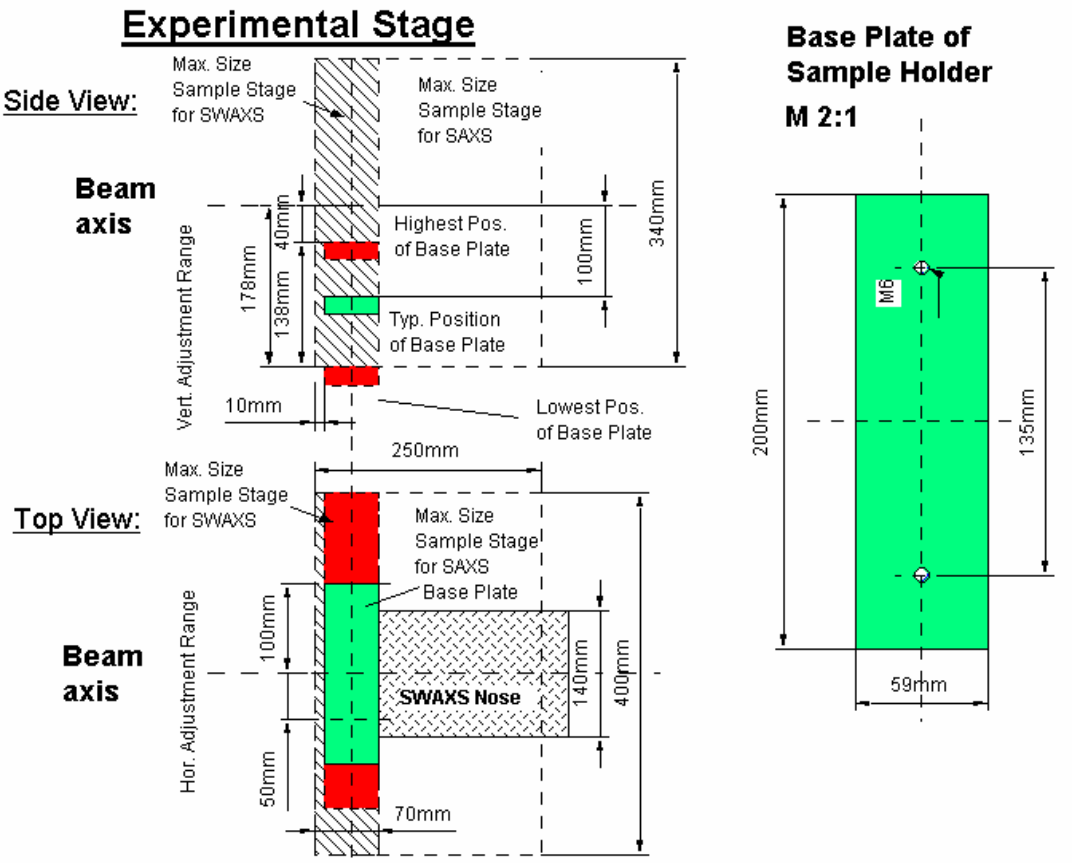

Figure 7. Maximum dimensions and alignment range of the sample holder to be mounted via a base-plate onto the standard alignment stage (left), and dimensions of the base-plate (right).

2. Sample Holders

As standard equipment for liquid samples Paar capillaries (diameter: 1 and 2 mm) are used thermostated with the KHR (electrical heating) or KPR (Peltier heating/cooling) sample holders (Anton Paar, Graz, Austria). For use in these sample holders flow through capillaries and Gel holders are standard equipment. Temperature scans can be performed with KHR (25-300 °C) or KPR (-30-70 °C). Typically the precision and the stability of this systems is 0.1 °C. Additionally thermostats for temperature control or cooling proposes can be used at the beamline (-40 - 200 °C). Helium and Nitrogen gas bottles are available at the beamline, for other gases please contact the beamline responsible.

Multiple-sample holders can be mounted onto the standard sample manipulator. At present holders are available for measuring in automatic mode up to 30 solid samples at ambient temperature or up to 4 liquid or gel samples in the temperature range 0 – 95 °C.

3. Online Exhaust System

At the experimental station is available a custom-built fume cover and chemical exhaust system for toxic gases. Thus it is possible to e.g. study in-situ chemical reactions, during which toxic gases might develop.

4. Stopped Flow Apparatus

A commercial stopped flow apparatus (manufactured by Bio-Logic, Paris, France), especially designed for Synchrotron Radiation SAXS investigations of conformation changes of proteins, nucleic acids and macromolecules, is available. The instrument consists of a 4 syringe cell with 3 mixer modules manufactured by Bio-Logic. Each syringe is driven independently from the others by an individual stepping-motor, which allows a high versatility of the mixing sequence (flow-rate, flow duration, sequential mixing). For example, injection sequences using one or up to 4 syringes, unequal filling of syringes, variable mixing ratio, reaction intermediate ageing in three- or four-syringe mode etc.. The solution flow can be entirely software-controlled via stepping motors, and can stop in a fraction of a millisecond.

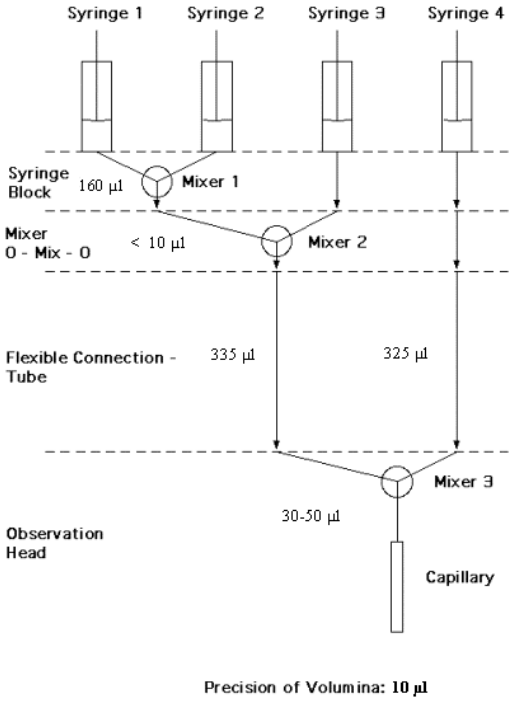

Figure 8. Sketch of the stop flow system.

The software allows the set-up of the shot volumes of each of the 4 syringes in a certain time interval. Up to 20 mixing protocols can be programmed. Additionally macros for the repeated execution of individual frames can be defined. Furthermore, the input and output trigger accessible for user operation can be programmed. In the usual operation modus the start of rapid mixing sequence is triggered from our X-ray data-acquisition system (input trigger).

After the liquids have been rapidly mixed, they are filled within few ms into a 1 mm quartz capillary - situated in the X-ray beam- , which is thermostated with a water bath. Depending on the diffraction power of the sample time resolutions of up to 10 ms can be obtained.

The main parameter of the system are:

- Thermostated quartz capillary (1 mm)
- Temperature stability 0.1 °C
- Total sample used per mixing cycle (shot volume): 100 µl
- Maximum 2θ angle of 45°
- Total Volume 8 ml
- Dead volume 550 µl
- Speed: 0.045 – 6 ml/s
- Duration of flow 1 ms to 9999 ms/Phase
- Dead time: 1 ms
- Reservoir volume: 10 ml each

Further information can be found at the webpage: http://www.bio-logic.fr/

5. Grazing Incidence Small Angle X-ray Scattering

Grazing incidence studies on solid samples, thin film samples or Langmuir-Blodget-films can be performed using a specially designed sample holder, which can be rotated around 2 axes transversal to the beam. Furthermore the sample can be aligned by translating it in both directions transversal to the beam. The precisions are 0.001 deg for the rotations and 5 µm for the translations. Usually the system is set to reflect the beam in the vertical direction. According to the required protocol and the actual assembly of the rotation stages ω, θ, 2θ and φ scans can be performed.

6. Temperature Gradient Cell

A temperature gradient cell for X-ray scattering investigations on the thermal behaviour of soft matter manybody-systems, such as in gels, dispersions and solutions, has been developed. Depending on the adjustment of the temperature gradient in the sample, on the focus size of the X-ray beam and on the translational scanning precision an averaged thermal resolution of a few thousands of a degree can be achieved.

7. Flow-through Cell

The flow through cell works in a simple manner: Special quartz capillaries (Glas Technik & Konstruktion, Schönwalde/Berlin) of 1.5 mm diameter and wide openings of about 3 mm at each end, can be inserted into the standard Anton Paar sample holder, which allows various temperature treatments (T-range 25-300 or –30-70 °C, respectively). Thin tubes are connected directly to the capillary ends and a constanst flow is achieved by a peristaltic pump.

8. IR-Laser T-Jump System for Time-Resolved X-ray Scattering on Aqueous Solutions and Dispersions

The Erbium-Glass Laser available at the SAXS-beamline (Dr. Rapp Optoelektronik, Hamburg, Germany) delivers a maximum of 4 J per 2ms pulse with a wavelength of 1.54 µm onto the sample. The laser-beam is guided by one prism onto the sample, which is filled in a glass capillary (1 or 2 mm in diameter) and Peltier or electronically thermostated in a metal sample holder (A. Paar, Graz, Austria). With a laser spotsize of maximal 7 mm in diameter a sample-volume of maximal 5.5 µl or 22 µl, respectively, is exposed to the laser-radiation. In a water-solutions/dispersions with an absorption coefficient of A = 6.5 cm^{-1} T-jumps up to 20°C are possible.

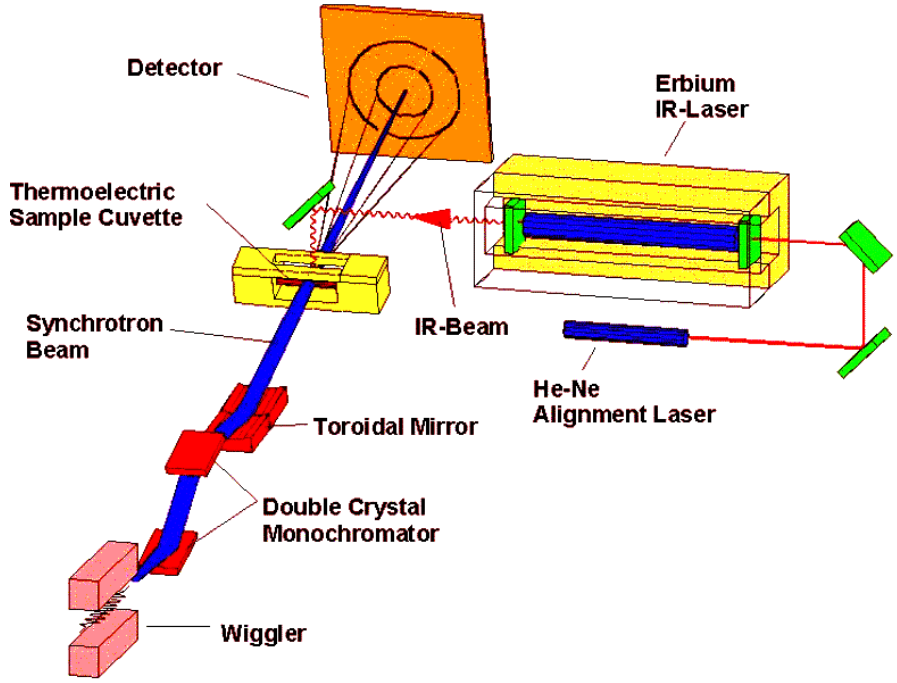

Figure 9. Sketch of the T-jump set-up.

9. High Pressure Cell System

SWAXS measurements of samples under pressure can be performed from 1 to 2500 bar, from 0 to 80 °C in the scattering angle region up to 30 degrees, both in the static or time-resolved mode, e.g. p-jump or p-scan, with a time-resolution down to the ms range. Precise pressure scans of any speed within a broad range (e.g. ca. 1.0 bar/s - 50 bar/s in the case of water as pressurising medium, and a typical sample volume) can be performed. Alternatively, dynamic processes can be studied in pressure-jump relaxation experiments with jump amplitudes up to 2.5 kbar/10ms in both directions (pressurising and depressurising jumps).

In most applications diamond windows of 0.75 mm thickness (each) are used. The transmission of one pair (entrance and exit window) is 0.1 at 8 keV, i.e. lower than 0.3, the value for the originally used 1.5 mm thick Be-windows. However the loss in intensity is more than compensated for by the considerably lower background scattering of diamond thus leading to higher q-resolution in the experiments.

The sample thickness can be 0.6-4.0 mm, with a volume of approximately 0.5-3 mm^3 completely irradiated by pin-hole collimated (< 1.0 mm diameter) X-rays.

The pressure cell system is flexible and can be built according to the needs of the particular experiment. Normally, a liquid (water, ethanol or octanol) is used as pressurising medium.

But in principle, also gaseous media can be employed as well. N_2 has been successfully tested, and measurements in supercritical CO_2 became frequent.
Beside bulk measurements on samples in transmission set-up, also grazing incidence experiments using silicon wafer with highly aligned samples on its surface inserted in the high-pressure cell have been carried out successfully.

10. Oxford Cryostream Cooler

The Cryostream cooler creates a cold environment only a few millimeters from the nozzle position. The temperature and the flow of the nitrogen gas stream is controlled and regulated by a Programmable Temperatur Controller based on an 'in stream' heater and a thermo-sensor before it passes out over the sample.

The system has been especially developed for X-ray crystallography to perform diffraction experiments on e.g. shock frozen bio-crystals. However, the programmable temperature controller allows further implication for SAXS-experiments, e.g., rapid temperature drops in solvents. The design of the Cryostream Cooler facilitates:

- Nitrogen stream temperatures from -190 to 100 °C
- Stability of 0.1 °C,
- Refill without any disturbance of the temperature at the sample
- Temperature ramps can easily be carried out remotely controlled with scan rates up 6 °C/min
- Individual temperature protocols can be cycled
- T-jumps in both directions can be performed by rapid transfer of the sample in a pre-cooled or -heated capillary using an fast syringe driver reaching a minimum temperature of -80 °C. Here, typical scan rates are about 15 °C/sec with a total process time in the order of 10 sec.

Further information can be found at the webpage: http://www.oxfordcryosystems.co.uk/

11. In-line Differential Scanning Calorimeter (DSC)

The in-line micro-calorimeter built by the group of Michel Ollivon (CNRS, Paris, France) allows to take simultaneously time-resolved synchrotron X-ray Diffraction as a function of the Temperature (XRDT) and high sensitivity DSC from the same same sample.
The microcalorimetry and XRDT scans can be performed at any heating rate comprised between 0.1 and 10 °C/min with a 0.01 °C temperature resolution in the range -30/+130 °C. However, maximum cooling rates are T dependent and 10°C/min rates cannot be sustained below 30°C since cooling efficiency is a temperature dependent process. Microcalorimetry scans can be recorded independently, and also simultaniously, of X-ray patterns. The microcalorimeter head can also be used as a temperature controlled sample-holder for X-ray measurements while not recording a microcalorimetry signal. Isothermal microcalorimetry is also possible when a time dependent thermal event such as meta-stable state relaxation or self-evolving reaction, is expected. The sample capillaries have a diameter of 1.5 mm and are filled over a length of 10 mm.

12. The 2D CCD-camera System

The CCD has a 115 mm diameter input phosphor screen made of a gadolinium oxysulphide polycrystalline layer. The screen is coupled by means of a fiber optic to the image intensifier. The image intensifier is coupled again with an additional taper to the CCD itself. The achieved spatial resolution of a pixel is 79 μm for the whole set-up.
The number of pixels is 1024 x 1024 and they can be pinned down to 2 x 2 and 4 x 4. The dynamic range of the CCD is 12 bit. The dark current of the CCD is in the order of 100 ADU (off-set) and the readout noise (read out speed: 10 MHz) is in the order of 6 ADU. (The CCD is cooled by multistage Peltier element for reducing the dark noise.) The intensifier gain is adjustable between 200 and 20000 photons full dynamic range. Typical readout times and exposure times are 150 ms and 100 ms, respectively. The readout times can be reduced down to 100 ms by using the pinning mode of the CCD. Between the frames additional wait times can be programmed e.g. for reducing the radiation damage in the sample or to extend the time for measuring long time processes.
For the external control a TTL trigger signal is provided (active low, when the CCD is accumulating an image), which is used to control the electromagnetic fast shutter of the beamline on one hand. On the other hand this signal can be used also to trigger processes as requested by the user.
The CCD is controlled by Image Pro+, which also includes non too sophisticated data treatment capabilities. The program is featuring a comprehensive set of functions, including:

- flat fielding/background corrections
- enhanced filters and FFT
- calibration utilities (spatial and intensity)
- segmentation and thresholding
- arithmetic logic operations
- various measurements, like surface, intensity, counts, profiles
- advanced macro management

The data are stored in 12 bit – TIFF format. At the present state up to 300 full images (1024 x 1024) can be recorded by the system, but a strict conservation of the timing sequence is maintained only for the first 15 - 17 frames until the RAM memory is full. Afterwards the images are stored in the virtual memory on the hard disk. At present a software development for the CCD readout system is under way to improve the stability of the readout cycles.
For the treatment of the 2D-data the programe FIT2D of Dr. Andy Hammersley is used. It allows to perform both interactive and ‘batch’ data processing. Furthermore FIT2D supports spatial, flat field and background corrections and elevated data-treatment like circular integration, segment integration and similar can be performed (see also the webpage: http://www.esrf.fr/computing /expg/subgroups/data_analysis/FIT2D/index.html).

13. Vantec Detector

The one-dimensional high count rate capable Vantec-1 Detector from BrukerAXS Inc. has an active area of 50 x 16 mm and reaches a spatial resolution of about 50 µm, which is smaller than the resolution obtained by the presently used Gabriel Type Gas detectors. Moreover its new gas amplification principle based on the Microgap technology [1] allows much higher count rates compared to the old system. Now the main limitation is the data acquisition system with its maximum integral count rate of about 1 MHz. In the present data acquisition system HCI (Hecus X-ray Systems, Graz, Austria) the detector has the following performance:

- Minimal time resolution: 11 µs
- Maximum No. of frames: 512 (depending on the no. of channels)
- Maximum integral count rate: 1 MHz

14. Tension Cell

Together with the external user group Schulze-Bauer/Holzapfel the research team constructed a general-purpose tension cell. This particular cell was designed for *in-situ* tensile testing with the particular feature that the sample could be completely immersed in a solvent (e.g. physiological solution), which is of particular interest for the blood vessel or collagen fiber testing. The sample container can be attached to a thermal bath to control the temperature in the range from 5 to 95 ºC. A screw with an appropriate opening for the passage of the X-ray beam can adjust the optical thickness of the sample container continuously and optimize the set-up for different sample geometries.
The fully remote controlled system allows to control not only the fiber extension from 0 to 50 mm, but also it records simultaneously the force signal in the range from 0 to 25 N and as an option the optically determined Video extensometer signal to measure the transversal contraction of the sample.

User Contribution

Material Science

NUCLEATION PROCESS OF NOBELE GOLD NANORODS AND GROWTH OF CdSe AND ZnS NANOPARTICLES

A. Antonello[1], D. Buso[1], A. Martucci[1], and J. Jasieniak[2]

1.) Dipartimento di Ingegneria Meccanica, Settore Materiali Università di Padova
2.) School of Chemistry, University of Melbourne

Introduction

The experiments done on the ELETTRA SAXS facilities have been focused on nucleation and growth of particles in solution. Particularly, gold nanorods kinetic studies under different composition parameters has been performed. In the remaining part of available beam time, CdSe and ZnS has been taken into account.

Experimental set-up

SAXS measurements have been performed on nanoparticles in solution. As far as static measurements were concerned, the solution was poured into a glass capillary. This was then irradiated with the X-ray beam and the scattering pattern was collected by a CCD camera.
For kinetic studies, the capillary was inserted in a flow circuit. The solution was withdrawn from the reaction flask by a peristaltic pump. This set-up, along with the possibility of running SAXS spectra with the desired frequency, allow one to follow the evolution of the particle in solution. In order to correlate with SAXS with UV/Vis absorption spectra, an "ocean optics" spectrophotometer was inserted in the circuit. This basically consists in a cell through which the solution flows. A light beam is brought into the chamber through an optical guide and travels perpendicularly to the liquid flow. The output signal is then driven to an analyser connected to a computer, from which data can be collected. It is then possible to set the instrumentation to collect spectra with a defined frequency. This experimental set-up permits to follow the variation of the system from SAXS data and from absorption data simultaneously.

Outline of experimental work

In the following paragraphs, a brief outline of the performed SAXS experiments will be presented.

Gold nanorods experiments

Measurement of static SAXS spectra have been done on prepared gold nanorods sample of five different aspect ratio. This will allow, along with TEM images, an easier correlation between scattering pattern and nanorods.
Kinetic studies of gold nanorods has been performed with the described experimental set-up.
The synthesis employed was the well known seeded-growth . This consists in injecting an aqueous solution of spherical gold nanocrystal (seed solution) in a aqueous solution containing CTAB and chloroauric acid (growth solution). In this condition the spherical particles grow in a preferential crystallographic direction to give rods.
The aspect ratio of the rods can be tuned in the range of 1,5 to 5 using different concentration of silver nitrate in the growth solution. The kinetic studies has mainly dealt with the tuning of this parameter. So, different concentrations for silver has been taken into account.
- Since the quality and aging of solution is an important parameter, the seed-solution was also monitored for 80 minutes, taking spectra every five minutes.

CdSe and ZnS experiments

As far as CdSe is concerned, the following experiments has been done:
Static measurement of CdSe nanoparticles dispersed in ethanol using two different capping agents: ammino-propanol and ammino-exanol. The purpose is to determine the effectiveness on the degree of dispersion of the particles in solution.

Static measurement of CdSe particles with different known sizes. These experiments will allow a confirm of the information resulting from SAXS spectra interpretation. These and the following experiences has been done using SAXS facilities in the short-camera modality. This set-up condition allow a better resolution in a range of smaller particle sizes.
Kinetic study of CdSe nanocrystal growth in solution. The synthesis consists in injecting a solution containing the selenium precursor into a solution containing the cadmium precursor heated up to 280°C.
This has been done using a heating mantel. Once the injection was performed, the solution was withdrawn by the pump through a copper capillary. This permits the solution to be cooled quickly to room temperature, so stopping the growth of particles before the solution entered the glass capillary. The instrument was set-up to take a spectra every 10 seconds.
The measure was initiated 20 seconds after the injection.
In this case, the "Ocean Optic" spectrophotometer was not use, due to non readily solvable problems with the sealing of pipes connect to this instrument.

Study on ZnS growth in solution

The synthesis was performed at room temperature in aqueous solution. The procedure is analogous to the one reported above for CdSe and consists in the injection of a sulphur precursor containing solution into a zinc containing one.
Since the reaction was supposed to be quite quick, a remote control of the injection was prepared. The procedure of measurement is similar to the one described above.
A spectra was collected every 10 seconds and also in this case the spectrophotometer was not used, because it soon got saturated due to the large concentration of particles achieved in this synthesis.

A detailed SAXS data analysis is still under way, and the results will be combined with results obtained by HRTEM measurement on these nanoparticles.

FORMATION OF GE-NANOCRYSTALS IN SiO_2 MATRIX BY MAGNETRON SPUTTERING AND POST-DEPOSITION THERMAL TREATMENT

U.V. Desnica[1], K. Salamon[2], M. Buljan[1], P. Dubcek[1], N. Radic[1], I.D. Desnica-Frankovic[1], Z. Siketic[1], I. Bogdanovic-Radovic[1], M. Ivanda[1], and S. Bernstorff[3]

1) R. Boskovic Institute, Physics Department, Bijenicka 54, HR-10000 Zagreb, Croatia
2) Institute of Physics, Bijenicka 56, HR-10000 Zagreb, Croatia
3) Sincrotrone Trieste, SS 14 km 163.5, 34012 Basovizza (TS) Italy

Semiconductor materials in the form of quantum dots (QDs) display a significant dependence of electronic, optical and other properties on the size of the nanoparticles [1-2]. Specifically, Ge quantum dots (Ge QDs) embedded in a transparent matrix exhibit intense photo- and electro-luminescence, strong third-order optical nonlinearities and tunable absorption, which are particularly strongly dependent on the nanoparticle size [3]. This enables the tunability of the nano-Ge band-gap over a considerable range of the visible light wavelengths. These physical properties of nano-Ge material makes it suitable for many electronic, optoelectronic and photonic applications, including integrated opto-couplers in micro-systems in biotechnology, etc [1].

Ge QDs were formed in SiO_2 by magnetron sputtering co-deposition in a multisource magnetron sputtering KJLC CMS-18 system, either in the form of thick films (400 nm thick) or as multilayered films containing 20 bi-layers. The substrate was ‹111› Si. Each bi-layer consisted of a layer of co-sputtered mixture of 40% mol Ge and 60% mol SiO_2 ('active layer'), and a layer of pure SiO_2, serving as a spacer between 'active' layers. The deposition temperature, T_d, ranged from room temperature to 700 °C. The as-deposited samples were subsequently thermally annealed for one hour in vacuum up to T_a = 1000 °C.

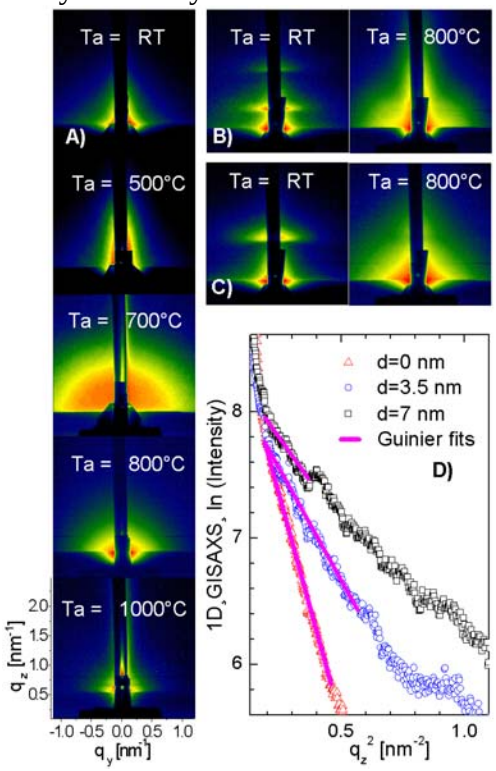

Figure 1: 2D GISAXS patterns from magnetron deposited Ge+SiO_2 layers at RT on ‹111› Si substrate, prior and after annealing at various temperatures, T_a, indicated in each figure. A) (first column): Thick (Ge+SiO_2) film. B) (2. and. 3. pattern in 1. row): Bi+layered films; thicknesses of each of the (Ge+SiO_2) and SiO_2 layers being 7 nm and 7 nm respectively. C) (2. and. 3. pattern in 2. row): Same as B), but thicknesses of each of the (Ge+SiO_2) and SiO_2 layers being 7 nm and 3.5 nm, respectively. D) 1D GISAXS profiles for samples annealed at 800 °C for different thickness of the SiO_2 layer serving as a spacer between (Ge+SiO_2) layers: a) d_{spacer}= 0, b) d_{spacer}= 3.5 nm, c) d_{spacer}= 7 nm.

This report presents few examples of the most interesting results obtained by the Grazing Incidence Small Angle X-ray Scattering (GISAXS) technique in studying the synthesis of Ge GDs, their properties and the self-organization of Ge QDs in SiO_2 after co-deposition at deposition temperature T_d = RT, followed by thermal annealing at T_a = 800°C.

Figure 1 shows 2D GISAXS patterns (for the grazing incidence X-ray beam penetration depth of about 200 nm) from Ge+SiO_2 films deposited at RT on Si substrate and subsequently annealed at the temperature T_a indicated in each pattern. Figure 1A refers to thick films (no spacer layer) while groups B and C refer to Ge+SiO_2/SiO_2 bi-layered films. In both layered films the (Ge+SiO_2) layers were 7 nm thick, while the SiO_2 spacer layers were either 7 nm (group B) or 3.5 nm (group C) thick. The pattern of RT deposited bi-layered films (group B and C) are characterized by "Bragg sheets", reflecting the bi-layered structure of the film. Figure 2D shows one-dimensional (1D) GISAXS profiles of samples annealed at 800 °C, whose 2D patterns are shown in Figs 2A, 2B and 2C. The 1D GISAXS plots were obtained by cross-sectioning the 2D pattern parallel to the z-axis close to the beam-stopper. The average cluster radii, R, as obtained from the Guinier approximation, are shown in Table 1. Obviously the insertion of SiO_2 spacer resulted in a dramatic reduction of the QDs size (steeper slope of ln I(q) versus q^2 dependence), as intended. Already spacers as thin as 3.5 nm, reduce the average radii by ca 50% (from 6.2±0.2 nm to 4.1±0.3 nm). Doubling the thickness of the spacer layer from 3.5 to 7 nm results in just a small further decrease of R. Hence, one can conclude that already a 3.5 nm spacer prevents a large majority of the Ge atoms from neighboring (Ge+SiO_2) layers to participate in the formation of GeQDs in any given (Ge+SiO_2) layer. For a thicker spacer layer (7 nm) the diameter of the Ge QDs is very close to the thickness of the (Ge+SiO_2) layer. It appears that Ge QDs in these (Ge+SiO_2) layers are practically exclusively formed from Ge atoms deposited in the same layer.
Additional results [4] (not shown): Cross-sectional TEM (Transmission Electron Microscopy) confirmed the growth of spherical QDs in parallel layers separated by SiO_2. Raman spectroscopy found that the formed QDs are amorphous Ge aggregates, which crystallize into Ge-QDs after annealing at T_a = 700 °C or higher. Rutherford Back Scattering (RBS) results revealed the successful Ge+SiO_2 deposition in the range RT till 500 °C. For higher T_d sticking of SiO_2 and even more of Ge reduces dramatically in comparison with RT deposition.

Thickness of the spacer layer (nm)	**Radius (nm) after T_a = 800 °C**
0 (thick film)	6.2±0.2
3.5 nm	4.1±0.3
7 nm	3.8±0.4

Table 1. The role of spacer layer on the size of Ge quantum dots formed in SiO_2 matrix:
Average radius of Ge Quantum Dots (in nm) as a function of the thickness of the spacer layers of pure SiO_2 deposited between the 7 nm thick (Ge+SiO_2) layers. All samples were deposited at RT and subsequently annealed at T_a = 800 °C. Except of the thickness of spacer layers all other parameters of the deposition and annealing were the same for all samples.

In conclusion, it has been shown that the insertion of spacer SiO_2 layers between (Ge+SiO_2) layers transforms the 3D growth of Ge QDs into a preferentially 2D growth (separate growth within each thin (Ge+SiO_2) layer). This resulted in a considerably smaller average size of Ge QDs in the layered films for the same T_a. The synthesis of well crystallized, moderately sized, spherical Ge QDs was achieved by post-deposition annealing in the 700-800 °C range.

References:

[1] A. P. Alivsatos, Science 271, 933-937 (1996), R.F. Service, ibid. 929-932
[2] W. Scorupa, L. Rebohle, T. Gebel, Appl. Phys. A 76, 1049-1059 (2003)
[3] C. Boested, T.van Buuren, T.M. Willey, N. Franco, L.J. Terminello,C.Heske, T.Moeller, Appl. Phys. Lett. 84 4065-69 (2004)
[4] U.V. Desnica, K. Salamon, M. Buljan, P. Dubcek, N. Radic, I.D. Desnica-Frankovic, Z. Siketic, I. Bogdanovic-Radovic, M. Ivanda, S. Bernstorff, Superlattices and Microstructures); in print

GISAXS STUDY OF METAL NANOCLUSTERS-SILICA COMPOSITE COATINGS

E.Girardin[1], C.Renghini[2], and G.Albertini[1]

1.) Dipartimento di Fisica e Ingegneria dei Materiali e del Territorio , Universita' Politecnica delle Marche, Via Brecce Bianche, 60131 Ancona, Italy
2.) Dipartimento di Scienze Applicate ai Sistemi Complessi, Università Politecnica delle Marche, Via Brecce Bianche, 60131 Ancona, Italia

Nanocomposite thin films consisting of metal-nanoparticle inclusions embedded in a transparent dielectric matrix have received considerable attention as a promising candidate for future all-optical photonic devices due to their attractive optical properties, large third order optical non linearity and fast time response [1,2]. Such nanocomposite thin film materials are often produced by the co-sputtering method because of its simplicity in process, flexibility in the materials combination and controllability in size distribution. The samples are then annealed to induce nucleation and growth of the clusters. The thermal treatment temperature is chosen in order to obtain clusters of the requested dimensions.
The samples were silica slabs (20x10x1 mm^3) coated by 1 micron of metal (10% vol. Ag, Au, Cu) nanoclusters-silica composites. They were processed by co-sputtering of SiO2 and metal (RF-sputtering), some samples on the substrate heated at 400°C, 600°C and 800°C. After deposition, the samples have been annealed at various temperature, (750°C, 850°C and 950°C for 1 and 3 hours). We expected the nanocluster size to be about 10-50 nanometer.

The GISAXS experiment were carried out on the SAXS beamline, using synchrotron radiation with wavelength λ=0.154 nm (photon energy of 8 KeV). A two dimensional CCD detector with 1024x1024 pixels, positioned perpendicular to the incident beam at a detector to sample distance 1.65 m, was used to record the SAXS intensity. The spot size was 4.8 x 0.25 mm. For each sample, a set of grazing angle of incidence was selected in the range $0.1° < \alpha < 1.140°$.

Results are still under evaluation, but from our first measurements we got indications that heating the substrate before the deposition will decrease the nanocluster size which is, as expected, around 20-50 nanometers. More time is necessary to study the effect of annealing.

References:

[1] P. Chakraborty , J. Mater.Sci.33, (1998) 2235
[2] E.M. Vogel, M.J. Weber, D.M. Krol, Phys. Chem. Glasses 32, (1991) 231

THE INFLUENCE OF POST DEPOSITION PLASMA TREATMENT ON SnO_x STRUCTURAL PROPERTIES

D.Gracin[1], K.Juraic[1], A. Gajovic[1], P. Dubcek[1], I.Djerdj[2], N.Tomasic [3], S.Krajnovic [4], M.Milun [4], and S.Bernstorff[5]

1.) Rudjer Boskovic Institute, Bijenicka 54, 10000 Zagreb, Croatia
2.) Department of Physics, Faculty of Science, University of Zagreb, POB 331, HR-10002 Zagreb, Croatia
3) Faculty of Science, Institute of Mineralogy and Petrography, University of Zagreb, Horvatovac bb, HR-10000 Zagreb, Croatia
4) Institute of Physics, Bijenicka 46, HR-10000 Zagreb, Croatia
5) Sincrotrone Trieste, SS 14, km 163.5, Basovizza (TS), Italy

Typical amorphous silicon solar cells are deposited on glass covered by transparent conductive oxide (TCO). The active layer, amorphous silicon with a thickness of about 0.5 μm, is deposited as p–i–n structure that ends with an Al thin film as back electrode. The TCO as the front electrode has to meet several demands: high optical transmittance, low electrical resistance and a moderate rough surface in order to enable a certain degree of light scattering. The tin-oxide (SnO_x) is widely used as TCO material. In the standard production procedure, the thin Si films are deposited on SnO_x using high frequency discharge in gas mixtures with substantial hydrogen content. In order to study the influence of this kind of plasma on the SnO_x structural properties, 0.7 μm thick SnO_x films deposited on glass are exposed to RF hydrogen plasma, and are then characterized by optical transmittance measurements, X-ray diffraction (XRD Rietveld method), grazing incidence small angle X-ray scattering (GISAXS, SAXS beamline at the synchrotron ELETTRA), scanning electron microscopy (SEM-JEOL T300, operated at 15,) and X-ray photoemission spectroscopy (XPS).

The average layer transmittance after hydrogen plasma treatment is lowered by 10–20% and the spectral distribution of the transmittance is changed indicating that plasma treatment influences the chemical composition as well as the surface morphology. The changes of the morphology are clearly seen on SEM micrographs shown in Fig. 1. The as-deposited film (Fig. 1a) had a uniform appearance on presented magnification (the bars in Fig. 1 correspond to 10 μm). After plasma treatment, there are visible changes in the morphology. The energy dispersive spectroscopy (EDS) analysis of the dark spots in Fig. 1b and analysis by changing the focus of the optical system, show that the dark spots are craters on the surface of the film.

The analysis of the films by XPS spectroscopy (Fig. 2) shows that plasma treatment results in significant changes in the Sn chemistry. As can be seen from the profile analysis (the inert in Fig. 2), after plasma treatment the contribution tin atoms in Sn and SnO related energy states increases on the expense of SnO_2. Combining the results of SEM and XPS, it can be concluded that the hydrogen plasma etched away part of surface layer, most probably through the process of SnO reduction and possibly accompanied with hydride formation.

The recorded XRD patterns of the investigated SnO_x thin films were subsequently refined by the Rietveld method shows that the as-deposited films are nano-crystalline, with a typical average crystallite size between 10 and 40nm and a preferred [2 0 0] orientation. By exposure to hydrogen plasma, the degree of preferential orientation slightly decreases, the average crystal size gets smaller and the micro-strain increases. This indicates that the influence of the plasma treatment, besides of the surface etching, extends into the depth of the samples as well. The increase of strain is most probably due to diffusion of hydrogen into the material along grain boundaries and micro-voids. The changes in crystal sizes and orientation are consistent with the surface etching, as observed by SEM.

GISAXS of as-deposited samples, recorded at the critical angle, (Fig. 3a) indicates nano structures in the shape of non-truncated pyramids on the surface and in the near-surface layer,

whose sizes agree well with those of the nanocrystals observed by XRD. After plasma treatment, their shape close to the surface is greatly rounded and the GISAXS signal becomes isotropic (Fig. 3b), consistent with the observed plasma surface etching. The results of the analysis of shape, individual size and depth distribution of the ‘‘particles’’ (presumably voids) in the material, calculated from GISAXS obtained at various angles are plotted in Fig. 4. The shape is described by the dimensions in two directions, parallel and perpendicular to the surface. The GISAXS angle is represented as the difference between the critical and the actual angle where the zero value corresponds to the surface of the sample while the highest value in Fig. 4 corresponds to a depth of about 0.7 μm below the sample surface. The as-deposited samples (open symbols in Fig. 4) had the voids larger in the direction perpendicular to the surface (‘‘Rg vertical’’, open circles in Fig. 4) than in the direction parallel to the surface (‘‘Rg horizontal’’, open squares in Fig. 4), indicating a columnar structure. After plasma treatment, the average size of the voids in the direction parallel to the surface did not change while in the direction perpendicular to the surface it increased substantially. This increase is also clearly visible for the grazing incident angles well above the critical angle, which means that the changes occurred also deep in the sample.

The GISAXS results, together with the results of the Rietveld analysis, support the assumption that the hydrogen plasma also influences sample layers as deep as 0.7 μm below the surface, possibly through voids associated with the columnar structure of the as grown film.

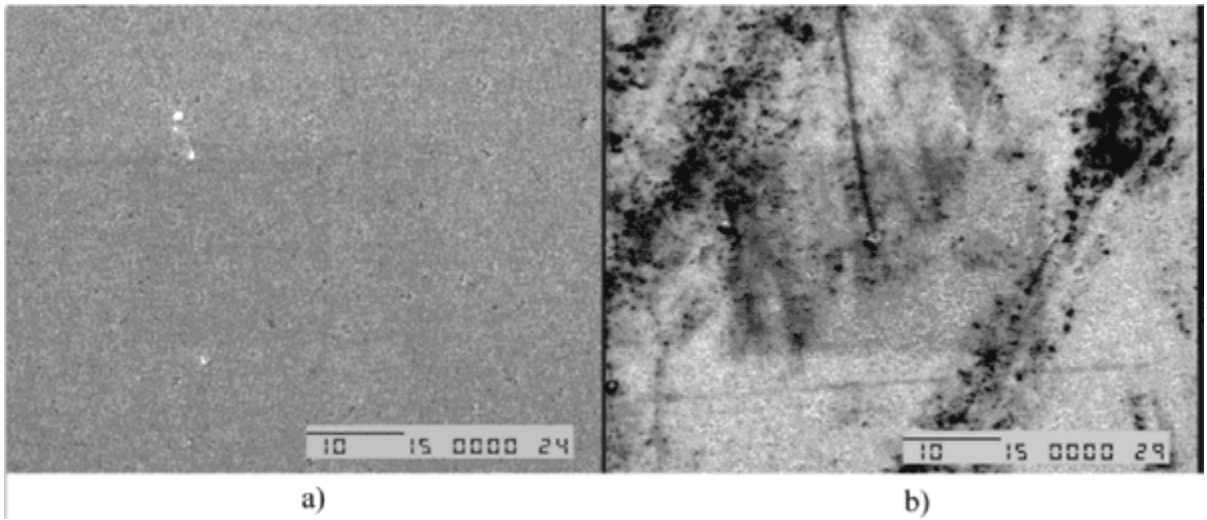

Figure 1. SEM micrographs of SnO_x on glass before (a) and after (b) plasma treatment. The bars correspond to 10 μm.

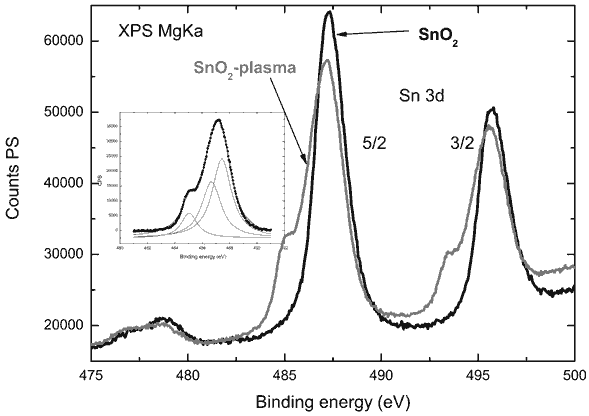

Figure 2. XPS spectra of a SnO_x layer before and after hydrogen plasma treatment. The deconvolution of the spectral line into the three contributions corresponding to Sn, SnO and SnO_2 is plotted in the insert.

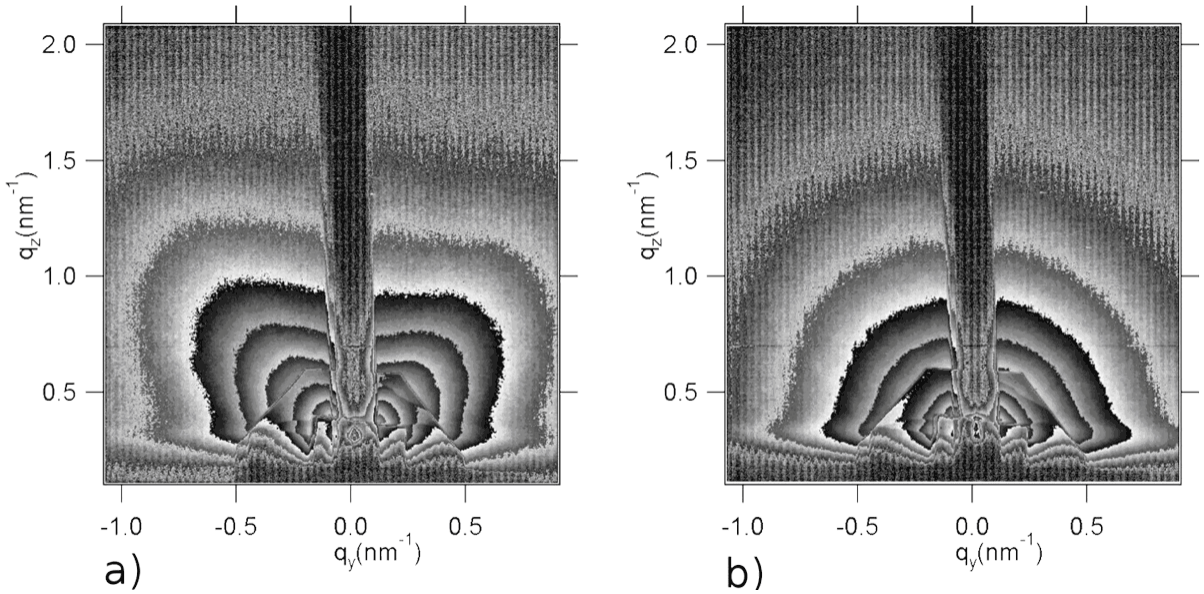

Figure 3. 2D GISAXS pattern before (a) and after (b) plasma treatment.

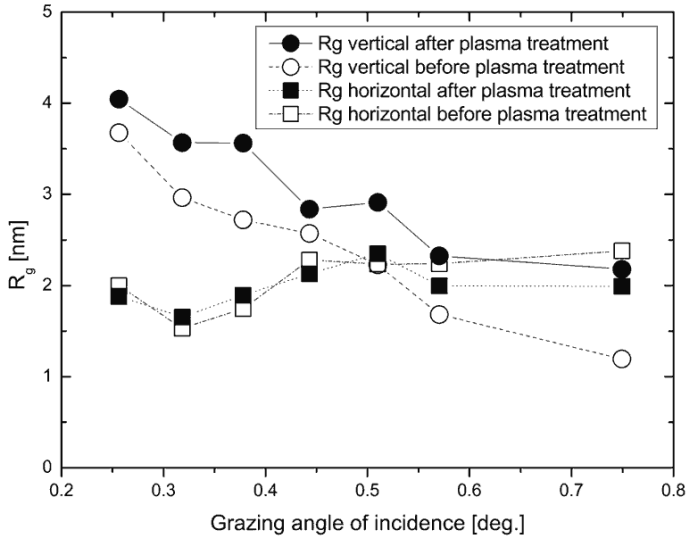

Figure 4. Guinier radius, Rg, vs. grazing angle of incidence for SnO_x before (open symbols) and after (full symbols) hydrogen plasma treatment calculated for the directions perpendicular (''Rg vertical'') and parallel (''Rg horizontal'') to the surface.

References:

[1] D.Gracin, K. Juraić, A. Gajović, P.Dubček, I. Djerdj, N. Tomašić, S. Krajinović, M. Milun, S. Bernstorff, Vacuum 82, 266-269 (2007)
[2] D.Gracin, B.Etlinger, K.Juraic, A.Gajovic, P.Dubcek, S.Bernstorff, Vacuum 82, 205-208 (2007)

STRUCTURAL CHARACTERIZATION OF THIN AMORPHOUS Si FILMS

D. Grozdanić[1], B. Rakvin[2], B. Pivac[2], P. Dubček[2], N. Radić[2], and S. Bernstorff[3]

1.) Faculty of electrical engineering and computing, University of Zagreb, Zagreb, Croatia
2.) R. Bošković Institute, P.O. Box 180, Zagreb, Croatia
3.) Sincrotrone Trieste, SS 14, km 163.5, Basovizza (TS), Italy

The intrinsic morphology of pure amorphous silicon (a-Si) on the nanometric scale has been an intriguing issue for more than two decades. This is mainly due to the fact that the actual morphology depends on several parameters such as: the method of preparation and the thermal history of a particular sample, as well as on many other structural properties [1,2]. It is known that a-Si deposited either by vacuum evaporation or sputtering almost inevitably contains nm-sized voids, which may or may not be connected. The existence of such structures within the a-Si has been confirmed by electron diffraction [3] and has been inferred from clustering of dangling bonds [2]. Still structural changes in a-Si during the course of thermal annealing are not completely characterized especially since the starting structure of a-Si is very much dependent on the preparation conditions.
Different techniques are employed for such studies and one of them – electron paramagnetic resonance (EPR) – describes very well the changes during annealing [4,5].
However, not all unsaturated bonds are paramagnetically active, and therefore we shall complement such information with structural measurements performed with grazing incidence small-angle X-ray scattering (GISAXS). SAXS is a well established technique for the detection of void distribution in a-Si and it has been applied with success to both a-Si and a-Si:H [6,7].

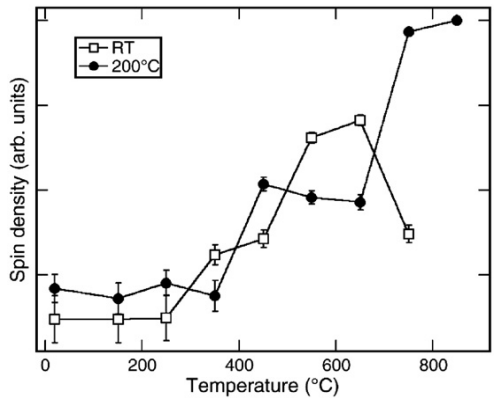

Figure. 1. Spin density versus annealing temperature of a-Si films deposited on substrates held at room temperature (open squares) or at 200°C (black dots), respectively. After deposition, each sample was divided into several pieces, which were then annealed each at only one fix temperature for 1h in vacuum. Thus the shown data points were collected on different sample pieces.

Figure 1 shows the variation of the spin density as a function of the annealing temperature for samples deposited either at RT or at 200 °C. As shown in the figure the spin density does not vary much until about 250 °C for the sample deposited at RT, or until about 350 °C for the sample deposited at 200 °C. For the sample deposited at RT annealing at temperatures above 250 °C produced a monotone increase in the spin density which passes through a maximum for annealing between 600 and 700 °C where it decreases again. On the other hand the spin density for the sample deposited at 200 °C increases strongly for annealing temperatures in the range 350–450 °C. Then it decreases slightly until about 650 °C, after which it increases again strongly for higher temperatures. A similar behavior was observed by Brodsky et al. [8], and they explained their results with cracking of newly formed crystals. Due to the specific method of deposition, i.e. magnetron sputtering, it is very likely that our material is loaded with voids that might coalesce at higher temperatures. In order to verify this behavior of film inhomogeneity we have employed GISAXS.

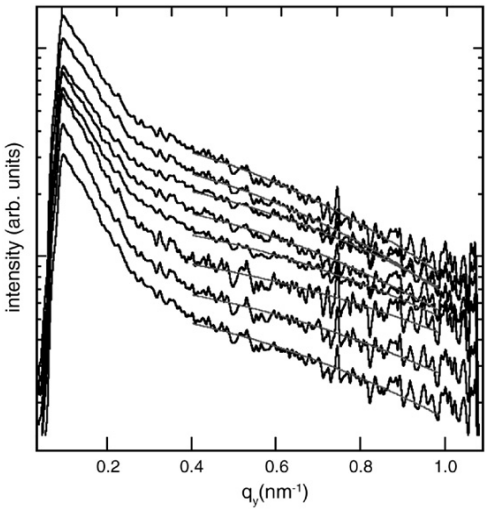

Figure 2. 1D intensity cuts taken from two dimensional scattering patterns for samples sputtered at room temperature, and annealed at a fix temperature of RT, 150, 250, 350, 450, 550, 650, and 750°C (from bottom to top).

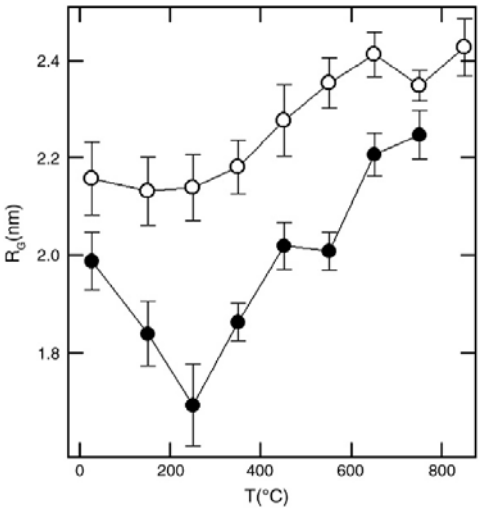

Figure 3. Guinier radius of inhomogeneities vs. annealing temperature for the samples sputter deposited at room temperature (empty circles) or at 200ºC (full circles).

Figure 2 shows GISAXS scans which were obtained from a complete series of samples (produced by sputtering on a substrate held at room temperature, and subsequent annealing in vacuum of the different sample pieces at different, fix temperatures in the range RT (for the lowest curve) up to 750 °C (highest curve). The intensities for q_y=0.3 nm^{-1} have been used to determine the sizes of the inhomogeneities by curve fitting. The so obtained results for both sample series (i.e. with substrates held at room temperature or at 200 °C during sputtering of the layers) are displayed in Fig. 3. In the case of the samples sputtered at room temperature, the typical size of the inhomogeneities decreases with annealing temperature up to 150 °C, where this trend is reversed, and the size increases up to 2.4 nm at the highest annealing temperature. For the sample sputtered at 200 °C, the sizes are smaller but the temperature behavior is similar. The inhomogeneities size is significantly reduced upon annealing to 250 °C, and above this temperature it increases with annealing temperature, showing a small dip at about 550 °C. These results are in good agreement with the variation of the spin density as a function of the annealing temperature (compare Fig. 3 to Fig. 1). Our GISAXS results on annealed samples have shown that upon annealing up to about 250 °C, the a-Si structure relaxes and thus produces a reduction in void size. However, upon annealing at higher temperatures voids grow or coalesce forming larger ones supported very likely by nanocrystal growth. We have shown that the results of both techniques correlate very well. This correlation we understand in the way that a number of voids present in the a-Si matrix relaxed this matrix so that the dominant contribution of the dangling bonds comes from the void region.

References

[1] S. Roorda, W.C. Sinke, J.M. Poate, D.C. Jacobson, S. Drierker, B.S. Dennis, D.J. Eaglesham, F. Spapen, P. Fuoss, Phys. Rev., B 44 3702 (1991).
[2] D.L. Williamson, S. Roorda, M. Chicoine, R. Tabti, P.A. Stolk, S. Acco, F. Saris, Appl. Phys. Lett. 67 226 (1995).
[3] S.C. Moss, J.F. Graczyk, Phys. Rev. Lett. 23 1167 (1969).
[4] P.A. Thomas, M.H. Brodsky, D. Kaplan, D. Lepine, Phys. Rev., B 18 3059 (1978).
[5] B. Pivac, B. Rakvin, R. Reitano, Nucl. Instrum. Methods Phys. Res., B Beam Interact. Mater. Atoms 147 132 (1999).
[6] J. Shinar, H. Jia, R. Shinar, Y. Chen, D.L. Williamson, Phys. Rev., B 50 7358 (1994).
[7] P. Dubček, B. Pivac, S. Bernstorff, R. Tonini, F. Corni, G. Ottaviani, Nucl. Instrum. Methods Phys. Res., B Beam Interact. Mater. Atoms 200 110 (2003).
[8] M.H. Brodsky, R.S. Title, K. Weiser, G.D. Pettit, Phys. Rev., B 1 2632 (1970).

ULTRAFAST NUCLEATION AND GROWTH STUDY OF CALCIUM CARBONATE BY SAXS

B. Marmiroli[1], H. Amenitsch[1], M. Rappolt[1], G. Grenci[2], L. Businaro[2], B. Sartori[1], and P. Laggner[1]

1.) Institute of Biophysics and Nanosystem Research, Austrian Academy of Sciences, Schmiedlstraße 6, Graz, Austria
2.) TASC-INFM-CNR at Elettra Synchrotron, S.S. 14 km 163.5, Trieste, Italy

The motivation of our work has been the study of the first stages of crystallization in the sub millisecond (< 100 µs) time regime by SAXS. The desired time resolution has been obtained by using a free jet micromixer [1].
The mixer is based on hydrodynamic focusing: the side flows squeeze the inlet one into a thin stream, and molecules from the side flows rapidly diffuse across the inlet stream. Since in microfluidics only laminar flow is present, mixing is based on diffusion, which can be precisely controlled, and the length scale over which the fluids must diffusively mix is reduced [2]. After mixing, the time evolution of any subsequent reaction is separated spatially in the steady-state flow. The time resolution is reached by scanning along the free jet after the mixing and probing therefore different residence times. Time resolution is determined by the flow speed.
A free jet system has been selected to overcome the fouling on the walls and circumvent background scattering from the walls.

Previous studies of the scattering of the Calcium Carbonate reaction through a mechanically fabricated cross channel device with triangle cross section 100 µm high, 200µm wide, showed that no reaction was detected. There is thus the need of micromixers of smaller dimensions. We therefore decided to design and fabricate a custom made microfluidic device.

To design the mixer, flow simulation has been conducted with a commercially available code. The resulting geometry presents a length of the channel after focusing of 500 µm, a width of 10 µm, an exit nozzle 8 µm wide, a minimum width of 6 µm and a depth of the channels of 100 µm. The free jet has a speed of 10 m/s at the nozzle exit.

The geometrical parameters of the device are very stringent, so the micromixer has been fabricated by Deep X-ray Lithography (DXRL), which is a unique technique to obtain high aspect ratio microstructures [3].

The focusing effect has been investigated by injecting fluorescein with a concentration of 1 mM in the central channel at a flow rate of 100 µl/min and water in the side channels at the same flow rate. These are not the operating conditions of the device during the chemical reaction, as the ratio of the side flow to the central one and the speed of the jet at the exit are lower. Anyway, these conditions are better for the visualization of the structure of the hydrodynamic focusing (as shown in figure 1). The fluid paths are in line with the one predicted by simulations [3].
Then, the nucleation and growth of calcium carbonate has been studied by synchrotron SAXS. Results show that the chemical reaction is detectable (figure 2) and the time of the first accessible measurement can reach 49 µs.

This experiment demonstrates that the microfabricated rapid mixer with a free jet is a useful tool for studying the evolution of ultrafast chemical reactions, opening a wide field of investigation from both the chemical and the biological point of view.
We now intend to conduct more tests to determine the evolution of the chemical reaction and to apply simultaneous WAXS detection to follow the formation of crystalline polymorphs.

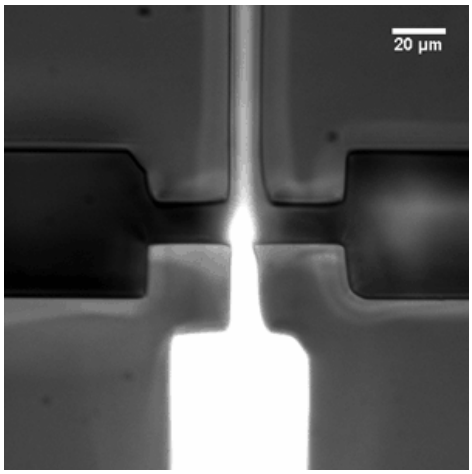

Figure 1 Focusing effect investigated by injecting fluorescein with a concentration of 1 mM in the central channel at a flow rate of 100 µl/min and water in the side channels at the same flow rate.

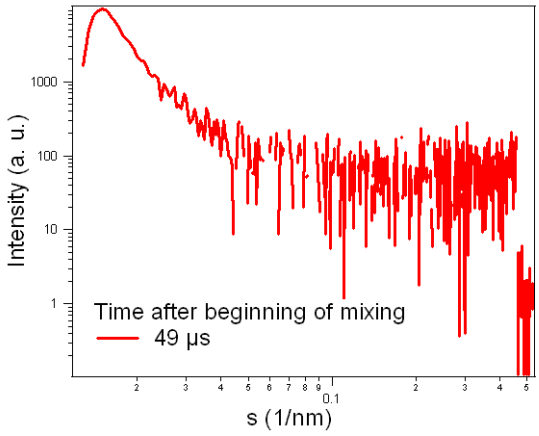

Figure 2 Scattering data of the reaction at the nozzle exit

Acknowledgements

This work has been supported by European Project SAXIER - 011934.

The authors wish to thank: Dr. M. Rappolt and Dr. F. Cacho for useful discussion, Dr. H. Coelfen for advice with the chemical reaction, Dr E. Ferrari for optical imaging, and Dott. G. Birarda and C. Morello for technical support.

References:

[1] H. Haberkorn, D. Franke, T. Frechen, W. Goesele and J.Rieger, Early stages of particle formation in precipitation reactions-quinacridone and boehmite as generic examples, J. Colloid Interf. Sci. 259, 112-126 (2003)

[2] J. B. Knight, A. Vishwanath, J. P. Brody, and R. H. Austin, Phys. Rev. Lett., 1998, 80, 3863

[3] E. W. Becker, W. Ehrfeld, P. Hagmann, A. Maner, and D. Muenchmeyer, Microelectronic Engineering, 1986, 4, 35

[4] B. Marmiroli, G. Grenci, H. Amenitsch ,B. Sartori, A. Gosparini , P. Laggner, L. Businaro, Jet micromixer for studying ultrafast chemical reactions by Small Angle X-ray Scattering,Microfluidics for X-ray Nanoanalytics Symposium, Graz (Austria), 13-14/02/08

THIN FILMS OF COMPLETELY IMMISCIBLE Ag-W SYSTEM

N. Radić[1], P. Dubček[1], M. Ristić[1], S. Musić[1], R. Grötzschel[2], Ž. Skoko[3], and S. Bernstorff[4]

1.) Rudjer Bošković Institute, POB 180, Zagreb, Croatia
2.) Forschungzentrum Rossendorf, Dresden (OT Rossendorf), BR Deutschland
3.) Faculty of Sciences, Zagreb, Croatia
4.) Sincrotrone Trieste, Basovizza (TS), Italy

Thin films of completely immiscible Ag-W system [1,2] have been prepared in a wide range of composition by codeposition of pure silver and pure tungsten sputtered by two independently controlled magnetron sources. The deposition rate onto the substrates (glass, alumina, sapphire, mono-Si) at room temperature was about 20 nm/min, and the final film thickness was about 0,5 μm.
The chemical composition of the prepared films has been determined by the RBS technique. The structure of the prepared films was examined by the XRD, GISAXS and SEM methods. No completely amorphous films have been obtained in the composition range $Ag_{94}W_6$-$Ag_{12}W_{88}$. A supersaturated solid solution Al(W) with fcc structure is formed with <30 at. % W, while a bcc solid solution is formed for higher tungsten content. The SEM analysis reveals a significant variation across the examined composition range: at the fcc crystalline range boundary a densely packed film of rather uniformly sized 20-30 nm particles is sparsely dotted with well-developed crystalline several hundred nanometers large particles. On the W-rich crystalline side the grass-like surface of the film is decorated on top by 20 nm sized particles at about 50-100 nm distance (Fig.1).

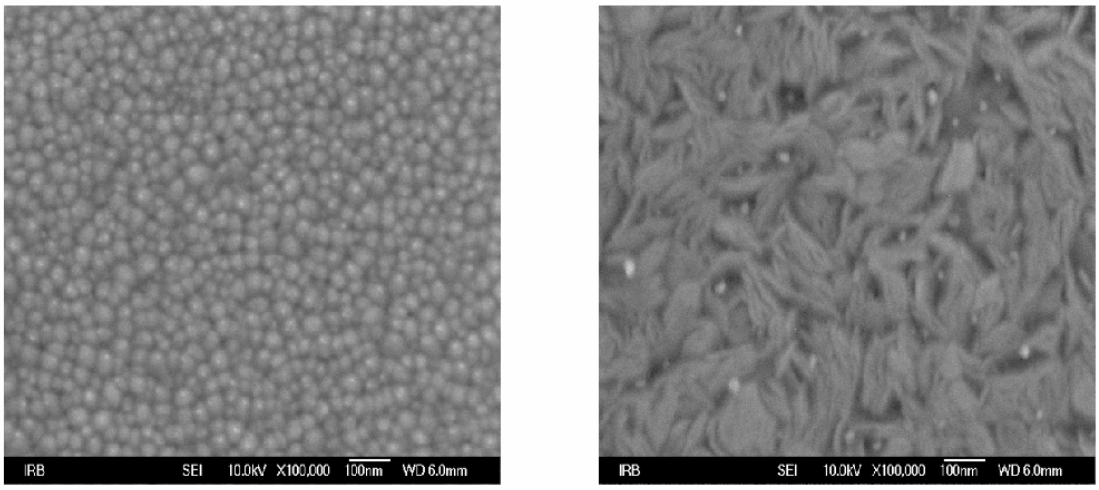

Figure 1. SEM (JEOL JSM-7000F) pictures of AgW and AgW films taken at 100.000 x magnification.

The general trend from the Ag-rich end towards the W-rich end for the bulk/body of the film is a decrease in compactness, while the particles atop the film surface decrease in size from several hundreds of nanometers to about ten nanometers.
The GISAXS measurements have been performed at ELETTRA, at the SAXS beamline, with a X-ray beam energy of 8 keV (λ= 1.54 Å), and employing a 2-dim CCD detector (1024 x 1024 pixels). The 2-dim scattering contours (Fig.2) were analyzed by taking horizontal (along q_z = 1.20 nm^{-1}) and vertical (q_y = -0.08 nm^{-1}) cuts vs scattering angle.

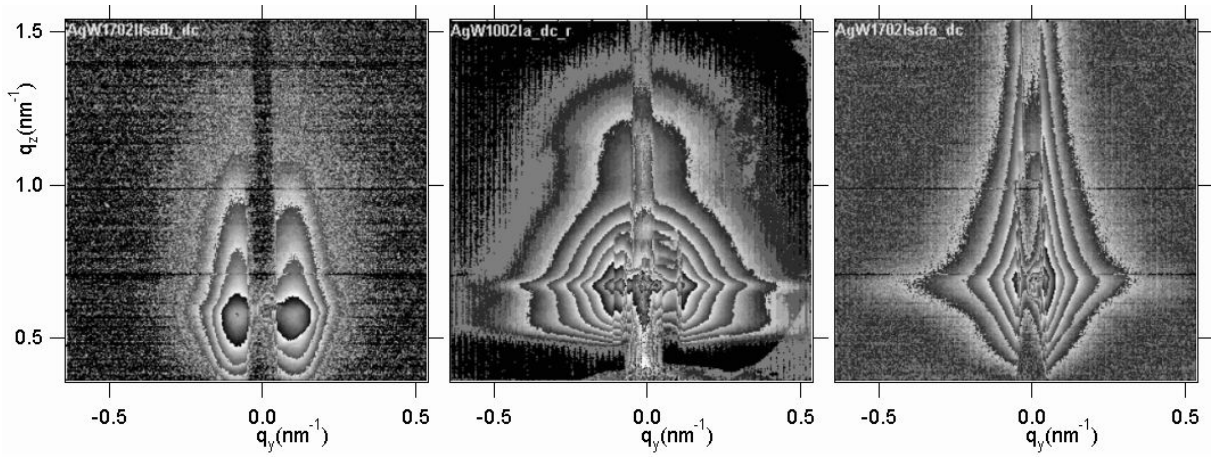

Figure 2. The 2-dim scattering intensity for $Ag_{95}W_5$, $Ag_{55}W_{45}$ and $Ag_{12}W_{88}$ thin films, respectively.

Apart from the Porod (q^{-4}) type scattering above about $q_z = 1.2nm^{-1}$ (coming from the contrast between the disordered part and nanocrystals that are embedded in the film), there is a particle-like scattering at the smaller angles. The Guinier approximation was used in order to obtain the typical sizes of the inhomogeneities as a function of composition for both directions of the scattering.

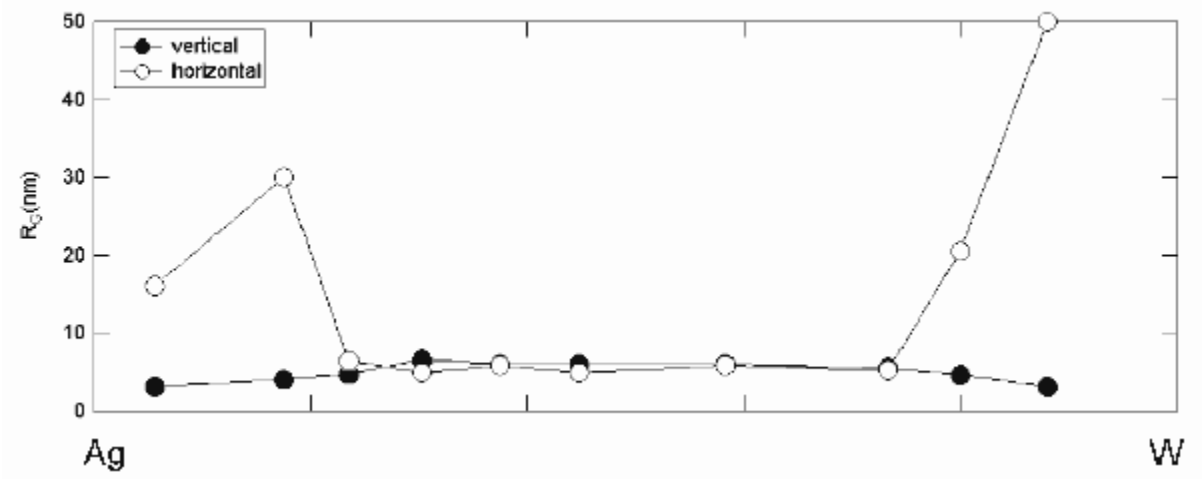

Figure 3. Size of the inhomogeneities in the Ag-W thin films: R_G was derived from GISAXS patterns for two directions of 1-dim cut: vertical (●), and horizontal (O).

The results are presented in Fig.3. As seen, at both ends of the phase diagram platelet-like inhomogeneities are observed. However, in the nanocrystallinity range of Ag-W thin films, the GISAXS results refer to the isotropic inhomogeneities in electron density of about a few nm in size, presumably corresponding to the intercrystalline matter/voids.

References:

[1] R.F. Zhang, Y.X. Shen, H.R. Gong, L.T. Kong, and B.X. Liu. J. Phys. Soc. Jpn. 73, 2023 (2004)
[2] X. D. Dai, J. H. Li, H. B. Guo, and B. X. Liu. J. Appl. Phys. 101, 063512 2007

INVESTIGATION OF STACKING FAULTS IN SEVERELY PLASTICALLY DEFORMED (SPD) METALS BY IN-SITU SYNCHROTRON WAXS, PART I: FACE CENTERED CUBIC METALS (FCC)

E. Schafler[1], M. Kerber[1], A. Wieczorek[1], G. Ribárik[2], T. Ungàr[2], S. Bernstorff[3], and M. J. Zehetbauer[1]

1.) Institute of Materials Physics, University of Vienna, A-1090 Vienna, Austria
2.) Department of General Physics, Eötvös University Budapest, H-1518 Budapest, Hungary
3.) Sincrotrone ELETTRA, Basovizza, I-34012 Trieste, Italy

The specially designed micro-tensile testing machine enabled the mounting of very small samples (see Figure 1) prepared from High Pressure Torsion (HPT) billets of 8 or 10mm in diameter and about 1mm in thickness. For the acquisition of up to 6 reflections the new detector system of the type INEL CPS590 covering a 2theta-range of 90° has been employed. By this means several problems with the background correction occurring when single profiles are measured using several single position sensitive detectors have been avoided. One session with 15 shifts were used to set up and perform this investigation. At first different samples of Cu and Ni which have been subjected to different degrees of deformation by HPT, in order to produce different states of the microstructure, have been investigated by X-ray diffraction only statically (without additional tensile deformation). It was possible to find the optimum experimental setup and this has been used to characterize the initial microstructural state carefully. Selected samples have been subjected to tensile deformation, while in parallel diffraction pattern have been recorded.

The evaluation of the measured data by multiple whole profile analysis for Cu succeeded with initial very interesting results [1]. In Figure 2 the engineering stress is plotted against the engineering strain showing on the one hand the high strength of this material, on the other hand the preserved good ductility. This is very unusual for common polycrystalline materials when decreasing the grain/subgrain size, but it seems to be an unique property of bulk nanostructured materials produced by methods of severy plastic deformation (SPD). So current research interests are focused on the clarification and explanation of this behaviour, the present results are very promising in this respect.

The analysis of the diffraction patterns recorded during short deformation breaks by X-ray Multi-Reflection Profile Analysis (MXPA) revealed a reduction of the coherently scattering domain size from about 100 nm to 60 nm (see Figure 3). While during additional deformation of conventional materials at cold working conditions the defect density increases, the situation is vice versa in the present case. Figure 3 presents an astonishing result for the dislocation density: during the further deformation of the highly distorted and fragmented material, the dislocation density decreases. The interpretation of this behaviour is difficult and requires further necessary investigations by complementary methods. But not only low-dimensional defects like dislocations contribute to the the deformation of this material: The investigation by the MXPA method yields a considerable quantity of stacking faults (Figure 4) increasing with deformation, whose existence could be observed qualiatively several times in nanostructured materials by transmission electron microscopy (TEM) [2, 3]. These outstanding results with respect to the question of the deformation mechanisms of nanostructured materials will be of high interest and importance for the currently intense discussions in this field.

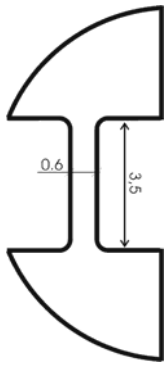

Figure 1. The dimensions of the micro tensile samples.

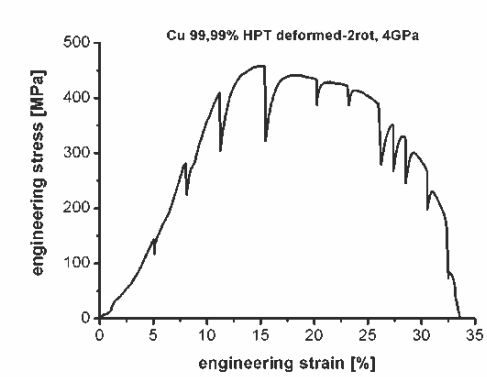

Figure 2. The stress-strain curve (engineering) for HPT Cu.

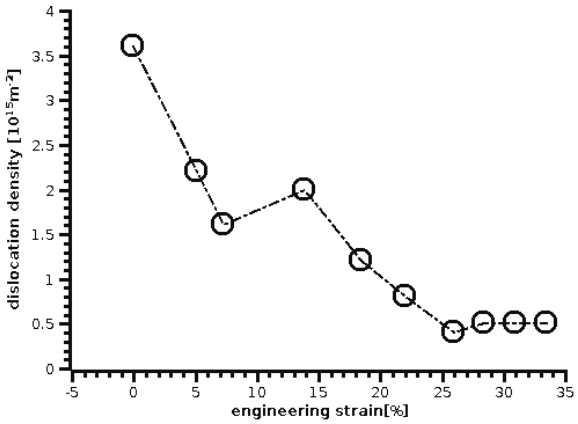

Figure 3. The evolution of the dislocation density with additional tensile straining.

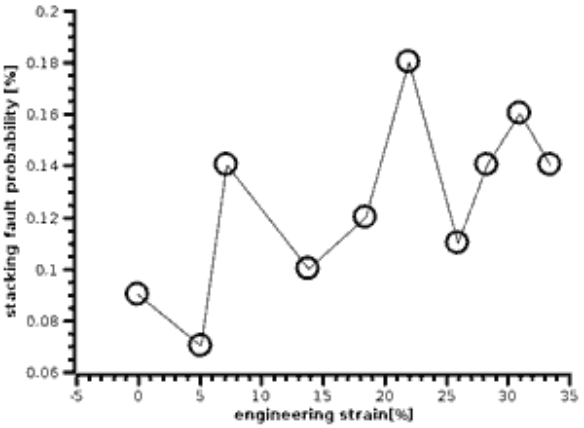

Figure 4. The evolution of the stacking fault probability with additional tensile straining.

References:

[1] M. Kerber, E. Schafler, A. Wieczorek, G. Ribarik, S. Bernstorff, M. Zehetbauer, Symp. Bulk Nanostructured Materials, Aug. 2008, Ufa, Russsia
[2] X. Z. Liao, F. Zhou, E. J. Lavernia, S. G. Srinivasan, M. I. Baskes, D. W. He, Y. T. Zhu, Appl.Phys.Lett. 83 (2003) 632
[3] X. Z. Liao, F. Zhou, E. J. Lavernia, D. W. He and Y. T. Zhu, Appl.Phys.Lett. 83 (2003) 5062

NANOSCALE Ge ISLANDS ON FACETED Si(113) STUDIED BY GRAZING-INCIDENCE SMALL-ANGLE X-RAY SCATTERING

Th. Schmidt[1], M. Speckmann[1], R. Hildebrand[1], S. Bernstorff[2], and J. Falta[1]

1.) Institute of Solid State Physics, University of Bremen, Otto-Hahn-Allee 1, 28359 Bremen, Germany
2.) Sincrotrone Trieste, Strada Statale 14, km 163.5, 34012 Basovizza / Trieste, Italy

Ge quantum dots are of high interest for application in Si based electronic and optoelectronic devices. For instance, it is discussed that the limitations with respect to light emitters, arising from the indirect bandgap of the group IV semiconductors can be overcome in quantum dot structures [1, 2]. Fabrication via self-assembly, though most promising in terms of scalability and mass production, generally does not offer a precise control of the size distribution of the quantum dots, the homogeneity of which, however, plays an important role for technological applications. As we have already shown earlier [3, 4], submonolayer adsorption of Ga on Si(111) leads to a modulation of the surface chemical potential and results in an improved spatial dot-dot correlation and size distribution. An even more pronounced influence of Ga pre-adsorption is found on Si(113). Upon Ga saturation of the Si(113) surface, a well-ordered array of facets with alternating (112) and (115) orientation is found [5]. For subsequent Ge growth, the formation of small Ge islands aligned at these facets has been observed [6]. In the present study, the morphology of such Ge islands is investigated by grazing-incidence small-angle x-ray scattering (GISAXS).

The samples were prepared by molecular beam epitaxy. Ga was deposited on clean Si(113) at 550°C until saturation was achieved and the surface was completely faceted, as monitored by in-situ high-resolution low-energy electron diffraction. Then, Ge was grown at a substrate temperature of 450°C. Fig. 1 (a) shows a typical real-space image obtained by ex-situ scanning electron microscopy (SEM). Corresponding GISAXS patterns are shown in Fig. 2. Owing to surface oxidation at ambient conditions, no clear indication of a regular substrate facet arrangement is observed with GISAXS. However, inclined streaks are found in the data, as pointed out in Fig. 2 (a). Contradicting Friedel's rule, these streaks do not appear symmetrically for $\pm q_{\|}$ and therefore cannot be attributed to a two-dimensional spatial correlation. Instead, they are well explained in terms of crystal truncation rods (CTRs) emerging from the side facets of the Ge islands. This is also confirmed by the dependence on the azimuthal orientation with respect to the incoming beam. If the beam impinges along the [–1,1,0] crystal orientation [Fig. 2 (a)], streaks are found for $q_{\|} < 0$ only, whereas the streaks appear exclusively at $q_{\|} > 0$ when the sample is rotated by 180°, cf. Fig. 2 (c). No streaks are observed for the incoming beam along [3,3,–2], as shown in Fig. 2 (b). For facet CTRs, straight lines are expected which start at the position of the direct beam and extend more or less upwards, with an inclination equal to the tilt angle of the corresponding facets. However, due to x-ray reflection at the surface, the CTR streaks show significant intensity only for an exit angle near the critical angle. Further, x-ray reflection leads to a mirrored streak starting from the position of the specularly reflected beam and extending more or less downwards, with the same above-mentioned inclination. From the observed inclination angle of 30° ± 2° and from the azimuthal orientation, the corresponding facets are identified as (111) facets. Moreover, also the average facet width (perpendicular to [–1,1,0]) can be quantified by GISAXS. From a line profile as indicated in Fig. 2 (d), a streak full width at half maximum is extracted that corresponds to a facet width of $2\pi/\delta q \approx 100$ nm for this sample. It is, of course, intriguing why only one type of side facets appears in the GISAXS patterns. In this respect, the SEM images are instructive, as they reveal the strong asymmetry of the Ge islands. In Fig. 1 (b), a single Ge island is depicted, superimposed by a sketch of the facet arrangement. The

width of the (111) facet along [3,3,–2] is in good agreement with the GISAXS results, therefore the height of this island can be estimated to 55 nm, which in turn implies an inclination angle as large as 80° for the opposite facet. For such steep facets, the related intensity in the GISAXS pattern occurs at much larger q|| and therefore is not visible with the experimental setup chosen here.

The results presented here are very promising for future experiments. In contrast to most microscopy techniques, GISAXS can also be applied to buried structures and will, therefore, shed a light on how the morphology of such Ge islands is affected during silicon overgrowth.

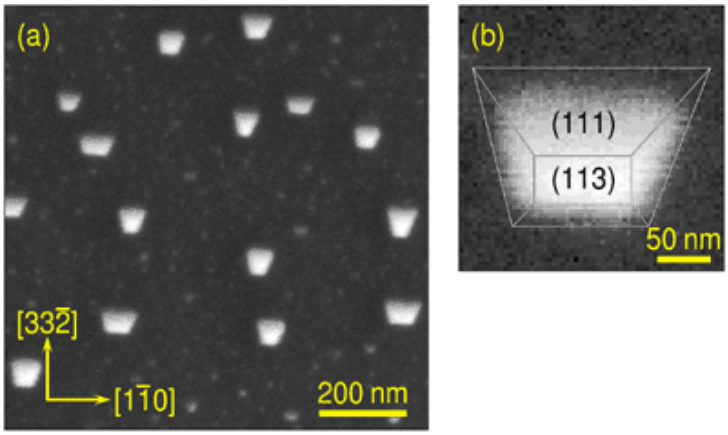

Figure 1. SEM image (a) obtained after Ge growth at 450°C on faceted, Ga-terminated Si(113). An average island is shown at larger magnification in (b), facets are indicated.

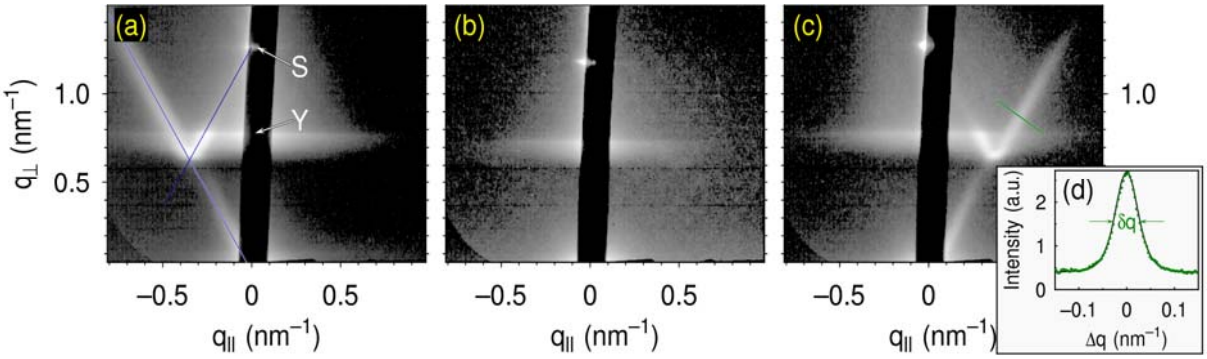

Figure 2. GISAXS patterns obtained from the sample shown in Fig. 1, for different azimuthal orientations of the sample. The incoming beam is parallel to [–1,1,0] (a), [3,3,–2] (b), and [1,–1,0] (c). The center of the detector near $q_{||}$ = 0 was covered with an Al stripe. In image (a), the facet streaks are indicated by thin blue lines. The position of the Yoneda peak (Y) and the specular spot (S) is also indicated. A profile through a facet streak, along the green line in image (c), is shown in plot (d).

References:

[1] G. Abstreiter, P. Schittenhelm, C. Engel, E. Silveira, A. Zrenner, D. Meertens and W. Jäger; Growth and characterization of self-assembled Ge-rich islands on Si; Semicond. Sci. Technol. 11, 1521 (1996)

[2] J. Konle, H. Presting, H. Kibbel, K. Thinke, and R. Sauer; Enhanced performance of silicon based photodetectors using silicon/germanium nanostructures; Sol.-State Electron. 45, 1921 (2001)

[3] Th. Schmidt, S. Gangopadhyay, J. I. Flege, T. Clausen, A. Locatelli, S. Heun, and J. Falta; Self-organized 2D nano-patterns after low-coverage Ga adsorption on Si(111); New J. Phys. 7, 193 (2005)

[4] Th. Schmidt, J.I. Flege, S. Gangopadhyay, T. Clausen, A. Locatelli, S. Heun, and J. Falta; Alignment of Ge nano-islands on Si(111) by Ga-induced substrate self-patterning; Phys. Rev. Lett. 98, 066104 (2007)

[5] T. Clausen, Th. Schmidt, J. I. Flege, J. Falta, A. Locatelli, T. O. Mentes, S. Heun, and F. Z. Guo; Real-time low-energy electron microscopy study of Ga adsorption and facet array formation on Si(113); e-J. Surf.Sci. Nanotech. 3, 379 (2005)

[6] Th. Schmidt, T. Clausen, J. I. Flege, S. Gangopadhyay, A. Locatelli, T. O. Mentes, F. Z. Guo, S. Heun, and J. Falta; Adsorbate induced self-ordering of germanium nano-islands on Si(113); New J. Phys. 9, 392 (2007)

NOVEL IN SITU SET UP TO STUDY AEROSOL AND NANOPARTICLES IN THE GAS PHASE USING SAXS

I. Shyjumon, M. Rappolt, B. Sartori, P. Laggner, and H. Amenitsch

Institute of Biophysics and Nanosystems Research, Austrian Academy of Sciences, Graz, Austria

Materials with ordered and well defined nano-pores are widely used in catalysis, separation process, drug delivery, optics, nano-devices etc [1]. A very promising approach for the synthesis of such mesostructured materials is the evaporation induced self-assembly (EISA) process [2,3], which is based on the surfactant mediated structuring mechanism and highly ordered mesostructured particles can be produced with a few seconds of process time.

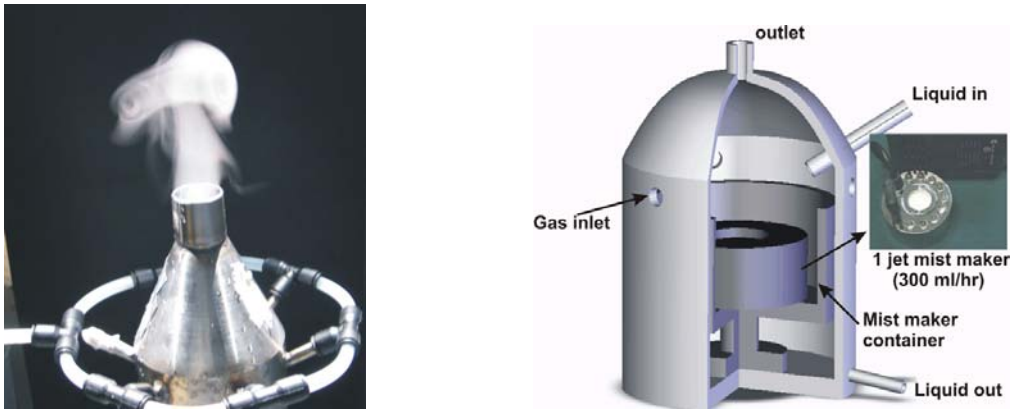

Figure 1: Left – photo of the working fog generator and right -3D schematic of it together with a photo of the mist maker.

For this purpose an in-house built aerosol generator setup for in situ gas phase studies of aerosol and nanoparticles has been constructed [4]. The aerosol generator with an ultrasonic ceramic disk mist maker provides high enough particle concentrations for structural gas phase analysis by synchrotron small angle x-ray scattering (for water ~4×10^8 droplets/ s with a droplet size of ~2.5µm), shown in Fig 1. The working principle was proved by scattering of gold nanoparticles [4]. For evaporation induced self-assembly studies of nanostructured particles, an additional thermal treatment chamber was included in the setup. Following the aerosol generator a quartz tube, 1 m long and 36 mm inner diameter that can be heated up to 300 °C, using a heater tape.

The first on-line gas phase data with our setup for mesostructured silica particles are presented for different thermal treatments, shown in Fig. 2(a) also presented the corresponding shift of the unit cell parameter a at different temperatures in the gas is shown in Fig 2(b). The competition between the rates of evaporation and silica condensation governs mainly the structure and ordering processes. The decay of unit cell parameter a with temperature is due to the core CTAB shrinkage.

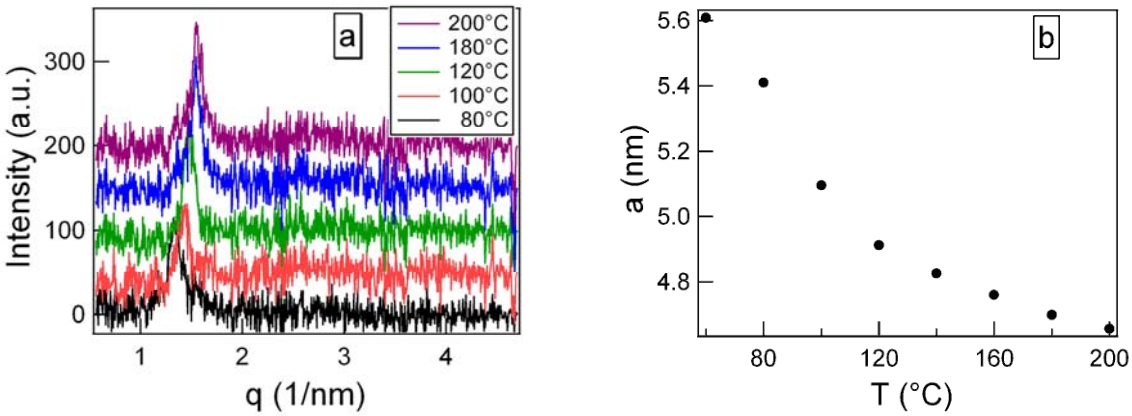

Figure 2. (a) Scattering data (stack plot) of silica aerosol in the gas phase at different temperatures, and (b) the evolution of the unit cell parameter a with temperature.

Scanning electron microscope imaging revealed the average particle size to be ~1 µm. Furthermore, to quantify their internal nanostructure, diffraction experiments of deposited silica aerosols were carried out and the corresponding electron density map indicates a silica wall thickness of about 1 nm (Fig.3).

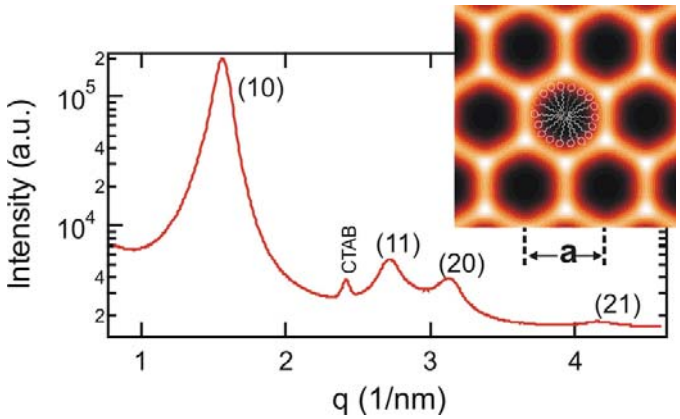

Figure 3. Diffraction data for deposited mesostructured silica aerosol particles. The dryer temperature was 150 °C and the CTAB/Si ratio was 0.14. The (10), (11), (20), and (21) reflections of the hexagonal phase of the silica aerosol are indicated together with the reflection from CTAB crystals. The inset illustrates the corresponding electron density map.

Acknowledgements

The authors wish to thank C. Morello for technical support.

References:

[1] D. Grosso, et al., Chem. Mater., 14, 931 (2002)
[2] Y. F. Lu, H.Y.Fan, A. Stump, T.L. Ward, T. Rieker, and C.J. Brinker, Nature, 398, 223 (1999)
[3] C. Boissiere. et al., Chemical Communications, 2798-2799 (2003)
[4] I.Shyjumon et al., Review of Scientific Instruments, 79, 043905 (2008).

GAS PHASE STUDY OF SILICA AEROSOL MESOSTRUCTURING

I. Shyjumon, M. Rappolt, B. Sartori, P. Laggner, and H.Amenitsch

Institute of Biophysics and Nanosystems Research, Austrian Academy of Sciences, Graz, Austria

Preparation of mesostructured particles in a controlled way find application in high end technology. Such mesostructured materials are prepared by self assembly process of organic and inorganic composites, in which the mesoscopically organized organic part acts as the structure directing agent for the inorganic phase [1].

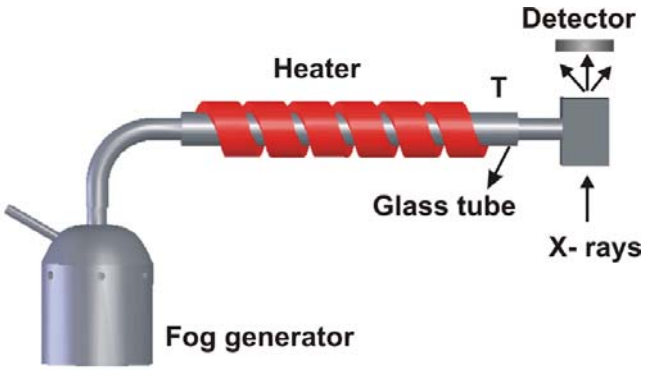

Figure 1. *In situ* set-up for the study of EISA of aerosol particles, schematic.

A new set-up for the EISA study of mesostructured aerosol particles was constructed with a temperature treatment chamber (dryer), shown in Fig.1 [2]. There are different parameters that decide the final mesostructure formed such as the micelle shape, the concentration of the surfactant and the nature of the interaction. Aerosol particles are produced from a precursor solution with TEOS:CTAB:H_2O:HCl (molar ratio 1:0.14:41:0.13) [3].

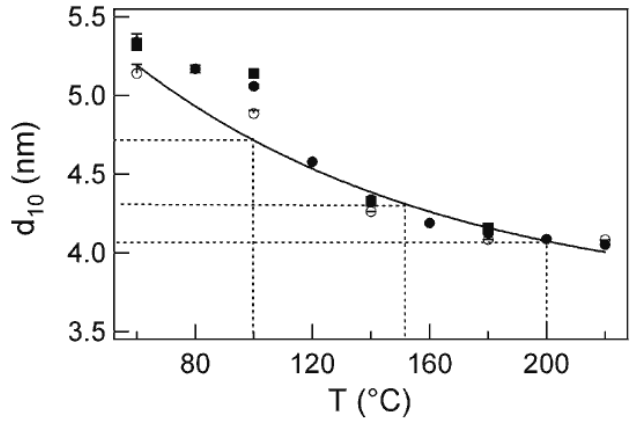

Figure 2. Temperature dependence of d-spacing at different solution aging, ● ~2 hrs, ■ ~7 hrs, ○ ~14 hrs at a flow of 5 SLM.

Gas phase data are recorded at different dryer temperatures at a flow of 5 SLM and the experiments were repeated at different solution aging. Fig. 3 shows the d-spacing shrinkage with dryer temperature in gas phase for data recorded at different solution aging. A pronounced decrease can be seen between 100 to 150 °C, thereafter the slope $\Delta d/\Delta T$ drops below 0.05 Å/°C, whereas little influence on solution aging is observed.

From the deposited particles the diffraction data were obtained and the data was interpreted using a simple two region model, which contains two density regimes with a corona of uniform density. Fig. 3 shows the model fit of the integrated intensities for samples prepared at different dryer temperatures; Table 1 summarizes the results of the fits. It is seen from the fit results that the lattice decrease is due to both the shrinkage of the CTAB core as well as of the Si matrix with temperature.

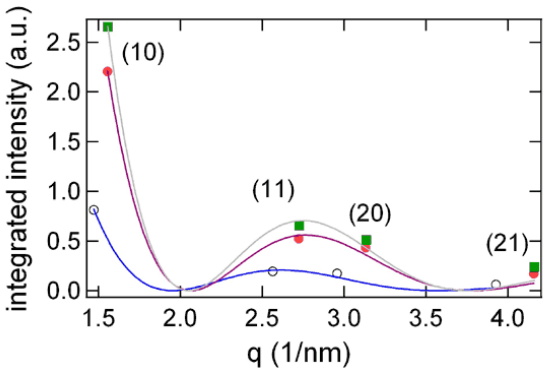

Figure 3. Model fit for the integrated intensities for samples prepared at different dryer temperatures, ○ – 80 °C, ● – 150 °C, ■ – 200 °C.

T (°C)	R1 (nm)	a (nm)	Si matrix (nm)
80	1.96±0.04	4.93±0.01	1.01±0.08
150	1.86±0.04	4.66±0.01	0.95±0.07
200	1.87±0.03	4.66±0.01	0.93±0.07

Table 1. Radius of the core R1, cell parameter a and the silica matrix thickness at different dryer temperatures T, flow rate = 5 SLM, CTAB/TEOS ratio = 0.14.

Acknowledgements

The authors wish to thank C. Morello for technical support.

Reference:

[1] D. Grosso, et al., Chem. Mater., 14, 931 (2002)
[2] I. Shyjumon et al., Review of Scientific Instruments, 79, 043905 (2008)
[3] C. Boissiere et al., Chemical Communications, 2798-2799 (2003)

IN SITU SWAXS STUDY OF SELF-ASSEMBLED PE-PEO BLOCK COPOLYMER IN LIQUID PRECURSOR OF UNSATURATED POLYESTER THERMOSET

C. Sinturel[1], M. Vayer[1], R. Erre[1], and H. Amenitsch[2]

1.) Centre de Recherche sur la Matière Divisée, 1 B rue de la Férollerie, 45071 Orléans Cedex 2, France
2.) Institute of Biophysics and Nanosystems Research, Austrian Academy of Sciences, Schmiedlstr. 6, 8042 Graz, Austria

We have recently reported the preparation of nanostructured polymers obtained from self-organized structures of low molecular weight polyethylene-block-polyethylene oxide block copolymers (EEO, 1400 g.mol^{-1}) dispersed in unsaturated polyester (UP) liquid precursors of thermoset system.[1] From this previous study, we stressed the importance of the curing temperature because uncured system exhibited LCST type behaviour upon heating, with a macro-phase separation occurring at 75°C in the studied range of compositions. Curing at a temperature lower than 75°C prevented macro-phase separation and allowed us to form unusual final morphology, with nanostructures consisting in EEO platelets dispersed in a cured matrix of crosslinked unsaturated polyester network.

In this study, we focus on the behaviour of the non initiated systems that can undergo macro-phase separation upon heating since no crosslinking occur. Particularly, our aim is to carefully investigate the variation of molecular assembly and crystallinity of the block copolymer in the system upon heating, particularly at temperature above 75°C. For this purpose, we perform a set of experiment combining *in situ* SAXS and WAXS time resolved measurements upon heating and cooling of non initiated blends of EEO and UP.[2] Figure 1 presents the typical SWAXS pattern obtained for non initiated blends.

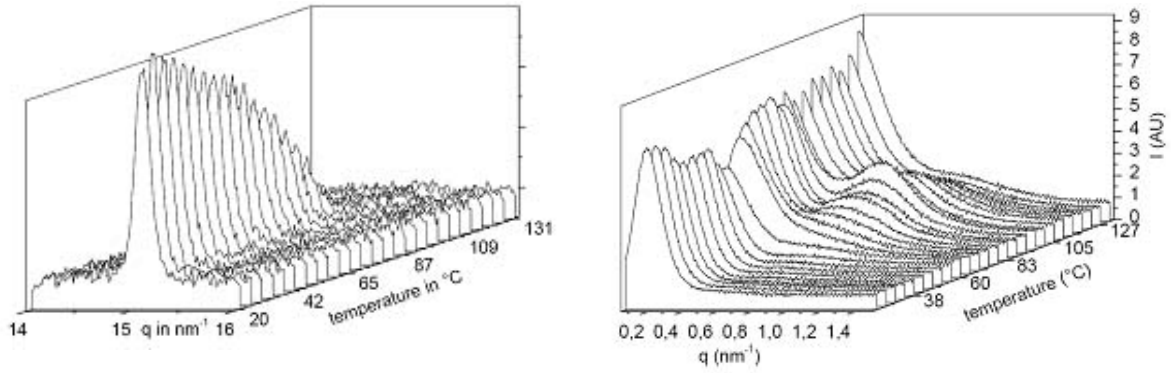

(a) (b)

Figure 1. Typical temperature dependence of the SAXS (a) and WAXS (b) profile of UR/EEO blends (here 80/20) upon heating from RT to 135°C at 5°C/min

In SAXS (Figure 1a) initial pattern is characterised in this case (20% of EEO) by a correlation peak located at 0.20 nm^{-1} (31 nm). As temperature increases, this peak decreases whereas in the meantime, a broader peak appears between 0.40 and 1.20 nm^{-1}, with a maximum at 0.72 nm^{-1} corresponding to 8.7 nm in real space. It can be noticed that this transition towards lower long spacing appears in the temperature range of the macro-phase separation described above. During the phase separation, the system goes from an homogeneous media composed of dispersed EEO platelets towards an heterogeneous system, containing EEO rich domains and UR rich phase. The SAXS results are thus consistent with this transition where aggregations of the platelets are likely to occur, leading to a reduction of the platelets inter-distance.

Initial WAXS diffraction pattern (Figure 1b) clearly exhibits the intense PE(110) diffraction peak at 15.2 nm^{-1}. Upon heating, the PE(110) diffraction peak gradually decreases from 70°C and vanishes at 105°C. It corresponds to the gradual melting of the PE domains, and is confirmed by the in situ DSC traces. It can be seen that the melting of the PE domains (60°C-105°C) coincides with the beginning of the phase separation (75°C). At this temperature, the system thus evolves from lamellae of EEO (with crystalline PE) dispersed in UR towards separated macro domains of EEO rich phase where PE domains gradually melt.

WAXS results can explain the behaviour of the broad scattering peaks around 0.7 nm^{-1} observed in SAXS. Such broad peaks are generally attributed to the correlation hole effect, originating from the molten diblock copolymer in the disorder state.[3] In our case, it can be seen that this peak appears well before the total melting of the PE domains. If the scattering in the final stage (105-130°C) can be indeed interpreted as molten diblock in the disordered state, the scattering in the range 75°C-105°C could be more likely interpreted as intermediate state composed of segregated domains of PE and PEO.

It can be seen from this SWAXS time resolved study that melting of the PE domains and aggregation of the platelets (i.e. macrophase separation) are highly correlated. This can be seen when plotting the integrated scattering intensity of the SAXS profile and the integrated intensity of the PE(110) diffraction peak of the WAXS pattern versus the temperature (figure 2).

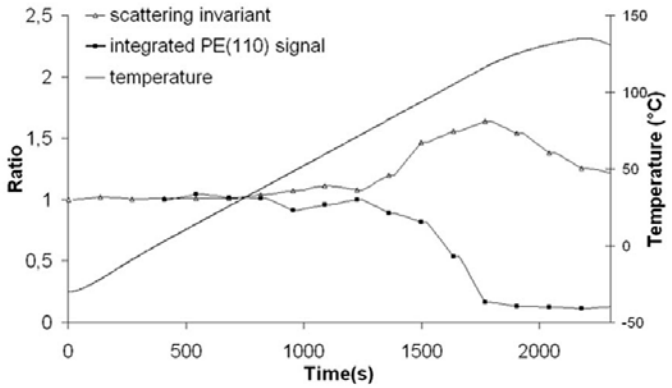

Figure 2. SAXS integrated intensity and PE(110) integrated intensity (ratio over the initial value) for UR/EEO 80/20 blend upon heating from RT to 135°C at 5°C/min

References:

[1] C. Sinturel, M. Vayer , R. Erre, H. Amenitsch; Macromolecules 40, 2532-2538 (2007)
[2] C. Sinturel, M. Vayer , R. Erre, H. Amenitsch; Submitted to polymer
[3] L. Leibler; Macromolecules 13, 1602-1617 (1980)

Life Science

HOW DOES CROSS-BRIDGE ATTACHMENT VARY WITH LOAD DURING SHORTENING AND LENGTHENING?

M.A. Bagni[1], G. Cecchi[1], B. Colombini[1], C.C. Ashley[2], P.J. Griffiths[2], H. Amenitsch[3], and S. Bernstorff[4]

1.) Dipartimento di Scienze, Università degli Studi di Firenze, Viale G.B. Morgagni 63, Firenze, I-50134, Italy 2.) University Laboratory of Physiology, Parks Road, Oxford, OX1 3PT, U.K
3.) Institute of Biophysics and X-ray Structure Research, Austrian Academy of Sciences, SchmiedlstraβE 6, A-8042 Graz, Austria
4.) Sincrotrone Trieste, Area Science Park, Basovizza/TS, I-34012, Italy

The contractile apparatus of skeletal muscle, like all striated muscles, is arranged in a quasi-crystalline lattice which gives rise to a complex spectrum of X-ray reflections. The equatorial reflections, which are aligned perpendicular to the muscle cell axis, have their spacings and intensities determined by the radial distribution of mass within the actin and myosin filament lattice. These filaments are arranged in overlapping lattices and are aligned along the muscle axis. During contraction of the muscle, the S_1 moieties of myosin bind to the actin filament in the overlap region (cross-bridges), and cause filament sliding by tilting of the S1 lever arm domain (the power stroke), accompanied by the hydrolysis of ATP. The direction of sliding, determined by the actin filament polarity, is to increase the degree of filament overlap and to shorten the axial length of the entire actin-myosin filament structural complex (the sarcomere) and hence of the whole muscle. The two most prominent equatorial reflections, 10 and 11, are the most intense in the entire muscle X-ray pattern. Upon S1 binding to actin in an isometric tetanus, 10 intensity (I_{10}) fell to 0.59 of its relaxed intensity, and 11 intensity (I_{11}) increased to 2.23. This intensity reversal is more or less directly proportional to the degree of S1-actin interaction when varied by changes in $[Ca^{2+}]$ [1] or by the pharmacological agent BDM [2] and is a highly sensitive probe of S1 binding. In contrast, neither of these reflections is sensitive to the power stroke event, as shown by the absence of an intensity change in either reflection accompanying the synchronized power stroke which follows a sudden change in muscle load.

In contrast, the meridional reflections, which occur along the axis of the muscle fibre and arise from the axial mass distribution within the sarcomere, are much more sensitive to S1 structural changes than to attachment *per se*. M3 reflection intensity (I_{M3}) is the strongest of all the non-equatorial reflections in the X-ray pattern, and occurs at a spacing equal to the period of the distribution of S1 moieties projecting from the myosin filament. The power stroke induced by either an increase or decrease in muscle load causes a large fall in I_{M3}, explicable if the average S1 axial mass density is maximal during isometric contraction, and net tilting to either pre- or post-power stroke structural sates of S1 causes a decrease in axial mass density [3,4]. It is therefore an important probe of S1 structure.

During contraction, a step change in axial load causes the muscle to shorten or lengthen at a constant velocity according to a well studied parameter of the contractile system, the force-velocity curve. The variation of force with shortening velocity may result either from a reduction in the number of actin-bound S1 or from a decreased load per cross-bridge. Instantaneous stiffness, a measure of S1 attachment, suggests that both effects contribute, but recently it has been shown that stiffness may be an unreliable index of attachment when force is changing because of the unknown contribution and properties of filament compliance. We therefore studied changes in I_{M3}, I_{10} and I_{11} during shortening and lengthening in order to detect changes S1 attachment. Bundles of intact muscle fibres from the interosseal muscles of Rana esculenta were mounted between a motor and a force transducer (sarcomere length 2.2μm by laser diffraction) and tetanised by electrical stimulation at 17Hz at 4°C. During the tetani, either ramp shortening or lengthening was imposed on the bundle by the motor. For shortening, the ramp was preceded by a step release, sufficiently large to immediately drop

tension to its isotonic level at that shortening velocity. Simultaneously, the X-ray pattern was recorded on a 2D CCD detector (camera length 2.65m) during the ramp phase of the length change, and also during the period after the ramp was completed. All intensities were corrected for integrated intensity over the whole pattern to compensate for fluctuations in source intensity, bundle movement in the beam and changes in the length of bundle exposed to X-rays. In addition I_{M3} was corrected for two dimensional broadening in reciprocal space due to the loss of axial alignment of adjacent filaments during contraction.

Shortening data were collected at mean forces of $0.40P_o$, $0.58P_o$ and $0.79P_o$. The corresponding values of I_{11}/I_{10} were 2.23, 1.92 and 2.20. The corresponding isometric values were 0.60 (relaxed) and 2.44 (tetanised). The largest change during shortening was therefore ca. 72% of the change between relaxed and tetanised states, suggesting at most a 28% reduction in cross-bridge attachment. I_{M3} increased to 1.65 fold relaxed intensity during isometric contraction. The corresponding values during shortening were 1.13, 1.02 and 1.78, indicating an 80% intensity reduction at the highest velocity of shortening. This indicates that the fall in force during shortening can be accounted for partially by reduction of cross-bridge numbers evident in I_{11}/I_{10}, but must also entail a change in mean lever tilt from the isometric state to account for the larger I_{M3} change. The power stroke event is approximately exponential in form, with a rate constant of the order of thousands of reciprocal seconds. The highest shortening velocities used in this study were ca. 0.4nm per half sarcomere per second, so a power stroke of 10nm would be diminished by a negligible amount by shortening and cross-bridges should develop full force. But if they remain actin-bound for a substantial time after power stroke completion, the force generated would be discharged by shortening, and S1 tilt would gradually approach its unloaded value, affecting I_{M3} but not I_{11}/I_{10}.

During stretching to achieve a maintained force of $2.12P_o$, I_{11}/I_{10} was 2.59 while I_{M3} was 1.44 fold its relaxed value, a fall of 32% compared to its isometric intensity. The increase in I_{11}/I_{10} is consistent with an 8% increase in actin-bound S1, which would be insufficient to account for the 2.12 fold higher force. Furthermore, the fall in I_{M3} is not consistent with increased cross-bridge formation, but with a change in S1 tilt. After termination of the ramp, force was maintained at $1.62P_o$, while I_{M3} increased to 1.64, close to its isometric value. I_{11}/I_{10} rose to 3.06, suggesting a 34% increase in cross-bridge number above isometric levels. These findings suggest that during the stretch, force enhancement is principally due to an elevated force per cross-bridge and hence in S1 tilt, reflected in the fall in I_{M3}. In contrast, the elevation of force after the stretch was completed seems much better accounted for by an increase in cross-bridge number coupled with a smaller increase in force per cross-bridge. This could occur if stretch extended cross-bridges before detachment to produce a higher average force. If stretch also reduced the detachment rate constant for S1 from actin, new bridges would form with their normal attachment kinetics, while strained bridges would remain attached longer, contributing extra force, but having a smaller effect in total I_{M3}.

References:

[1] L.C. Yu, J.E. Hartt and R.J. Podolsky. Equatorial X-ray intensities and isometric force levels in frog sartorius muscle. J. Mol. Biol. 132, 53-67 (1979)

[2] P.J. Griffiths, M.A. Bagni, B. Colombini, H. Amenitsch, S. Bernstorff, C.C. Ashley and G. Cecchi. Effects of the Number of Actin-Bound S1 and Axial Force on X-Ray Patterns of Intact Skeletal Muscle. Biophys. J., 90, 975-984 (2006)

[3].H.E. Huxley, R.M.Simmons, A.R. Faruqi, M.Kress, J. Bordas, and M.H.J. Koch. Changes in the X-ray reflections from contracting muscle during rapid mechanical transients and their structural implications. J.Mol. Biol., 169, 469-506 (1983)

[4] M. Irving, V. Lombardi, G. Piazzesi and M. Ferenczi. Myosin head movements are synchronous with the elementary force generating process in muscle. Nature, 357, 156-158. (1992)

THE INFLUENCE OF CONCENTRATION AND PH ON THE BOVINE SERUM ALBUMIN STRUCTURE

L.R.S. Barbosa[1,2], M.G. Ortore[2], R. Sinibaldi[2], F. Spinozzi[2], P. Mariani[2], and R. Itri[1]

1.) Instituto de Fisica da Universidade de São Paulo, Rua do Matão Travessa R, 187, São Paulo, Brasil
2.) Dipartimento di Scienze Applicate ai Sistemi Complessi, Università Politecnica delle Marche, Via Brecce Bianche, Ancona, Italy

There is an increasing interest on the study of protein-protein interactions, due to the large amount of fields that this subject is related to. Haemoglobin, for instance, could exceed 300 g/l [1] on living organisms and there are some evidences that the high concentration is responsible to the protein activity. There is also a huge interest in crowded proteins environments due to the development of recombinant proteins as therapeutic agents [1,2]. On the other hand, protein interactions and further aggregation processes are very important in understanding many physiological diseases such as Alzheimer or Kreutzfeld-Jacob and Parkinson diseases, which are caused by protein or peptide association phenomena [3].
Bovine Serum Albumin (BSA) is probably one of the most studied proteins in the last decades. It corresponds to the most abundant protein, accounting for 60% of the total globular protein in blood plasma [4,5], where its concentration can vary from 35 up to 55 mg/ml in the blood plasma [1,4] depending on the species. Its function is associated to the binding and transport of several small molecules such as fatty acids, dyes, metals, as well as several pharmaceutical compounds [4-6]. Despite the large amount of research dealing with the physical-chemical properties of BSA under different conditions, small attention has been paid on pH unfolding as a function of protein concentration. Small Angle X-Ray Scattering (SAXS) technique is a powerful tool to the study of proteins and biopolymers in solution [7,8]. In the present report we show a study concerning the influence of concentration and pH variation on BSA structure and interactions.

Figure 1 shows SAXS experimental intensities with the best fitting curves (solid lines). At pH 2.0 (see Fig. 1A), the protein is partially unfolded, and hence no fit was performed under this condition. All the other scattering curves were analyzed simultaneously via a global fitting process [9]. The protein form factor is kept unaltered in the pH range from 4.0 up to 9.0, regardless the concentration. The protein volume was obtained by the Monte Carlo method on the basis of the protein data bank (PDB) structure of human serum albumine, which is compatible to 90% sequence homology with the BSA.
Concerning the structure factor parameters, we found that the presence of an attractive potential, combined with a repulsive Coulomb term, was necessary to fit the SAXS curves [9-11]. Thus, the fitting parameters of the interaction potential are the protein effective diameter, its surface charge, the attractive potential at contact, *J*, and its range *d* (a better description of this potential can be found elsewhere [9,11]). It was evidenced that the values of *J* were only concentration-dependent and decrease for increasing protein concentrations. This decrease of the attractive potential as a function of protein amount in solution was already previously suggested and it is still a matter of debate [11]. Concerning the parameters related to the repulsion interaction, the fitted protein effective diameter was around 64(2) Å for all pH conditions (from pH 4.0 up to 9.0), in agreement with other studies [11], and the protein surface charges were obtained at each different pH condition. In a pioneer work, Tanford and Buzzel [12] calculated the effective charge on the BSA surface as a function of the pH and ionic strength and their results are in agreement with ours. It is interesting to notice that even at the isoelectric point, the protein could have some residual charge on its surface. This can be due to the binding of salts that composed the buffer [12], such as chloride ions.

In the present work we did not evidence protein structural transitions from pH 4.0 up to 9.0, disproving some previous literature results [4]. Even more interesting is the fact that we are able to provide protein-protein interaction parameters that successfully reproduce the structure factor in the whole investigated pH range and protein concentration condition. Protein surface charges present a satisfactory agreement with previous literature results [12] and the attractive terms show a protein concentration dependence, which may suggest further hypothesis about their physical meaning.

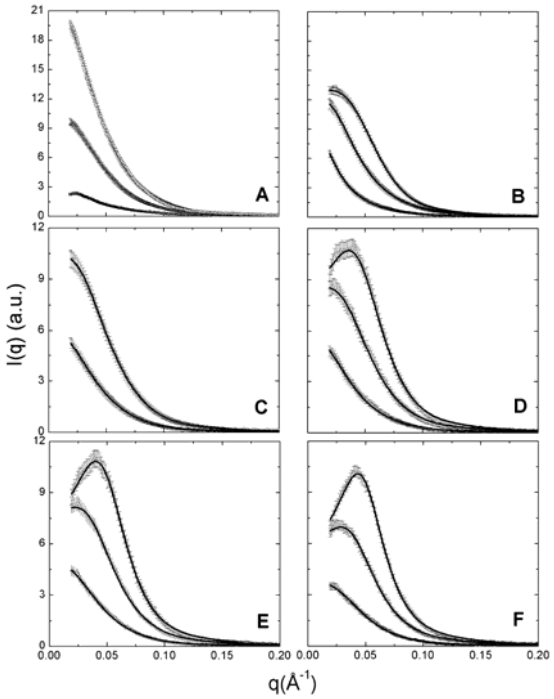

Figure 1. SAXS curves of the systems composed of BSA at 10, 25 and 50 mg/ml at pHs 2.0 (A), 4.0(B), 5.4 (except the one composed of BSA 50 mg/ml, where dimmers formation were evidenced) (C), 7.0(D), 8.0(E) and 9.0(F).

References

[1] J. Guo, N. Harn, A. Robbins, R. Dougherty, C. R. Middaugh,; Stability of helix-rich proteins at high concentrations; Biochem. 45 - 8686 – 8696 (2006)

[2] S. J. Shire, Z. Shahrokh, J. Liu; Challenges in the development of high protein concentration formulation. J Pharm Sci. 93 - 1390-1402 (2004)

[3] F. Chiti and C. M. Dobson; Protein misfolding, functional amyloid, and human disease Annual Reviwe on Biochem. ; 75 - 333-366 (2006)

[4] T. Peters Jr, All about albumins: biochemistry, genetics and medical applications. San Diego, 1996.

[5] D. C. Carter, J. X. Ho; Structure of serum albumin. Adv. Protein Chem., 45 - 153 – 203 (1994)

[6] S. Curry, H. Mandelkow, P. Brick, and N. Franks; Crystal structure of human serum albumin complexed with fatty acid. Nat. Struct. Biol. 5 - 827 (1998)

[7] D. I. Svergun, V. Petokhov; Analysis of X-ray and neutron scattering from biomacromolecular solutions. Curr Opin in Struct Bio. 17 - 562-571 (2007)

[8] J. Trewhella; Insights into biomolecular function from small-angle scattering. Curr. Opin. Struct. Biol. 7 - 702–708 (1997)

[9] R. Sinibaldi, M. G. Ortore, F. Spinozzi, S. Funari de Souza, J. Teixeira, P. Mariani, P; SANS/SAXS study of the BSA solvation properties in aqueous urea solutions via a global fit approach. European Biophysics Journal; DOI 10.1007/s00249-008-0306-z (2008)

[10] J. Narayanan and X. Y. Liu, Protein interactions in undersaturated and supersaturated solutions: A study using light and X-ray scattering; Biophys. J. 84, 523 (2003)

[11] F. Zhang, M. W. A. Skoda, R. M. J. Jacobs, R. A. Martin, C. M. Martin, F. Schreiber; Protein interactions studied by SAXS: Effect of ionic strength and protein concentration for BSA in aqueous solutions Journal of Physical Chemistry B 111 -. 251-259 (2007)

[12] C. Tanford, and J. G. Buzzel; The viscosity of aqueous solutions of bovine serum albumin between pH 4.3 and 10.5. J. Phys. Chem. 60 - 225-231 (1956)

EFFECT OF CERAMIDE ON STRUCTURE AND FLUCTUATIONS IN TERNARY LIPID MODEL-SYSTEMS

B. Boulgaropoulos, P. Laggner, and G. Pabst

1.) Institute of Biophysics and Nanosystems Research, Austrian Academy of Sciences, Graz, Austria

Sphingomyelin (1-O-phosphorylcholine-2-N-acylsphingosine) is a major lipid component of eukaryotic membranes. Like all sphingolipids, sphingomyelin is characterized by an amide linkage between the sphingosine and a fatty acid moiety. It can be enzymatically hydrolized to phosphocholine and ceramide, which has gained much attention as an important signaling molecule in vital cell processes such as apoptosis (programmed cell death), differentiation and senescence. [1-3].

Applying synchrotron small angle X-ray scattering (SAXS) we have studied the global structural and elastic properties of dioleoyl phosphatidylcholine (DOPC)/egg sphingomyelin (SM)/cholesterol(chol) mixtures, substituting SM gradually for ceramide (cer). The ceramide content of the system was increased from 0 to 10 mol% ceramide. The lipid model systems were studied as a function of temperature (Temperature scans from 20 to 50°C) under physiologically relevant conditions.

The SAXS patterns were analyzed by applying a full q-range model [4], from which the lamellar repeat distance, the bilayer thickness, the bilayer separation and the fluctuation parameter were calculated.

Increasing ceramide concentration [T = const.] leads on average to an increased lamellar repeat distance, an increase of the bilayer thickness, whereas the bilayer separation and the membrane flexibility stay constant. With increasing temperature the lamellar repeat distances increases for all ceramide concentrations.

Our studies show, that ceramide induces order in the lipid model system, even at low concentrations.

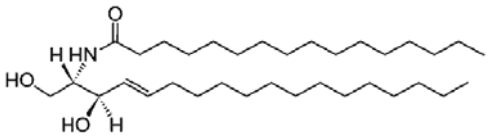

Figure 1. Molecular structure of N-Palmitoyl-D-erythro-Sphingosine (C16:0 Ceramide)

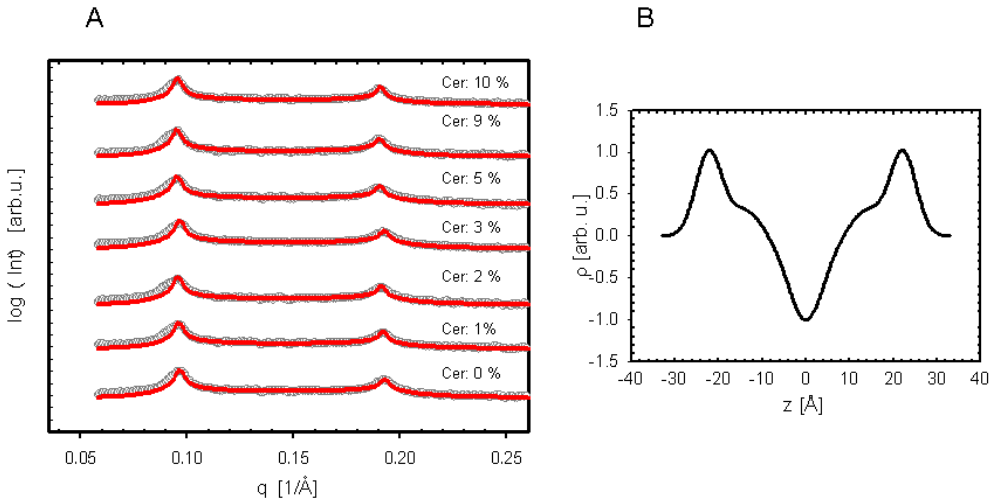

Figure 2. A: X-ray scattering patterns of DOPC/SM:Cer/Chol with fits (solid red lines), temperature: 37 °C, ceramide concentration: 0-10 mol % and B: calculated electron density profile of DOPC/SM:Cer/Chol (Temperature: 37 °C, ceramide concentration: 5 mol %).

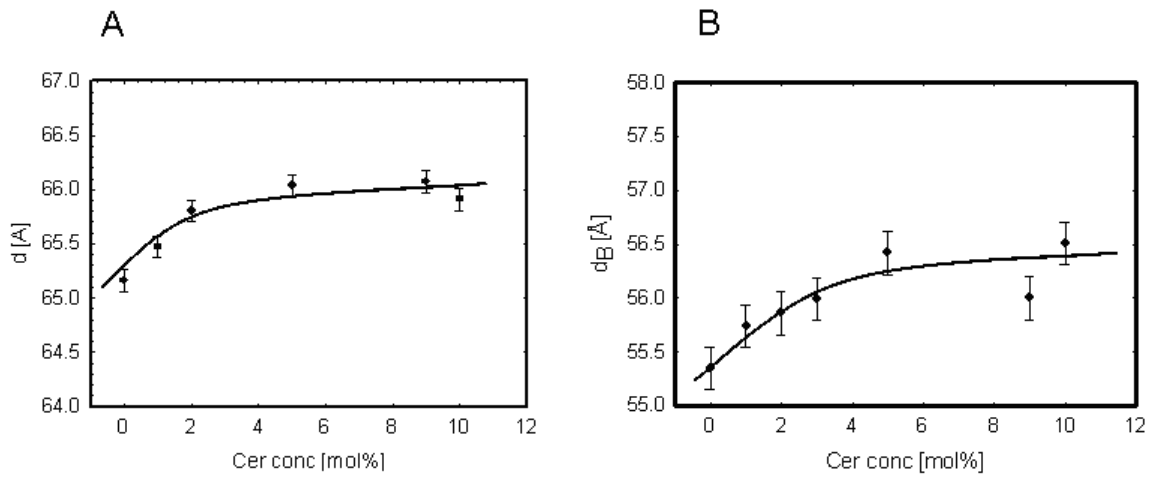

Figure 3 calculated parameters from the fits to the X-ray scattering patterns. (A: lamellar repeat distance d [Å], B: bilayer thickness d_B [Å])

References

[1] Kolesnick, R. and Y. A. Hannun, Ceramide and apoptosis, Trends in Biochem. Sc. 24, 224-225 (1999)
[2] Kolesnick, R., The therapeutic potential of modulating the ceramide/sphingomyelin pathway, J. Clin. Invest. 110, 3-8 (2002)
[3] Hannun, Y. and L. M. Obeid, The Ceramide-centric Universe of Lipid-mediated Cell Regulation: Stress-Encounters of the Lipid Kind, J. Biol. Chem. 277, 25847-25850 (2002)
[4] G. Pabst, Global Properties of Biomimetic membranes, Biophys. Rev. Lett. 1, 57 (2006)

ON THE CORRELATION BETWEEN PHASE EVOLUTION OF LIPOPLEXES/ANIONIC LIPID MIXTURES AND DNA RELEASE

G. Caracciolo[1], D. Pozzi[1], R. Caminiti[1], C. Marchini[2], M. Montani[2], A. Amici[2], and H. Amenitsch[3]

1.) Department of Chemistry, University of Rome "La Sapienza," P.le A. Moro 5, 00185 Rome, Italy
2.) Genetic Immunization Laboratory, Department of Molecular Cellular and Animal Biology, University of Camerino, Via Camerini 5, 62032 Camerino (MC), Italy
3.) Institute of Biophysics and Nanosystems Research, Austrian Academy of Sciences, Schmiedelstrasse 6, A-8042 Graz, Austria

Nowadays, synthetic cationic lipids, which form stable complexes with polyanionic DNA (lipoplexes), are considered the most promising nonviral gene carriers [1]. One of the major obstacles to efficient transfection is the low level of DNA release from lipoplexes. Recent studies [2,3] put forward two main concepts: (i) anionic lipids adopting nonlamellar phases are more efficient in releasing DNA from lipoplexes than those forming lamellar phases; (ii) the ability of cationic lipids to promote nonbilayer structures in combination with anionic phospholipids facilitates DNA release and results in higher transfection efficiency [3].

In the present study, we provide experimental evidence against that hypothesis. Here, we report on three lipoplex formulations [DOTAP-DOPC (A), DC-Chol-DOPE (B), and DOTAP-DOPC-DC-Chol-DOPE (AB)] that form lamellar phases when mixed with anionic DOPG, while promoting the formation of nonbilayer structures when mixed with anionic DOPA. Synchrotron small angle x-ray diffraction (SAXD) was applied to study the structural changes of lipoplexes upon interaction with anionic liposomes (ALs). Lipoplex/AL mixed dispersions were prepared by mixing solutions of AL and preformed lipoplexes at different charge ratios R=A/Lc (moles of anionic lipid/moles of cationic lipid). All SAXD measurements were performed at the Austrian SAXS station of the synchrotron light source ELETTRA (Trieste, Italy) [4].

Fig. 1 (panel A) shows some representative SAXD patterns of A/DNA/DOPG mixtures as a function of the anionic/cationic charge ratio R. At R=0 (no anionic lipid added), the sharp (00l) peaks (marked with an asterisk) are caused by alternating lipid bilayer/DNA monolayer lamellar structure (L_α^c phase) with periodicity $d=2\pi/q_{001}=65$ Å. As the DOPG concentration is increased in the mixture, the lamellar phase of A/DNA lipoplexes changed remarkably. Indeed, for $0<R<1$, the SAXD patterns were dominated by diffraction maxima of the L_α^c phase of A/DNA lipoplexes, while, for $R>1$, Bragg peaks of the highly swollen lamellar phase of pure DOPG were observed (indicated by diamonds). Panel B of Fig. 1 shows the evolution of the d spacings of the different phases of A/DNA/DOPG mixture as a function of R. In regime I, only lamellar lipoplexes were found to exist. In this regime, a characteristic structural feature of the A/DNA/DOPG mixture was the extensive swelling of the lamellar phase of A/DNA lipoplexes that accompanied its enrichment with DOPG molecules (lamellar d spacings are indicated with open circles). In regime II, lamellar lipoplexes were progressively disintegrated and started to coexist with excess DOPG. In regime III, only the fluid DOPG bilayers were found. We conclude that, all over the compositional range investigated, A/DNA lipoplexes retained their lamellar arrangement up to complete disintegration by anionic DOPG (Fig. 1, panel C). Fig. 2 (panel A) shows SAXD patterns of A/DNA/ DOPA mixtures as a function of R. For $0<R<0.2$, only lamellar lipoplexes were found to exist. In this stage, the DNA lattice was diluted by the anionic lipid. This can be seen in SAXD scans where d_{DNA} changes from 38.6 Å at R=0 up to about 41.9 Å at R=0.2. As the DOPA concentration is increased in the mixture, a lamellar-hexagonal phase transition occurred. At R=0.5, the diffraction pattern was still dominated by lamellar peaks, but we also observed three Bragg peaks that were indexed as the (10), (11), and (20) reflections of an

inverted hexagonal phase (indicated by diamonds) with a 71.3 Å structural unit. The initial lamellar phase of A/DNA lipoplexes persisted up to R~2. For R>2, the SAXD patterns of the A/DNA/DOPA mixture were dominated by a hexagonal phase, with a unit cell of 75.5 Å. Additional reflections were also seen. Such reflections arose from pure DOPA coexisting with hexagonal lipoplexes. Panel B of Fig. 2 shows the phase diagram of A/DNA/DOPA mixtures. In regime I, only lamellar lipoplexes were detected (lamellar d spacings are indicated with open circles). In regime II, lamellar and hexagonal lipoplexes coexisted. The increase of both the lamellar (open circles) and the hexagonal (open triangles) spacings is consistent with the inclusion of DOPA molecules within A membranes. This finding indicates that DOPA molecules penetrated within A membranes and promoted a lamellar-hexagonal phase transition (Fig. 2, panel C). Lastly, in regime III, hexagonal lipoplexes were found to coexist with pure DOPA. Very similar results were obtained with B/DNA and AB/DNA lipoplexes.
Furthermore, we applied gel electrophoresis to examine the release of DNA from lipoplexes by anionic lipids. As Fig. 3 unambiguously shows the DNA releasing activity of DOPG and DOPA was very similar for all lipoplex formulations tested.
In conclusion, we have shown that (i) the anionic lipids with a disposition to form lamellar phases (such as DOPG) may be DNA releasers as good as the anionic lipids with a propensity to form nonlamellar phases (such as DOPA); (ii) the extent of DNA release from lipoplexes by anionic lipids does not universally correlate with the propensity of the lipoplex/anionic lipid mixtures to adopt nonbilayer motifs. Thus, our findings suggest that the proposed general correlation between the formation of nonlamellar phases and the extent of DNA release does not exist [5].

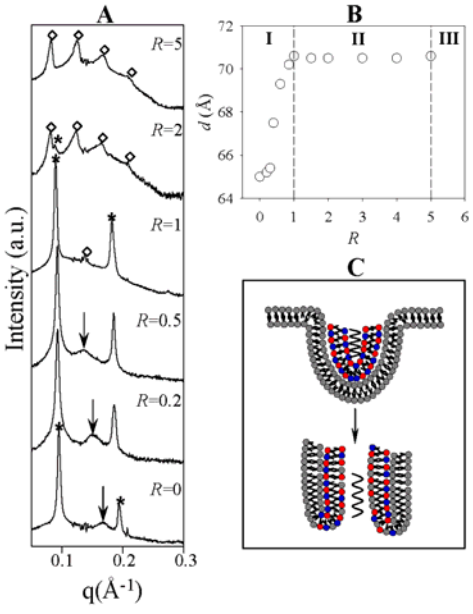

Figure 1. Panel A: SAXD patterns of A/DNA/DOPG mixtures as a function of the anionic/cationic charge ratio R. Panel B: phase diagram of A/DNA/DOPG mixture with differing DOPG content. Panel C: mechanism of interaction between lamellar lipoplexes and DOPG liposomes (gray).

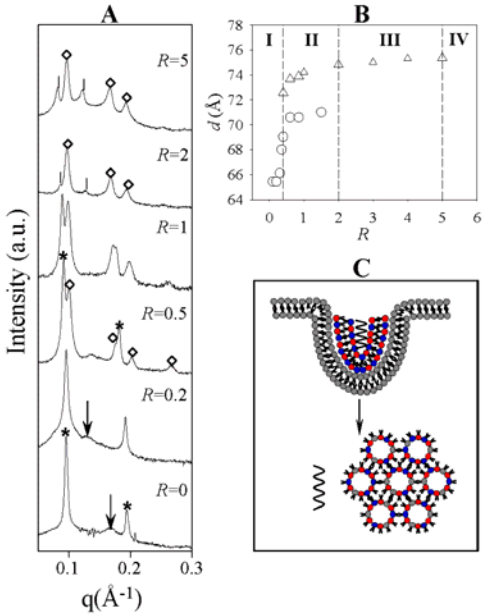

Figure 2. Panel A: SAXD patterns of A/DNA/DOPA mixtures as a function of the anionic/cationic charge ratio R. Panel B: phase diagram of A/DNA/DOPA mixture with differing DOPA content. Panel C: mechanism of interaction between lamellar lipoplexes and DOPA liposomes (gray).

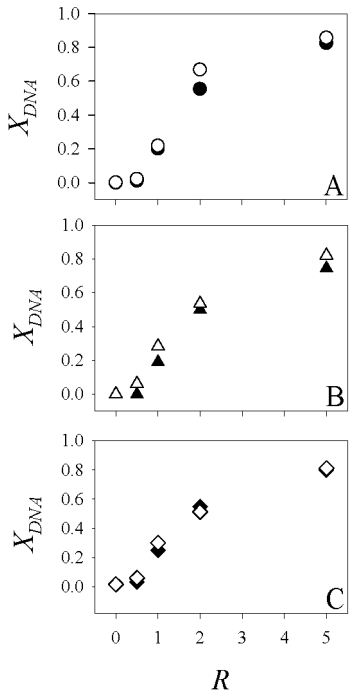

Figure 3. Fraction of DNA release, X_{DNA}, from A/DNA (panel A), B/DNA (panel B), and AB/DNA panel C) lipoplexes by DOPG (black symbols) and DOPA (white symbols).

References

[1] M. C. Pedroso de Lima, S. Simões, P. Pires, H. Faneca and N. Duzgunesü, Cationic lipid-DNA complexes in gene delivery: From biophysics to biological applications, Adv. Drug Delivery Rev. 47, 277-294 (2001)

[2] Y. S. Tarahovsky, R. Koynova and R. C. MacDonald, DNA Release from Lipoplexes by Anionic Lipids: Correlation with Lipid Mesomorphism, Interfacial Curvature, and Membrane Fusion, Biophys. J. 87, 1054-1064 (2004)

[3] L. Wang, R. Koynova, H. Parikh and R. C. MacDonald, Transfection Activity of Binary Mixtures of Cationic O-Substituted Phosphatidylcholine Derivatives: The Hydrophobic Core Strongly Modulates Physical Properties and DNA Delivery Efficacy, Biophys. J. 91, 3692-3706 (2006)

[4] H. Amenitsch, M. Rappolt, M. Kriechbaum, H. Mio, P. Laggner and S. Bernstorff, First Performance Assessment of the SAXS Beamline at ELETTRA, J. Synchrotron Radiat. 5, 506-508 (1998)

[5] G. Caracciolo, D. Pozzi, R. Caminiti, C. Marchini, M. Montani, A. Amici and H. Amenitsch, On the correlation between phase evolution of lipoplexes/anionic lipid mixtures and DNA release, Appl. Phys. Lett. 91, 1439031-1439033 (2007)

ENHANCED TRANSFECTION EFFICIENCY OF MULTICOMPONENT LIPOPLEXES IN THE REGIME OF OPTIMAL MEMBRANE CHARGE DENSITY

G. Caracciolo[1], D. Pozzi[1], R. Caminiti[1], C. Marchini[2], M. Montani[2], A. Amici[2] , and H. Amenitsch[3]

1.) Chemistry Department, University of Rome "La Sapienza," P.le A. Moro 5, 00185 Rome, Italy
2.) Genetic Immunization Laboratory, Department of Molecular Cellular and Animal Biology, University of Camerino, Via Camerini 5, 62032 Camerino (MC), Italy
3.) Institute of Biophysics and Nanosystems Research, Austrian Academy of Sciences, Schmiedelstrasse 6, A-8042 Graz, Austria

Cationic liposome-DNA (CL-DNA) complexes (lipoplexes) have been shown to be promising nonviral delivery systems for gene therapy applications. Clarifying the mechanisms of lipofection is of primary importance to increase the transfection efficiency of lipoplexes. Among physical chemical parameters affecting transfection efficiency (TE), the membrane charge density, σ_M, has recently been identified as a universal parameter that governs the TE behavior of lamellar lipoplexes in vitro. The purpose of this work was to investigate the TE behavior of multicomponent lipoplexes in the regime of optimal membrane charge density ($1<\sigma_M<2\times10^{-2}$ e/Å^2) and compare their performance with that of binary lipoplexes usually employed for gene delivery purposes [1,2]. In the region of optimal charge density, the universal Gaussian curve of TE versus σ_M is expected to be roughly constant [3]. By contrast, our TE data (not reported), when plotted versus σ_M did not exhibit such a saturated behaviour, but merged onto a Gaussian curve. We observed that maximum in transfection was obtained when multicomponent lipoplexes where used to transfect NIH 3T3 cells, while binary lipoplexes were definitely less efficient. To provide a rationale for discrepancy between our findings [3] and those previously reported [2], we investigated some physical–chemical features that might account for the superior transfection efficiency of the most efficient multicomponent lipoplexes such as their lipid composition, structure, propensity to be disintegrated by anionic liposomes (ALs) and ability to release DNA [4]. We studied the structural evolution of lipoplexes when interacting with anionic (cellular) lipids by means of synchrotron small angle X-ray diffraction (SAXD). All investigated lipoplexes were arranged into lamellar arrays, with distinct DNA packing densities reflecting their different membrane charge density. After interaction with anionic DOPA vesicles, used to simulate lipoplex-endosomal membrane interaction, all tested formulations exhibited a practically identical lamellar-inverted hexagonal phase change with minor differences in transition rate as a function of anionic/cationic charge ratios, *R*. (Fig. 1). Thus, we were not able to correlate the propensity of a given formulation to form non lamellar phases with distinct levels of TE. Another factor that is likely to be important in the efficiency of transfection is the dissociation of DNA from cationic lipids. Thus, we measured the extent of DNA release from different lipoplex formulations after interaction with ALs by electrophoresis on agarose gels as a function of increasing *R*. We observe (Fig. 2) that the molar fraction of DNA released, X_{DNA}, does not vary significantly with *R* with lipid formulations. This observation correlates well with our SAXD findings showing a virtually identical phase evolution of the tested lipoplex formulations as a function of *R*. As a result, neither the structural changes of lipoplexes upon interaction with anionic cellular lipids nor their ability to release DNA were found to correlate with TE. Based upon observations on the TE behaviour of multicomponent lipoplexes in the regime of low and optimal membrane charge density, our results suggest that the transfection efficiency may be strictly related to the composition of lipoplex formulations. In principle, the effective number of lipid components may also influence TE. To better test these suggestions, in Fig. 3 we plotted TE as a function of both DC-Chol/DOTAP and DOPE/PC ratios, while

the number of lipid components, *n*, was visualized by different colours (green: 1.5<*n*<2; blu: 2<*n*<2.5; red: *n*>2.5). We observe that TE peaked at DC-Chol/DOTAP=0.5 and DOPE/PC=0.5 when both cationic and neutral lipid species are mixed in equimolar ratio. Furthermore, an empirical trend was found that the transfection activity increases with the effective number of lipid components, *n*. Although the overall effect is quite obvious, we observed that not only the number of lipid components, but also lipid composition altered transfection activity. Our findings add a compositional degree of freedom, because efficiently transfecting complexes can be prepared from a broad range of lipids maximizing TE if composition is optimized. The exact physical-chemical reasons why multicomponent lipoplexes are more efficient than binary ones can not be stated unambiguously. However, some speculative arguments can be proposed. Among the barriers to transfection, escape from endosomal compartments is a major obstacle for efficient DNA delivery. The capacity of amphiphile molecules to perturb the endosomal bilayer structure will be of primary importance in facilitating the plasmid release. However, biological membranes are complex multicomponent systems consisting of mixtures of many different lipids and proteins. Accordingly, the superiority in TE of multicomponent lipoplexes may be related to the higher fusogenicity and compatibility of vesicles made of several lipid components with respect to single lipids or binary lipoplexes. This relationship between delivery activity and physical property can be rationalized on the basis of the known consequences of packing defects as well as large local density fluctuations that could be responsible for the enhanced fusogenicity of multicomponent blends of lipids. We therefore emphasize the importance of the lipid composition of both lipoplexes and target membranes and suggest that adapting lipoplex composition to the lipid composition of target cells may be a successful strategy for the rational design of superior cationic lipid carriers.

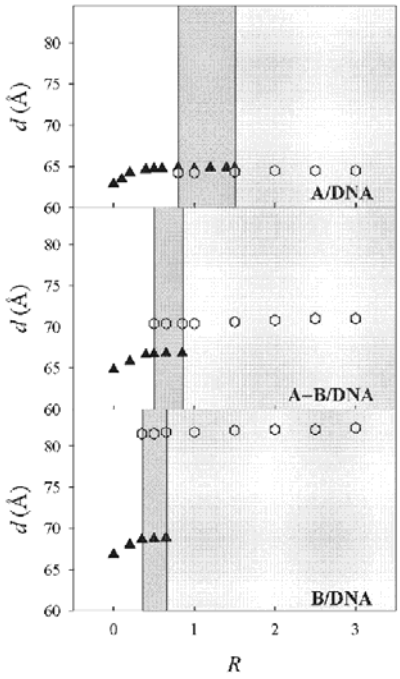

Figure 1. Phase diagram of DOTAP-DOPC/DNA, DOTAP-DOPC-DC-Chol-DOPE/DNA and DC-Chol-DOPE/DNA lipoplexes with differing DOPA content. Dashed lines separate regions occupied by lamellar lipoplexes (white panel), coexisting lamellar and hexagonal lipoplexes (dark grey panel) and hexagonal lipoplexes (light grey panel). Repeat spacings, d, of lamellar and hexagonal lipoplexes are indicated with black triangles and white hexagons, respectively.

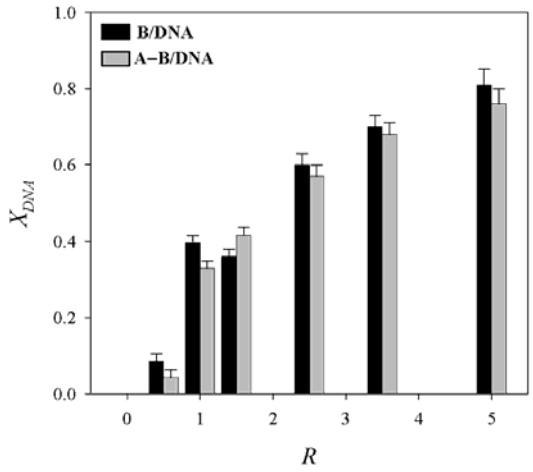

Figure 2. Molar fraction of DNA released, X_{DNA}, from DC-Chol-DOPE /DNA and DOTAP-DOPC-DC-Chol-DOPE/DNA lipoplexes by ALs as a function of increasing R

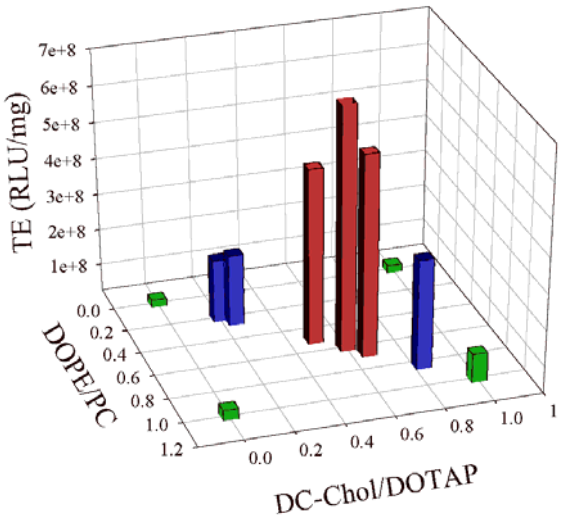

Figure 3. TE in RLU per milligram of cellular protein plotted as a function of both DC-Chol/DOTAP and DOPE/PC ratios. The number of lipid components, n was visualized by different colours (green: 1.5<n<2; blu: 2<n<2.5; red: n>2.5).

References

[1] K. K. Ewert, A. Ahmad, H. M. Evans, C. R. Safinya, Cationic lipid-DNA complexes for non-viral gene therapy: relating supramolecular structures to cellular pathways, Expert Opin. Biol. Ther. 5, 33-53 (2005)
[2] A. Ahmad, H. M Evans, K. K. Ewert, C. X. George, C. E. Samuel, C. R. Safinya, New multivalent lipids reveal bell-curve for transfection versus membrane charge density: nonviral lipid-DNA complexes for gene delivery, J. Gene Med. 7, 739-748 (2005)
[3] G. Caracciolo, C. Marchini, D. Pozzi, R. Caminiti, H. Amenitsch, M. Montani, A.Amici, Structural stability against disintegration by anionic lipids rationalizes the efficiency of cationic liposome/DNA complexes, Langmuir 23, 4498-4508 (2007)
[4] G. Caracciolo, D. Pozzi, R. Caminiti, C. Marchini, M. Montani, A.Amici, H. Amenitsch,, Transfection efficiency boost by designer multicomponent lipoplexes, Biochim. Biophys. Acta 1768, 2280-2292 (2007)

OBSERVATION OF A RECTANGULAR DNA SUPERLATTICE IN THE LIQUID-CRYSTALLINE PHASE OF CATIONIC LIPID/DNA COMPLEXES

G. Caracciolo[1], D. Pozzi[1], R. Caminiti[1],G. Mancini[2], P. Luciani[2], and H. Amenitsch[3]

1.) Chemistry Department, University of Rome "La Sapienza," P.le A. Moro 5, 00185 Rome, Italy
2.) IMC-CNR, Chemistry Department, University of Rome "La Sapienza", P.le A. Moro 5, 00185 Rome, Italy
3.) Institute of Biophysics and Nanosystems Research, Austrian Academy of Sciences, Schmiedelstrasse 6, A-8042 Graz, Austria

Over the last years complexes of DNA with cationic lipids (lipoplexes) have attracted much attention because of their potential use as nonviral gene delivery systems. Among the possible arrangements, the lamellar phase is largely the most abundant nanoscale architecture: this structure consists of smecticlike arrays of stacked bilayers with monolayers of DNA intercalated within the water gaps. The DNA strands usually exhibit 1D in-plane positional correlation, while in some cases 2D interbilayer coupling is manifested when DNA is embedded within lipid bilayers in the gel phase. Here we report, for the first time, on the observation of transbilayer correlation in the DNA ordering in the liquid-crystalline lipid phase. We also show that different DNA superstructures can be obtained by adjusting the membrane rigidity. The lipid component of lipoplexes was a binary mixture of dimyristoyl phosphatidylcholine (DMPC) and the cationic Gemini surfactant (2*R*,3*R*)-2,3-dimethoxy-1,4-bis(*N*-hex-adecyl-*N*,*N*-dimethylammonium) butane dibromide, **1**. Synchrotron small and wide-angle X-ray diffraction (SWAXD) measurements were performed at the Austrian SAXS station of the synchrotron light source ELETTRA (Trieste, Italy). In Figure 1 (top panel) the SWAXD patterns of isoelectric DMPC/**1**/DNA lipoplexes at low temperature (5 °C) are shown. The crystalline order of the lipids in the gel phase is revealed by the WAXD pattern showing a typical strong reflection. In the SAXD regime, we observe a set of equally spaced Bragg reflections arising from the membrane repeat distance $d=2\pi/q_{001}$=52.4 Å. In lamellar lipoplexes, the average thickness of the interlamellar water gaps corresponds to the diameter of DNA plus a hydration layer (d_W~20 Å). Because the complex consists of alternating layers of lipid and DNA, we could calculate the lipid bilayer thickness ($d_B=d-d_W$=32.4 Å). This value is in very good agreement with the bilayer thickness of pure DMPC/**1** aggregates (d_m=30.7 Å) [1]. Such a thickness was much lower (by some 15 Å) than that of pure DMPC (~47 Å)12 and was ~ 4.5 Å larger than that observed for the highly interdigitated phase of pure **1** bilayers [2]. Thus, our structural findings indicated that Gemini promoted the formation of interdigitated DMPC/**1** bilayers with a high degree of interpenetration of alkyl chains. Furthermore, the addition of DNA did not change significantly the membrane thickness of DMPC/**1** bilayers. In addition to the sharp lipid peaks (marked by stars), three diffuse reflections were seen and indexed as the (1,1), (1,3), and (1,5) reflections of a centered rectangular columnar DNA lattice, with lattice constants a=40.5 Å and b=104.8 Å. The systematic missing of (h,k) peaks with $h+k=2n+1$ confirmed the centered symmetry. As evident, the lattice parameter $b=2d$=104.8 Å was much smaller than that found in noninterdigitated bilayers. This result was due to the interdigitated nature of the gel phase of DMPC/**1** bilayers and was in good agreement with the findings of Koynova and MacDonald [3]. Upon heating, the WAXD patterns of DMPC/**1**/DNA lipoplexes showed that the lipid bilayers underwent a gel-liquid-crystalline phase transition that was completed between 35 and 50°C. Thus, the transition temperature of DMPC/**1** bilayers was found to be definitely higher than that of pure DMPC (T_m~24 °C). This indicated that Gemini surfactants raised significantly the transition temperature of the phospholipids. At 50 °C (Figure 1, middle panel), Bragg peaks in the SAXD regime show that the gel-liquidcrystalline transition is associated with an expansion of the lamellar repeat period, d, by 6 Å (d=58.4 Å). Nevertheless, the estimated thickness of

DMPC/**1** bilayers (d_m~38 Å) remains much lower (by some 10 Å) than that of pure DMPC (~47 Å). This finding suggested that thermal fluctuations reduced the degree of interdigitation, but a partial interdigitation persisted in the liquid-crystalline phase. In the interdigitated liquid-crystalline phases, the acyl chains are more motionally restricted than in the noninterdigitated liquidcrystalline phase but much more disordered than in their gel counterpart. Multiple DNA reflections are still observed but could not be indexed to a centered rectangular lattice (as in the low-temperature gel phase) nor to the simple DNA-DNA in-plane correlation usually observed in the liquid-crystalline phase of lipoplexes. Conversely, a simple rectangular phase is indexed with the measured sets of q values. DNA peaks are indexed to the (1,0) and (1,2), (1,3) reflections of a simple rectangular lattice with a=39.8 Å and b=58.4 Å. Here we emphasize that our structural findings are the first report of a transbilayer DNA superlattice in the liquid-crystalline phase. The unexpected reduction of the DNA spacing (less than 1 Å) probably reflects the decreased area per molecule and the increase in membrane charge density. At 65 °C, loss of interlamellar correlation occurred as revealed by the disappearance of the multiple DNA reflections from the SAXD pattern (Figure 1, bottom panel). In this temperature range (50 <T < 65 °C) the thermotropic behavior of DMPC/**1**/DNA lipoplexes resembled the typical behavior of lipoplexes. Indeed, the increase in temperature induced a reduction of the bilayer thickness by ~1.5 Å followed by a small expansion of the DNA spacing (~1 Å). At low temperatures, DNA arranged into a centered rectangular columnar phase intercalated between interdigitated bilayers in the gel phase (Figure 2, panel A) while, at higher temperatures (50 °C), DNA formed a simple rectangular DNA lattice between fluid but still partly interdigitated bilayers (Figure 2, panel B). At 65 °C, transbilayer coupling was lost and DNA superlattice was not observed (Figure 2, panel C). DNA lattice is coupled to the membrane rigidity by thermal motion. When bilayers are stiff (as in the gel phase) Coulomb repulsions between DNA strands favors a centered rectangular lattice. Upon heating, thermal fluctuations continuously raise. In the first stage, thermal motion possibly becomes strong enough that correlations are not well developed in centered rectangular lattices but a partial interlayer coupling still persists. In this case, a tendency to form a simple rectangular rather than centered structure would appear. When fluctuations become strong, interlayer coupling becomes weak and DNA strands in different layers are practically decoupled. The explanation for the observation of a DNA superstructure in the liquid-crystalline phase of DMPC/**1** membranes is likely to be their interdigitation. In conclusion this study is the first report of a DNA transbilayer ordering in the liquid-crystalline phase of lipoplexes.

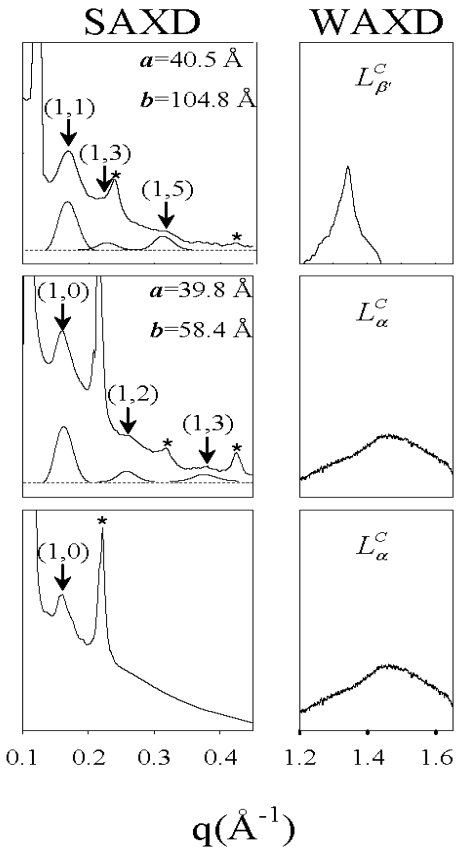

Figure 1. Small and wide-angle X-ray diffraction patterns of DMPC/1/DNA lipoplexes at different temperatures.

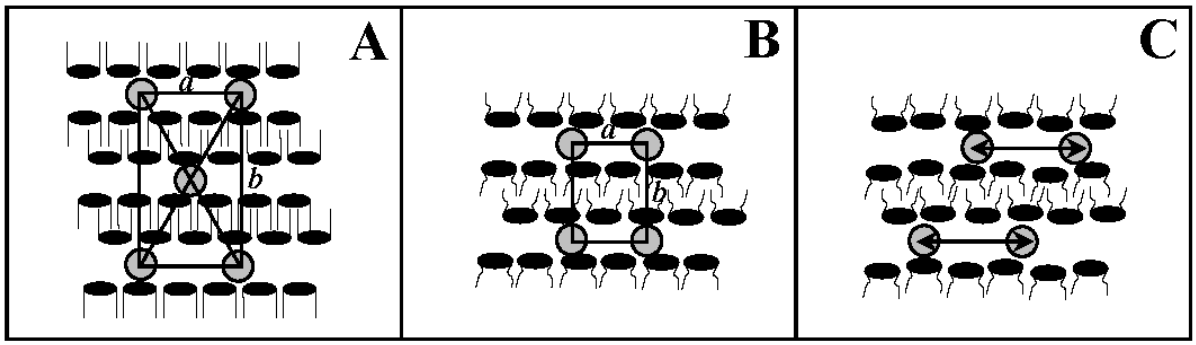

Figure 2. Schematic sketch of the local structure of the DNA ordering within DMPC/1/DNA lipoplexes as a function of temperature.

References:

[1] G. Caracciolo, S.Piotto, C. Bombelli, R.Caminiti and G.Mancini, Segregation and phase transition in mixed lipid films, Langmuir 21, 9137-9142 (2005)
[2] G. Caracciolo, G. Mancini, C. Bombelli, P. Lucani and R. Caminiti, The structure of gemini surfactants self-assemblies investigated by Energy Dispersive X-ray Diffraction, J. Phys. Chem. B 107, 12268-12274 (2003)
[3] R. Koynova and R. C. MacDonald, Columnar DNA superlattices in lamellar/O/-ethylphosphatidylcholine lipoplexes, Nano Lett. 4, 1475-1479 (2004)

ON THE PHASE BEHAVIOUR OF PHYTANTRIOL – AN ALTERNATIVE LIPID FOR THE FORMATION OF CUBOSOMES AND HEXOSOMES

Yao-Da Dong[1], Aurelia W. Dong[1], Heinz Amenitsch[2], Michael Rappolt[2], and Ben J. Boyd[1]

1.) Department of Pharmaceutics, Victoria College of Pharmacy, Monash University, Parkville, VIC 3052, Australia
2.) Austrian Academy of Sciences, Institute of Biophysics and Nanosystems Research, Graz, Austria

Introduction

Glyceryl monooleate has long been the lipid of choice for the study of bicontinuous cubic phases, transitions between them, and their role in biological processes. However, in the use of bicontinuous cubic phase structures for encapsulation in actual products such as drug delivery systems and functional foods, glyceryl monooleate has significant long term chemical stability issues due to the ester and unsaturated hydrocarbon functions. Hence, phytantriol (3,7,11,15-tetramethylhexadecane-1,2,3-triol), a lipid that has been used in cosmetics[1] and is available commercially in relatively high purity has received increasing attention in the last few years. It has demonstrated similar lyotropic phase behaviour to monoolein,[2] in particular that phytantriol also forms a bicontinuous cubic phase (Q_{II}) in excess water at ambient temperature, and inverse hexagonal phase (H_{II}) in excess water at higher temperatures (phase diagram reproduced in Figure 1 Panel B).[3] Previously we investigated the lyotropic phase behaviour of phytantriol obtained from Roche and found a much higher $Q_{II}+H_2O \rightarrow H_{II}+H_2O$ transition temperature (around 65°C)[4] than previously reported for phytantriol obtained from Kuraray (44°C).[3] We also demonstrated the rather dramatic suppression of the transition temperatures from 65°C to below ambient temperature by the addition of small quantities (5%) of a model lipophilic impurity (vitamin E acetate). Hence, we hypothesize that the differences between reported phase behaviour in the phytantriol + water system may be due to differing impurity profiles between phytantriol sourced from different commercial suppliers and sought to reconstruct the accurate phytantriol-water phase diagram using phytantriol from Roche.

Results

The rapid acquisition and versatile, multi-sample temperature control environment at the Elettra SAXS beamline allowed a rapid determination of the phase diagram, with complete temperature scans at 17 different compositions to facilitate highly accurate phase boundaries. We present an alternate phytantriol + water phase diagram for comparison to the previously published diagram in Figure 2 that may more accurately reflect the lyotropic phase behaviour of pure phytantriol. The phase diagram, illustrated in Figure 1 Panel A is based on the Roche phytantriol (now manufactured by DSM Nutritional Products). It was in broad agreement with that reported previously by Barauskas and Landh (based on Kuraray phytantriol),[3] however there were significant differences in a number of features.

- While the Q_{IIPn3m} to H_{II} to L_2 transitions with increasing temperature at high water content were still evident, the $Q_{II\ Pn3m}$ to H_{II} transition temperature (marked in Figure 1 Panel B), was found to be significantly higher than that previously reported. The $Q_{II\ Pn3m}$ persisted up to 58°C and H_{II} only existed from 60-62°C and transformed completely to L_2 phase at 64°C. Thus the range of existence of H_{II} phase was very narrow in comparison to that in Figure 1 Panel B.
- The phase progression at low temperatures (20°C) was also the same as previously reported. The progression from L_2 to L_α to $Q_{II\ Ia3d}$ to $Q_{II\ Pn3m}$ with increasing water content was observed. However, in the previously reported phase diagram, the boundary between the $Q_{II\ Ia3d}$ + $Q_{II\ Pn3m}$ transition region with $Q_{II\ Pn3m}$ (marked in Figure 1 Panel B) was at 25% water and the $Q_{II\ Pn3m}$ to $Q_{II\ Pn3m}$ + excess water boundary was at approximately 29%

water. In this study it was found that these transitions occur at a higher water content, with the former transition occurring at approximately 33% water. This is highlighted in Figure 2 where at 25C, the Roche phytantriol-water system with 27% water showed pure $Q_{II\ Ia3d}$ whilst Kuraray phytantriol showed pure $Q_{II\ Pn3m}$.

- The $Q_{II\ Ia3d} + Q_{II\ Pn3m}$ transition region (indicated by in Figure 1 Panel B), appeared as a 'nominal' transition region in the previously published phase diagram, but was found in this study to actually occupy a more substantial proportion of the phase diagram. This phase transition was found to span a region of 15% w/w water by composition, and a range of 40°C in temperature, and hence is a more dominant feature in this alternative phase diagram.

Lastly it was also noted that the melting temperature of the lamellar to L_2 phase at approximately 40°C is also slightly higher than that reported previously at 35°C.

Conclusion

We demonstrated key differences in phytantriol lyotropic behaviour depending on its commercial source. Further compositional analysis revealed differences in impurity profiles that support the above observations and are discussed in the full publication on this work.[6] In drug delivery applications, the phase structure has a dramatic effect on drug release from the matrix, with H_{II} phase displaying slower release than Q_{II}[5] by virtue of the generally small water channels. Hence there is a need to verify in detail the lyotropic behaviour of phytantriol between different commercial sources or even between manufacturing batches in order control the behaviour of these materials in commercial applications.

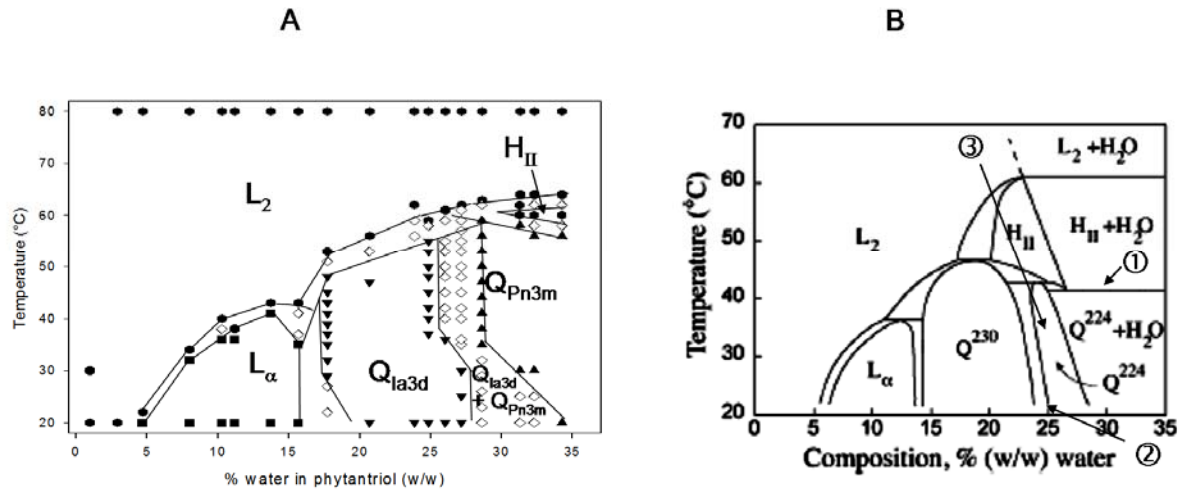

Figure 1.Panel A - Phase diagram for the phytantriol-water system determined by synchrotron-SAXS. The Roche phytantriol was utilised in the preparation of this phase diagram. Only data points that define phase boundaries are included in the figure. Circles define samples exhibiting reverse micellar phase (L_2); squares are lamellar phase (L_α), downward facing triangles are gyroid bicontinuous cubic phase ($QI_{I\ Ia3d}$), upward facing triangles are diamond bicontinuous cubic phase ($Q_{II\ Pn3m}$), hexagons are reverse hexagonal phase (H_{II}), open diamonds denote multiphase transition regions. Panel B - Reproduction of the phytantriol-water phase diagram from Barauskas et al. [3] The annotations on Panel B marked , and represent particular features of the phase diagram discussed in the text.

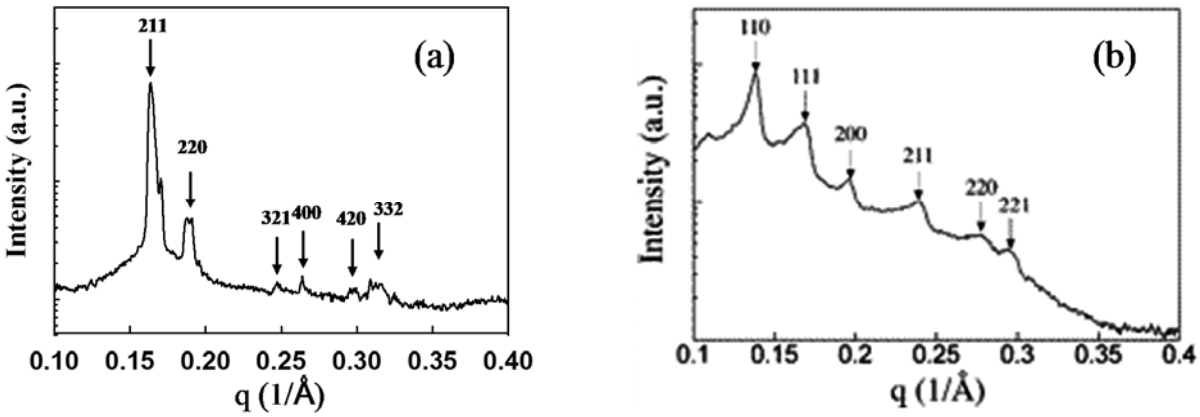

Figure 2. Representative X-ray diffractograms of (a) the cubic phase $Q_{II\ Ia3d}$ based on Roche phytantriol with 27% w/w water at 25 C (b) the cubic phase $Q_{II\ Pn3m}$ based on Kuraray phytantriol at the same condition reproduced from Barauskas et al. [3] The indexing of the Bragg reflections are indicated with their corresponding Miller indexes.

References

[1] E. Wagner, Panthenol and phytantriol in cosmetics. Parfuemerie und Kosmetik, 1994. 75: 260, 263-4, 266-7

[2] J. Briggs, H. Chung, and M. Caffrey, The temperature-composition phase diagram and mesophase structure characterization of the monoolein/water system. Journal De Physique II, 1996. 6: 723-751

[3] J. Barauskas, and T. Landh, Phase behaviour of the phytantriol/water system. Langmuir, 2003. 19: 9562-9565

[4] Y.-D. Dong, I. Larson, T. Hanley, B. J. Boyd, Bulk and Dispersed Aqueous Phase Behaviour of Phytantriol: Effect of Vitamin E Acetate and F127 Polymer on Liquid Crystal Nanostructure. Langmuir, 2006. 22: 9512-9518

[5] Boyd, B.J., M. Khoo, D. V. Whittaker, G. Davey. Lyotropic liquid crystalline phases formed from glycerate surfactants as sustained release drug delivery systems. Int. J. Pharm., 2006. 309:218-226

[6] Y-D. Dong, A. W. Dong, I. Larson, M. Rappolt, H. Amenitsch, T. Hanley, B. J. Boyd Impurities in commercial phytantriol significantly alter its lyotropic liquid crystalline phase behaviour. Accepted for publication 13th April in Langmuir, 2008

FORMATION AND PHASE TRANSITIONS IN LIQUID CRYSTALLINE DISPERSED PARTICLES USING TIME RESOLVED SAXS

Yao-Da Dong[1], Aurelia W. Dong[1], Heinz Amenitsch[2], Michael Rappolt[2], and Ben J. Boyd[1]

1.) Department of Pharmaceutics, Victoria College of Pharmacy, Monash University, Parkville, VIC 3052, Australia
2.) Austrian Academy of Sciences, Institute of Biophysics and Nanosystems Research, Graz, Austria

Introduction

'Cubosomes' (dispersed inverse cubic phase (Q_{II})) and 'hexosomes' (dispersed inverse hexagonal (H_{II}) phase) are of interest for the importance of non-lamellar liquid crystal structures in biology and they have also been proposed as potential drug delivery vehicles. [1] It has been accepted in the literature that the internal geometric structure of the 'parent' non-dispersed LC phase is retained in the particles on dispersion and that the particles 'are in effective thermodynamic equilibrium with their surroundings'.[2] However, we recently found that LC particles display supercooling, and that the effect is greater than that observed for the parent non-dispersed LC phase. Anomalous phase progressions on heating and cooling were also apparent, in particular the formation of the gyroid cubic phase in excess water which can only occur on kinetic dehydration of these systems.[3] Consequently in these experiments we aimed to further probe the supercooling effect.

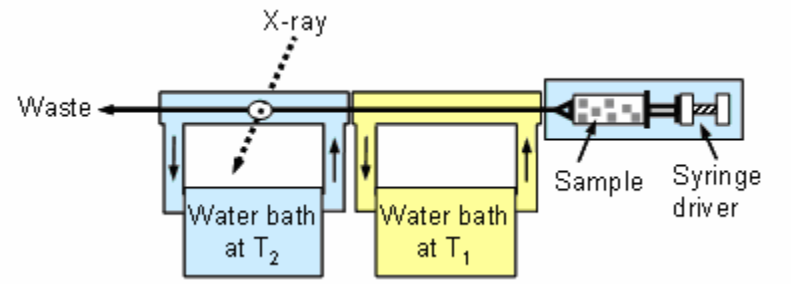

Figure 1. SAXS setup for the Temperature-drop (T-drop) experiments.

Results

Using a modification to the flow through cell at the Elettra SAXS beamline, shown schematically in Figure 1, we were able to rapidly change temperature of cubosome dispersion flowing through the capillary to allow observation of the thermal behaviour of dispersion systems at the final temperature by halting the flow. The system was validated for thermal flow by conducting T-jumps where T2>T1 and observing instant transition to the anticipated equilibrium phase structure. The three major findings arising from the T-drop experiments were:

- The extent of supercooling depends on the initial temperature (T1).
- The kinetics of particle metaphase transition through nucleation is rapid but the time required for the initial spontaneous nucleation depends on final temperature (T2).
- Unique metaphases formed during supercooling are highly stable until below a critical temperature where T-drop showed no supercooled metaphases.

Effect of initial temperature, T1: At equilibrium, phytantriol cubosome dispersion exhibits the $Q_{II\ Pn3m}$ phase structure at 53 °C. However, Figure 2(a) shows that for the phytantriol dispersion a T-drop from 90 – 53 °C produces L_2 phase 1 min after the T-drop whilst for a drop from 75 – 53 °C co-existing $Q_{II\ Pn3m}$ and $Q_{II\ Ia3d}$ cubic phases were evident (Figure 2(b)) in agreement with previously results on cooling at 1 °C/min. Similarly, a T-drop

of 75 – 40 °C showed $Q_{II\ Pn3m}$ + $Q_{II\ Ia3d}$ (Figure 2(c)) whilst 70 to 40 °C in Figure 2(d) showed only the

T1	Phase at T1	T2	Phase expected	Phase observed
90	L2	53	Pn3m	L2 (+Ia3d at 10 min)
75	L2	53	Pn3m	Pn3m + Ia3d
75	L2	40	Pn3m	Pn3m + Ia3d
70	L2	40	Pn3m	Pn3m
90	L2	30	Pn3m	Pn3m at 1 sec/10 min

Table 1. Phases present on T-drop for selected systems from T1 to T2 (°C). (italicised structures not expected from equilibrium phase behaviour at final temperature T2)
Note that the $Q_{II\ Ia3d}$ phase can only occur through 'kinetic dehydration' in excess water.

$Q_{II\ Pn3m}$ structure. Phytantriol dispersion is in the L_2 phase above 70 °C at equilibrium, hence it is surprising that the higher initial temperature causes greater supercooling for the system which is contradictory of the Mpemba effect. The Mpemba effect describes water at ambient temperature crystallizes at lower temperature than hot water due to greater effect of supercooling on the former.[4] One possible explanation is that the higher temperature minimises the crystal 'memory effect' allowing a greater extent of supercooling to occur.[5]

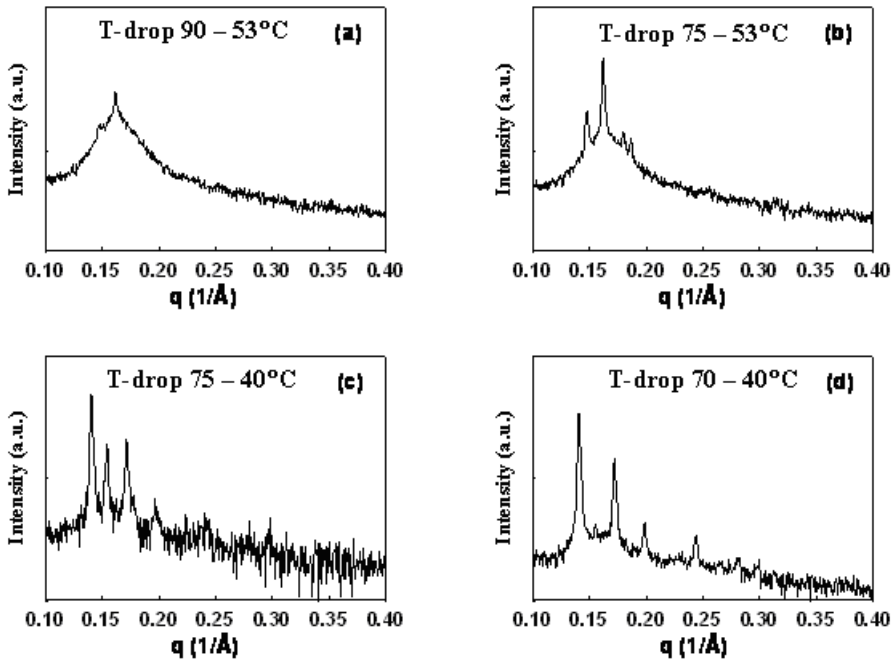

Figure 2. Representative X-ray diffractograms of phytantriol cubosome dispersion system 1 minute after T-drop: (a) 90 – 53°C (L_2 predominates); (b) 75 – 53°C ($Q_{II\ Pn3m}$ + $Q_{II\ Ia3d}$); (c) 75 – 40°C ($Q_{II\ Pn3m}$ + $Q_{II\ Ia3d}$) and (d) 70 – 40°C ($Q_{II\ Pn3m}$ predominates).

Effect of final Temperature, T2: Figure 3 demonstrates that these supercooled metaphases are not detected when the temperature is dropped to an even lower temperature than in Figure 2. Comparing Figure 3A and 3B the greater amplitude in T-drop to 30°C produced the equilibrium Pn3m structure just one second after 1 sec and was unchanged at 10 min. In contrast, at 10 min in Figure 3A, the Ia3d spacegroup was still dominant.

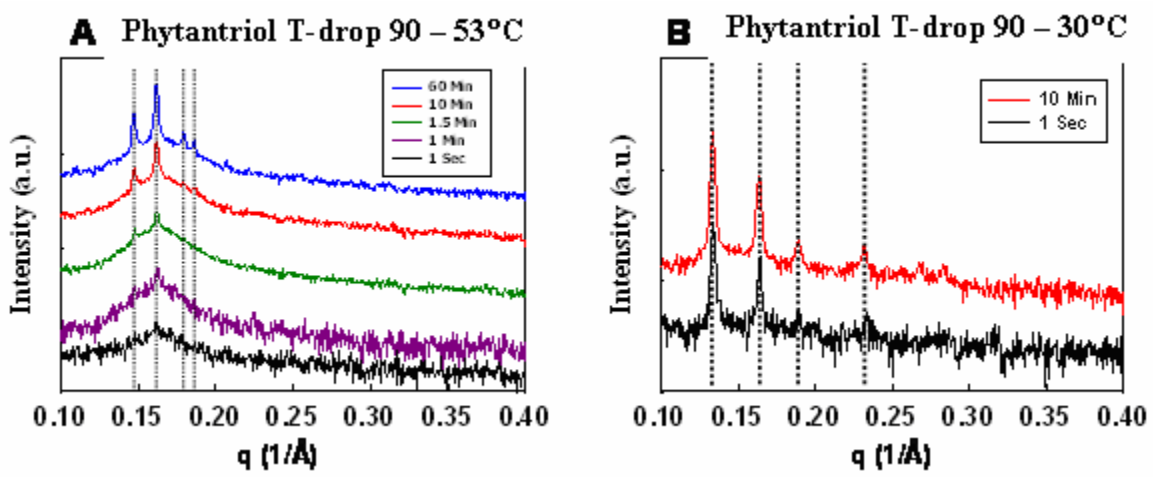

Figure 3. Representative X-ray diffractograms of Phytantriol dispersion T-drop (A) 90 – 53°C (L_2 + $Q_{II\ Pn3m}$ + $Q_{II\ Ia3d}$) over time and (B) 90 – 30°C ($Q_{II\ Pn3m}$) over time. Dotted lines highlight the positions of the Bragg reflections.

Kinetics of phase transitions: The T-drop for the phytantriol dispersion from 90 – 53°C in Figure 3A showed the kinetic of conversion from predominantly L2 phase initially to the $Q_{II\ Pn3m}$ and $Q_{II\ Ia3d}$ phase over around 30-60 min (although the Pn3m phase should be present at equilibrium). In Figures 3A the supercooled metaphase was relatively stable. No change in peak intensity or lattice dimension (peak shifts) can be detected between 30 and 60 min after the temperature drop. Isotropic to metaphase conversion of particles requires spontaneous phase nucleation within individual particles. The time required for spontaneous nucleation will vary depending on the final temperature. The slow conversion for phytantriol 90 – 53°C in Figure 3(a) is likely because of 53°C is very close to the phase boundary; a separate T-drop experiment at 75 – 56°C showed only the L_2 phase (data not shown). Therefore, the system requires much longer time for spontaneous nucleation to occur than other systems at lower temperatures.

These findings have important implications for the preparation and use of these materials under varying temperature conditions.

References

[1] Drummond, C.J., et al., Hydrophobic radiofrequency plasma-deposited polymer films: dielectric properties and surface forces. Colloids and Surfaces A: Physicochemical and Engineering Aspects, 1997. 129-130: p. 117-129
[2] deCampo, L., et al., Reversible Phase Transitions in Emulsified Nanostructured Lipid Systems. Langmuir, 2004. 20(13): p. 5254-5261
[3] Dong, Y.D., et al. Non-equilibrium phase behaviour for liquid crystals during heating and cooling IBN/Elettra Annual Report, 2006, pp. 80-82. Dong, Y.D., et al., Phase progression and supercooling effects in dispersed non-lamellar liquid crystalline systems. . Manuscript in preparation, 2006.
[4] Auerbach, D., Supercooling and the Mpemba effect: When hot water freezes quicker than cold. American Journal of Physics, 1995. 63(10): p. 882-885
[5] Blumstein, B.R., Memory effects of polymer liquid crystals: influence of thermal history of phase behaviour, in Mechanical and Thermophysical Properties of Polymer Liquid Crystals, W. Brostow, Editor. 1998, Chapman & Hall: London. p. 147-171

NOVEL STRUCTURES OF SURFACTANT-DNA COMPLEXES

S.K. Ghosh[1], A.V. Radhakrishnan[1], G. Pabst[2], V. A. Raghunathan[1], and A. K. Sood[3]

1.) Raman Research Institute, Bangalore – 560 080, India
2.) Institute of Biophysics and Nanosystems Research, Austrian Academy of Sciences, Schmiedlstrasse 6, A-8042 Graz, Austria
3.) Department of Physics, Indian Institute of Science, Bangalore - 560 012, India

We have studied the structures of complexes of DNA with the cationic surfactant cetyltrimethylammonium tosylate (CTAT), which is well known to self-assemble into long worm-like micelles in aqueous solutions. Three structures of these complexes are observed, depending on the DNA and CTAT concentrations in the solution, in contrast to DNA-cetyltrimethylammonium bromide (CTAB) complexes, which show only one structure in the same composition range. At high DNA and low CTAT concentrations a hexagonal structure is seen, which is similar to the one observed in DNA-CTAB complexes [1]. This is a close-packed structure of the two types of cylinders, with each DNA stand intercalated between three surfactant micelles. At lower
DNA concentrations, where the molar ratio of DNA base to CTAT is less than 1, a structure characterized by a square lattice is observed irrespective of the CTAT concentration. This is also a close-packed structure, where each DNA strand is surrounded by 4 micelles. At high DNA and CTAT concentrations another structure is seen, which is characterized by a two-dimensional hexagonal lattice. This lattice is a $\sqrt{3}$ x $\sqrt{3}$ superlattice of the hexagonal lattice present at lower CTAT concentrations. Figure 1 shows an electron density map of this structure obtained for a particular combination of the phases of the observed reflections. Modeling studies are underway to determine the structure of this phase. It is clear that the rich phase behaviour of the DNA-CTAT complexes is due to the competition between the tosylate ion and DNA to bind to the micelles, which is absent in the DNA-CTAB system.

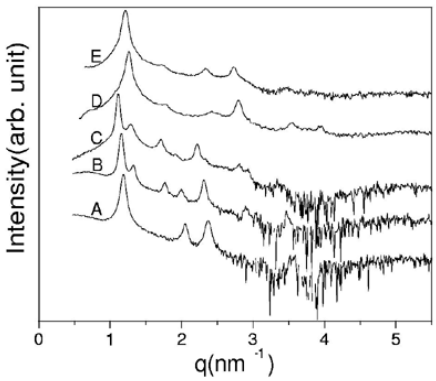

Figure 1. X-ray diffraction patterns of the different structures of CTAT-DNA complexes. (A) hexagonal, (B,C) hexagonal superlattice, (D,E) square.

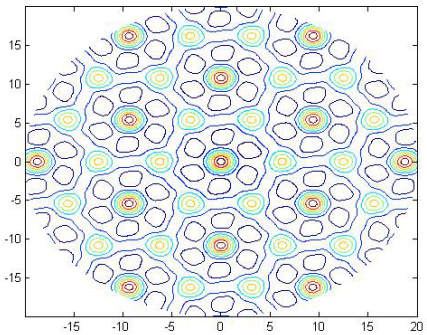

Figure 2. Electron density map of the hexagonal superlattice structure calculated from the diffraction data.

References

[1] R. Krishnaswamy, G. Pabst, M. Rappolt, V.A. Raghunathan and A. K. Sood; Structure of DNA-CTAB-hexanol complexes; Phys. Rev. E 73, 031904 (2006)

THE ROLE OF MEMBRANE HYDROCARBON CHAIN COMPOSITION IN INTERACTIONS WITH ANTIHYPERTENSIVE DRUGS

A. Hodzic[1], P. Zoumpoulakis[2], T. Mavromoustakos[2], M. Rappolt[1],P. Laggner[1], and G. Pabst[1]

1.) Austrian Academy of Sciences, Institute of Biophysics and Nanosystems Research, Graz, Austria
2.) National Hellenic Research Foundation, Institute of Organic and Pharmaceutical Chemistry, Athens, Greece

Stressful life style of modern human societies leads to many diseases and one of the growing indispositions related to this fact is hypertension. Thus, there is a strong need for novel effective drugs. One of the new categories of antihypertensive drugs consists of AT1 antagonists (SARTANs), whose action is based on blocking of the active site of the AT1 receptor [1].

The aim of the present study is to contribute to a basic understanding of the their molecular mode of action on membranes. We studied the influence of the SARTAN losartan on the global structure of phospholipid bilayers composed of pure dimyristoyl phosphatidylcholine (DMPC) and palmitoyl oleoylphosphatidylcholine (POPC) applying synchrotron small-angle x-ray scattering. Additionally, we also studied influences on the binary mixtures of DMPC/cholesterol and POPC/cholesterol. The observed effects were primarily related to bilayer interactions, whereas the membrane thickness remained largely unaffected.

Losartan led to a complete loss of positional correlations between adjacent bilayers for all single component model membranes. This can be explained by the negative surface charged conferred to the bilayers upon losartan insertion. The effect was however, counterbalanced upon the addition of cholesterol. Both, POPC and DMPC bilayers exhibited no positional correlations up to 5 mol% cholesterol, respectively. However, only POPC remained uncorrelated at 20 mol% and above, while DMPC/cholesterol bilayers exhibited multilamellar vesicles, i.e. a reentrant transition of the positionally uncorrelated bilayers into correlated ones. Our results may be understood in view of the different hydrocarbon chain packing densities in saturated versus unsaturated bilayers and their respective affinities to interaction with cholesterol. This shows that the insertion of losartan into the membrane may be overridden by a tighter bilayer interface and emphasizes the role of hydrocarbon chain composition in its mode of action.

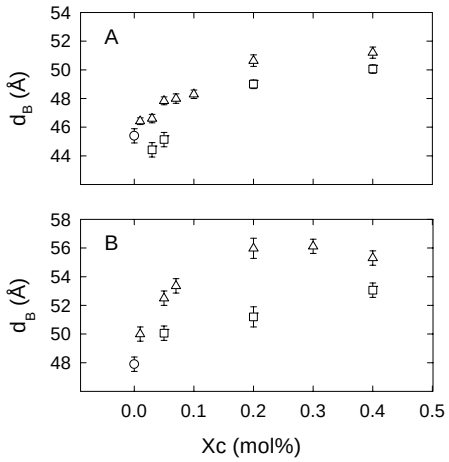

Figure 1. Bilayer thickness, d_B, from ternary mixture of POPC or DMPC with cholesterol and losartan. Panel A shows the concentration dependence of the DMPC membrane thickness (d_B), for pure lipid (o), in presence of different concentrations of cholesterol (Δ), and different concentrations of cholesterol with 2 mol% losartan, respectively (□). Panel B shows the concentration dependence of the POPC membrane thickness (d_B), for pure lipid (o), in presence of different concentrations of cholesterol (Δ) and different concentrations of cholesterol with 2mol% losartan, respectively (□).

References:

[1] T. Mavromoustakos et al.; Efforts to understand the molecular basis of hypertension through drug: membrane interactions; Curr. Top. Med. Chem. 4, 445-459 (2004)

INTERACTION BETWEEN NEW GEMCITABINE-SQUALENE PRODRUG AND A PHOSPHOLIPIDIC BILAYERS

B.Pili[1], C. Bourgaux[1], H.Amenitsch[2], P.Couvreur[1], and M.Ollivon[1]

1.) Univ .Paris-sud XI, Faculté de Pharmacie, UMR CNRS 8612, Chatênay-Malabry, France
2.) Austrian Academy of Sciences, Institute of Biophysics and Nanosystems Research, Graz, Austria

Introduction

Gemcitabine (2',2'-difluoro-2'-deoxycytidine) is a nucleoside analogue with antineoplastic activity against a wide range of solid tumours. To be active, the gemcitabine has to be phosphorylated, but only a low proportion of gemcitabine is converted to di- and triphosphate forms. Moreover, gemcitabine is rapidly and extensively deaminated in blood and in some tissues to the inactive uracil derivative, leading to a short plasma half-life and induction of drug resistance.

To protect gemcitabine from rapid metabolic inactivation, a new prodrug (the squalenoyl gemcitabine, SQgem, fig.1), coupling squalene to gemcitabine has been conceived in our laboratory [1]. Squalene is an acyclic isoprenoid chain ($C_{30}H_{50}$); it is a precursor in the biosynthesis of sterols and, as such, a common cellular component. SQgem molecules spontaneously form nanoassemblies of about 130 nm in water. In a previous study we have demonstrated that SQgem packed in an inverted hexagonal phase [2]. The SQgem exhibited greater anticancer activity in vitro in human cancer cells and, in vivo, in experimental leukemia.

We have studied the effect of SQgem on phospholipidic bilayers of 1,2–dipalmitoyl–sn–3-phosphatidylcholine (DPPC), employed both as a simple model of biomembrane and as potential drug carriers.

Experimental methods

DPPC was purchased from Avanti Polar Lipids (purity 99%), squalene from Fluka (purity 97%) and Gemcitabine·HCl from Sequoia Research Products. SQGem was synthesized in our laboratory.

SQgem/DPPC mixtures were dissolved in chloroform and then dried under vacuum. The dry films were hydrated in excess water with ultrapure Millipore water and vortexed at 55°C.

Small and Wide Angles X-ray Diffraction (SAXS-WAXS) experiments were carried out at the Austrian SAXS beamline of Elettra Synchrotron, using a microcalorimeter (Microcalix) as a sample holder which allows X-Ray diffraction patterns to be recorded as a function of temperature [3].

Results

Amphiphilic SQ-gem molecules, having a polar group that can anchor them to the aqueous interface, insert between the acyl chains of lipids.

Small-angle X-ray diffraction experiments demonstrated that, at room temperature, SQgem promotes the formation of a bicontinuous cubic phase in DPPC ($0.06 <$ molar ratio $r =$ [SQgem]/[DPPC] <0.25). An example of SAXS pattern is shown in Figure 2. Seven Bragg peaks were observed, whose positions (q) are in the ratios $\sqrt{2}$, $\sqrt{3}$, $\sqrt{4}$, $\sqrt{6}$, $\sqrt{8}$, $\sqrt{9}/\sqrt{10}$, $\sqrt{12}$. These Bragg peaks index as the (110), (111), (200), (211), (220), (221/ 310), and (222) reflections of a Pn3m bicontinuous cubic phase.

This phase was pure in the composition range ($0.11< r < 0.25$) and coexisted with the lamellar gel phase in the range ($0.06< r <0.11$).

Increasing the temperature to 50°C gave rise to SAXS patterns characteristic of the lamellar liquid-crystalline L_α phase, as shown for example in Figure 3. The d-spacing was almost identical to that of pure DPPC; it increased slightly with increasing r.

Conclusions

At room temperature SQgem is able to induce the formation of a Pn3m bicontinuous cubic phase in DPPC membranes in excess water, even at low concentrations. Note that a cubic phase (Ia3d) of pure DPPC is observed only in a very small region of the phase diagram, at high temperature and very low hydration.

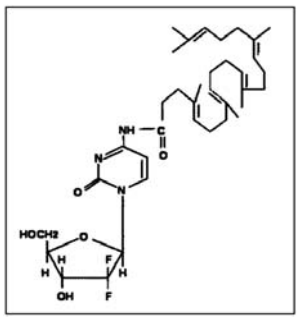

Figure 1. Squalenoyl gemcitabine (SQgem) prodrug structure.

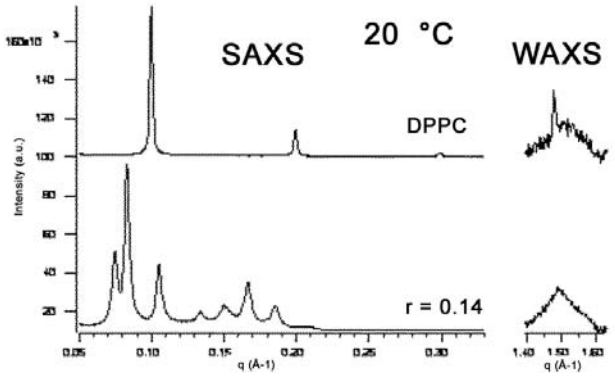

Figure 2. X-ray Diffraction profile at Small and Wide angles (linear scale) from pure DPPC and Sqgem/DPPC mixture at T=20°C. The composition is defined by molar ratio r = [SQgem]/[DPPC].

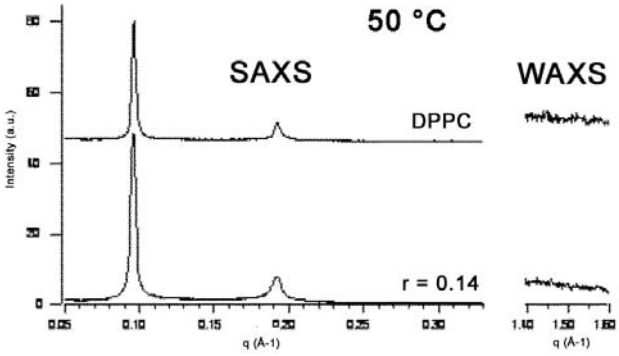

Figure 3. X-ray Diffraction profile at Small and Wide angles (linear scale) from pure DPPC and SQgem/DPPC mixture at T=50°C. The composition is defined by molar ratio r = [SQgem]/[DPPC].

References

[1] P.Couvreur et al; Squalenoyl nanomedicines as potential therapeutics; NanoLetters, 6(11), 2544-2548 (2006)

[2] P.Couvreur, L.H. Reddy, S.Mangenot, J.H.Poupaert, D.Desmaele, S.Lepetre Mouelhi, B.Pili, C.Bourgaux, H.Amenitsch and M.Ollivon; Discovery of new hexagonal supramolecular nanostructures formed by squalenoylation of an anticancer nucleoside analogue; Small 4(2), 247-253 (2008)

[3] M. Ollivon, G. Keller, C. Bourgaux, D. Kalnin, P. Villeneuve and P. Lesieur; DSC and high resolution X-ray diffraction coupling; J. Thermal Anal. and Calor. 85, 219–224 (2006)

ORIENTATION OF COLLAGEN FIBERS IN HUMAN ARTERIAL TISSUE UNDER STRAIN STUDIED BY FIBER DIFFRACTION

F. Schmid[1], F. Cacho[1], B. Sartori[1], M.Rappolt[1], G. Holzapfel[2], P. Laggner[1], and H. Amenitsch[1]

1.) Institute of Biophysics and Nanosystems Research, Austrian Academy of Sciences, Schmiedlstr. 6, 8042 Graz, Austria
2.) Graz University of Technology Institute of Biomechanics, Center of Biomedical Engineering, Kronesgasse 5-I, A-8010 Graz, Austria

The aim of our study is to understand how collagen fibers in human arteries behave when the tissue is exposed to load.

In mammalian tissue, collagen is widely found as building block of composite materials with mechanically diverse properties such as bone and skin. The key to provide strength as well as flexibility lies in the hierarchical architecture of collagen/matrix networks, which extends over several orders of magnitude in length scale. Arteries also contain collagen fibers, embedded in a matrix. There is great scientific interest in understanding the mechanics of arteries to improve existing medical treatments (e.g. ballon angioplasty) or to design artificial crafts. Modern constitutive mechanical models are capable of simulating the macroscopic stress-strain behavior quite accurately. Nevertheless, nanoscopic structural changes are not yet incorporated and therefore profound multilevel modeling is still missing. In constitutive models fibers are implemented via anisotropy directions, but they don't resemble real fiber networks yet. Moreover, precise *in situ* data about the fiber behavior like fiber orientation and fiber strain under macroscopic strain are not available.

Histological images show the presence of two main directions of collagen fibers. These are clearly visible when a cross-shaped sample is subjected to equi-biaxial stretch (Fig. 1). However in one dimensional stripe tests [3,4], only one diffraction peak is visible as soon as force is applied to the sample, as demonstrated in Fig. 2.

Another series of biaxial experiments have been designed to investigate this collapse of the collagen network by varying continuously the load conditions: from biaxial to uniaxial and reverse. These experiments demonstrated a relative fast orientation of the collagen network under medium strains in load directions. In particular, in this "locking" state during unaxial load the fibers cannot orient significantly more and a final angle of about 20° (FWHM) is reached independent of the direction - circumferential or longitudinal - in the tissue.

This phenomenon of fast orientation and locking under uniaxial load cannot be explained with the assumptions of an affine transformation of the fibers on the microscopic level, which are commonly used in the mathematical description of constitutive mechanical models. The experimental determination of the fiber behavior is therefore a prerequisite for the development and validation of new mechanical models.

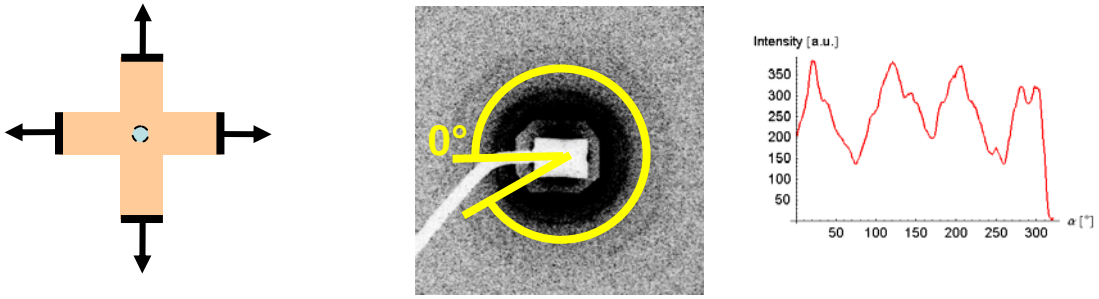

Figure 1: A cross shaped sample (left) was equi-biaxially stretched. The diffraction pattern (middle) shows the 2 main fiber directions. For clarity, the integration of the peak is shown on the right.

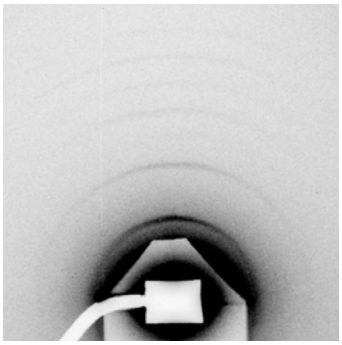

Figure 2: The diffraction pattern of a stripe sample. The sample was held vertically and stretched. Even detailed analysis of the peak areas reveals only one single peak.

Acknowledgements

The authors wish to thank C. Morello for technical support.

References

[1.] Cacho, F., Elbischger, P., Rodriguez, J., Doblare, M. & Holzapfel, G.A. 2007. A constitutive model for fibrous tissues considering collagen fiber crimp. Int J Non Linear Mech, 42, 391-402

[2.] Holzapfel,G.A. 2006. Determination of material models for arterial walls from uniaxial extension tests and histological structure. Journal of Theroetical Biology 238, 290-302.

[3.] Schmid, F., G.Sommer, M.Rappolt, P.Regitnig, G.Holzapfel, P.Laggner, and H.Amenitsch. 2006. Bidirectional Tensile Testing Cell for In Situ Small Angle X-ray Scattering Investigations of Soft Tissue. NIMB 246, 262-268.

[4.] Schmid,F., G.Sommer, M.Rappolt, C.A.J.Schulze-Bauer, P.Regitnig, G.A.Holzapfel, P.Laggner, and H.Amenitsch. 2005. In situ tensile testing of human aortas by time-resolved small-angle X-ray scattering. Journal of Synchrotron Radiation 12, 727-733.

EFFECT OF THE HUMAN ANTIMICROBIAL PEPTIDE LL-37 ON BACTERIAL MODEL MEMBRANES

E. Sevcsik, G. Deutsch, H. Amenitsch, and K. Lohner

Austrian Academy of Sciences, Institute of Biophysics and Nanosystems Research, Graz, Austria

Antimicrobial peptides are a class of substances that are thought to become an alternative to conventional antibiotics, which are often not effective anymore due to bacterial resistances. These peptides distinguish between foreign, e.g., bacterial and host cells based on differences in the composition of the cell membrane, however, the molecular mechanism of membrane disruption is still not clear [1]. The aim of our project was to study the interaction of the human antimicrobial peptide LL-37 with bacterial model membranes. DSC data showing a low-temperature phase transition at 29°C (Figure 1B) in conjunction with laboratory X-ray data indicated that LL-37 induces a ripple phase above 29°C in such membranes.

High resolution X-ray measurements and temperature scans were performed to allow us to further characterize this new phase thereby gaining information on the mode of interaction of LL-37 with bacterial membranes. This knowledge, in turn, will allow the design of novel peptide antibiotics killing their target cells by destruction of their phospholipid membrane integrity.

Specifically, the experiments were performed with mixtures of the negatively charged lipid dipalmitoyl-phosphatidylglycerol (DPPG) and the zwitterionic lipid dipalmitoyl-phosphatidylethanolamine (DPPE), which are the major components of cytoplasmic bacterial membranes. Liposomes of these lipids were prepared in the absence and presence of the peptide LL-37 and time-resolved scattering pattern were recorded following a defined temperature program. We succeeded in recording the SAXS and WAXS patterns as a function of temperature during a heating cycle, giving us detailed information of the low-temperature transition from the lamellar phase with a d spacing of 84 Å into the one with 124 Å (Figure 1A). Furthermore, high-resolution scattering pattern of the two phases were recorded that were analyzed with a global, full-q-range fitting model [2]. Parallel to the increase of the d spacing, also the phosphate-phosphate distance increases from 46.2 Å to 50.4 Å, which is an indication of a reorientation of the peptide in the lipid bilayer possibly involving the formation of a ripple phase. However, the second part of the project, identification of the ripple phase, was not as successful. Further experiments on oriented samples are planned to address this point.

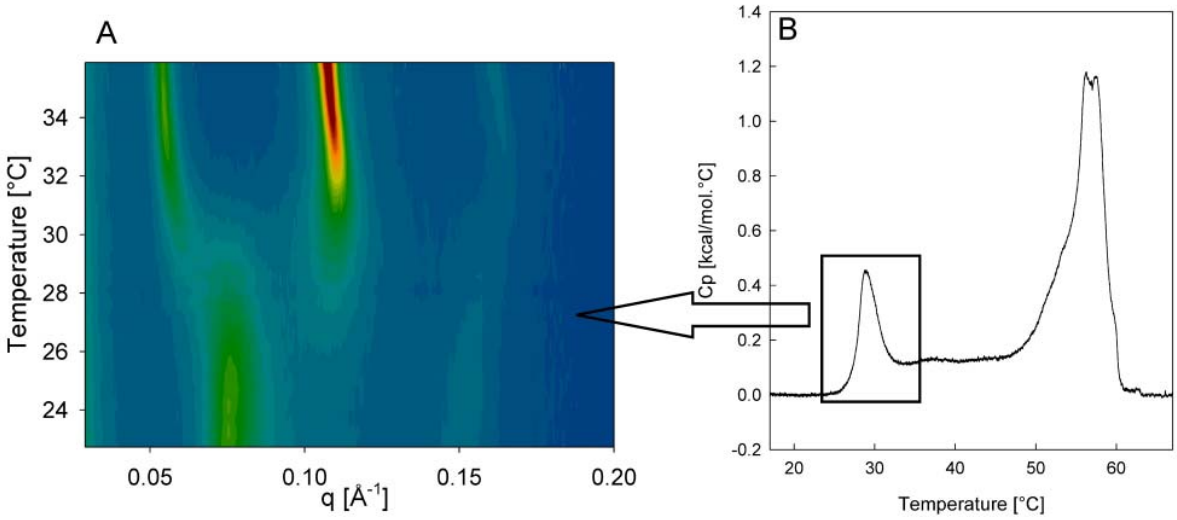

Figure 1. (A) Time-resolved SAXS patterns of the low-temperature transition observed for DPPE/DPPG 1/1 in the presence of 4 mol% LL-37. Exposure time was 60s for each frame. (B) Differential scanning calorimetry data of DPPE/DPPG 1/1 in the presence of 4 mol% LL-37. Scans were recorded at 30°/h.

References:

[1] B. Bechinger, K. Lohner, Detergent-like actions of linear amphipathic cationic antimicrobial peptides, Biochim.Biophys.Acta 1758, 1529-1539 (2006)

[2] G. Pabst, R. Koschuch, B. Pozo-Navas, M. Rappolt, K. Lohner, P. Laggner, Structural analysis of weakly ordered membrane stacks, J.Appl.Crystallogr. 63, 1378-1388 (2003)

CALCIUM TRIGGERED Lα-H2 PHASE TRANSITION MONITORED BY COMBINED RAPID MIXING AND TIME-RESOLVED SYNCHROTRON SAXS

A. Yaghmur, P. Laggner, B. Sartori, and M. Rappolt

Institute of Biophysics and Nanosystems Research (IBN), Austrian Academy of Sciences, Graz, Austria

Combining rapid mixing and X-ray scattering techniques has become an important tool for investigating the dynamics of structural transitions in the self-assembled systems [1-3]. It allows in-situ millisecond time-resolved experiments. In our present study, we carried out stopped-flow experiments combined with synchrotron SAXS for monitoring in-situ the structural transitions in DOPG/MO-based vesicles induced by rapidly added Ca^{2+} solutions. Our initial intention was to gain insight into the kinetics and the dynamics of the Ca^{2+}-induced self-assembly, and to detect also the possible formation of intermediate phases. The applied set-up is schematically illustrated in Figure 1.

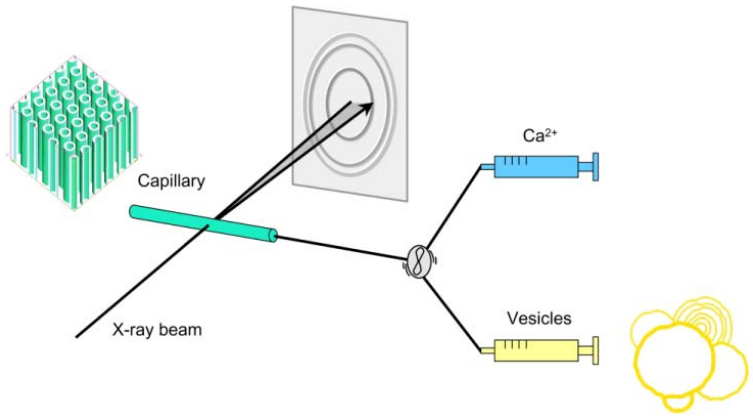

Figure 1. Schematic of the combined stopped-flow and synchrotron SAXS set-up. In the stopped-flow apparatus, one syringe contained a buffer with Ca^{2+} ions, whereas the other contained DOPG/MO-based vesicles. The rapid mixing was conducted within 10 ms and the formation of the inverse hexagonal phase (H_2) was followed by millisecond time-resolved SAXS.

Under static conditions, it was reported that two different bicontinuous cubic phases (Im3m or Pn3m) form by the addition of Ca^{2+} ions to DOPG/MO-based ULVs and MLVs [4]. However revisiting the same studies but under rapid-mixing conditions, fast and unexpected bilayer to monolayer transitions were observed, i.e. already at low Ca^{2+} concentrations the L_α phase transformed within milliseconds into the H_2 phase (Figure 2). Few seconds after the rapid mixing, no further changes in the fully formed H_2 phase were detected [5].

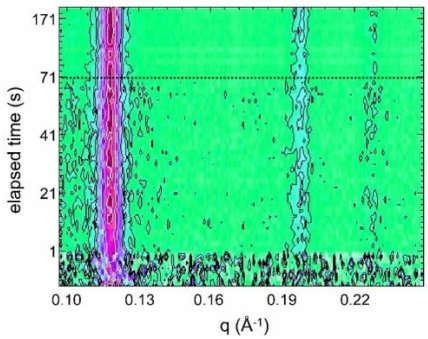

Figure 2. Time-resolved X-ray pattern of the rapid calcium-triggered H_2 phase formation at 50 °C. The vesicle dispersion contained DOPG/MO with a molar ratio 30:70 (7 wt% lipid), and the final salt concentration was 20 mM. The contour plot clearly displays the first three reflections of the H2 phase; no indication for the formation of an intermediate phase is spotted.

The driving force for the fast L_α-H_2 phase transition is the strong electrostatic interactions of Ca^{2+} ions with the phosphate group of the anionic DOPG lipid. The divalent cation is screening the repulsive forces between the negative charges of DOPG molecules in the membrane, and its strong binding enhances the negative spontaneous curvature of the

monolayers and causes a rapid collapsing of the vesicles. The rapid loss of the bilayer stability and the reorganization of the lipid molecules within ms support the argument that the transition mechanism is based on a leaky fusion of the vesicles.

At 20 °C, the transition from L_α to H_2 phase occurs via an intermediate phase with a bilayer structure (possibly Pn3m phase, Figure 3). This intermediate structure has a short lifetime (100-400 ms). In contrast at 50 ˚C, the impact of Ca^{2+} ions on the DOPG/MO membrane curvature is higher, and no formation of this intermediate phase was spotted.

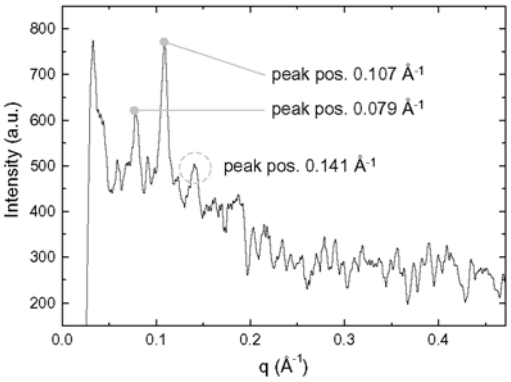

Figure 3. Intermediate formation at 20 ˚C. The SAXS pattern is averaged from the data taken in the range of 100-400 ms after the rapid mixing. It indicates a possible formation of bicontinuous cubic phase of the symmetry Pn3m. The observed Bragg peaks and their presented q-values, suggest a coexistence with the H_2 phase.

Our study demonstrates further that the sample preparation can have great influence on the calcium-induced nanostructures. For the formation of 'pellets', the excess of water has to be removed from the vesicular system, as done in ref. [4], and then under the influence of Ca^{2+} ions the formation of the cubic Im3m or Pn3m phases is observed (the published results have been reproduced). However, different results are obtained when real vesicles (lipidic nanostructures in excess water) are exposed to the same salt concentration. In this case, the H_2 phase forms and it is stable for at least two weeks. The differences are most probably explained throughout lower Ca^{2+} affinity in the 'pellet' situation or alternatively by the unintentional removal of a fraction of DOPG molecules, which would increase the impact of MO lipids in the remaining pellet system. These findings also show how important it is to study self-assembled nanostructures under realistic excess of water conditions.

Acknowledgments. AY is grateful to the Support by the European Community - Research Infrastructure Action under the FP6 "Structuring the European Research Area" Programme (through the Integrated Infrastructure Initiative "Integrating Activity on Synchrotron and Free Electron Laser Science") for refunding the expenses during the SAXS investigations in ELETTRA.

References:

[1] M. Gradzielski; Investigations of the dynamics of morphological transitions in amphiphilic systems; Curr. Opin. Colloid Interface Sci. 9, 256-263 (2004)
[2] M. Gradzielski; Vesicles and vesicle gels - structure and dynamics of formation; J Phys. -Condensed Matter 15, R655-R697 (2003)
[3] P. Panine, S. Finet, T.M. Weiss and T. Narayanan; Probing fast kinetics in complex fluids by combined rapid mixing and small-angle X-ray scattering; Adv. Colloid Interface Sci. 127, 9-18 (2006)
[4] T.S. Awad, Y. Okamoto, S.M. Masum and M. Yamazaki; Formation of cubic phases from large unilamellar vesicles of dioleoylphosphatidylglycerol/monoolein membranes induced by low concentrations of Ca^{2+}; Langmuir 21, 11556 (2005)
[5] A. Yaghmur, P. Laggner, B. Sartori and M. Rappolt; Calcium Triggered L -H2 Phase Transition Monitored by Combined Rapid Mixing and Time-Resolved Synchrotron SAXS; PLoS ONE, In press

MONOELAIDIN AQUEOUS DISPERSIONS: TUNING THE INTERNAL NANOSTRUCTURE CURVATURE FROM L_α TO V_2

A. Yaghmur, P. Laggner, and M. Rappolt

Institute of Biophysics and Nanosystems Research (IBN), Austrian Academy of Sciences, Graz, Austria

Cubosomes (aqueous dispersions of inverted type bicontinuous cubic phases, V_2) and hexosomes (aqueous dispersions of inverted type hexagonal phase, H_2) have very unique properties that set the stage for new potential applications in the area of food and pharmaceutical technologies [1-3]. These nanostructured fluids are tailored for solubilization of active molecules with different physicochemical properties (hydrophilic, hydrophobic, and amphiphilic active components), and for solubilizing proteins, and may also serve as nano-reactors [1;4].
In literature, monoelaidin (ME)/water system represents a good example on the lamellar-nonlamellar transition during membrane fusion analogue to that occurs in the biological cells under certain circumstances. In this context, one feature of the thermotropic behavior of the non-dispersed ME/water system that makes it of interest is the unique direct transformation under full hydration conditions from L_α to V_2 [5;6]. This behavior is very intriguing and it is different from that observed during investigating the impact of temperature on the majority of fully hydrated monoglycerides-based systems. For instance, the order of the phase transitions in monoolein (MO)/water and monolinolein (MLO)/water systems under full hydration conditions is V_2 (at ambient temperatures) via H_2 to fluid isotropic inverse micellar solution (L_2, at high temperatures) [7;8]. In a recent investigation, the analogue transformation from cubosomes via hexosomes to ELP (emulsified L_2 phase) was observed for the MLO-based aqueous dispersions during heating cycle from 25 to 94 ˚C [8].

In the present study, we report on the preparation and the characterization of colloidal nanostructured aqueous dispersion of the binary ME/water system. The stabilization of the dispersed particles was done by adding the polymeric stabilizer Pluronic F127 during the dispersing procedure. Herein, our major goal is to focus on answering the following main question: is it possible to induce a direct transition of vesicles to cubosomes by heating ME-based aqueous dispersion? For this purpose, it is important also to compare the internal nanostructure of ME-based aqueous dispersion to that of its corresponding bulk non-dispersed phase coexists with excess water.

Figure 1A presents the SAXS scattering curves for two ME-based aqueous dispersions and their corresponding bulk non-dispersed fully hydrated ME system at 20 °C. The dispersions were formed at different F127 concentrations: 0.25 and 0.5 wt%, respectively. It is worthy noting the nanostructure of the fully hydrated ME non-dispersed phase is well preserved (the internal nanostructure is identical to that of the corresponding non-dispersed phase). In both samples, the results show three peaks in the characteristic ratio for a lamellar (L_α) phase with a *d*-spacing of 50.4 Å. As shown in Figure 1B, at higher temperature (36 °C), the scattering curve (red line) shows the characteristic peaks for a cubic Im3m structure (cubosomes) and intriguingly the temperature increase shifts the peaks to lower q values and increases the structure parameter (the mean lattice parameter, α, is 167.3 Å). This behavior is very interesting and it is different for that observed during investigating the majority of monoglycerides-based systems [7;8]. For instance, it was found in MLO/water system that increasing temperature shifts the peaks to higher *q* values (the same trend is also valid for MO/water mixture and other studies done by Caffrey and co-workers) [7;8]. With a further increase of temperature, the observed peak positions suggest the formation of a dispersion with internal *Pn3m* cubic phase (bicontinuous, diamond type CD with a mean lattice

parameter, α, of 85.7 Å). In addition, the observed peaks shift to higher *q* value and there is a decrease in the lattice parameters. In a recent report, Conn et al. [6] proposed that the L_α phase in the binary non-dispersed ME/water system consists of closely packed onion vesicles. They hypothesized that the onion vesicle confines a highly swollen cubic phase that acts as a seed for the formation of an ordered bicontinuous cubic phase via the formation of stalks and then fusion pores.

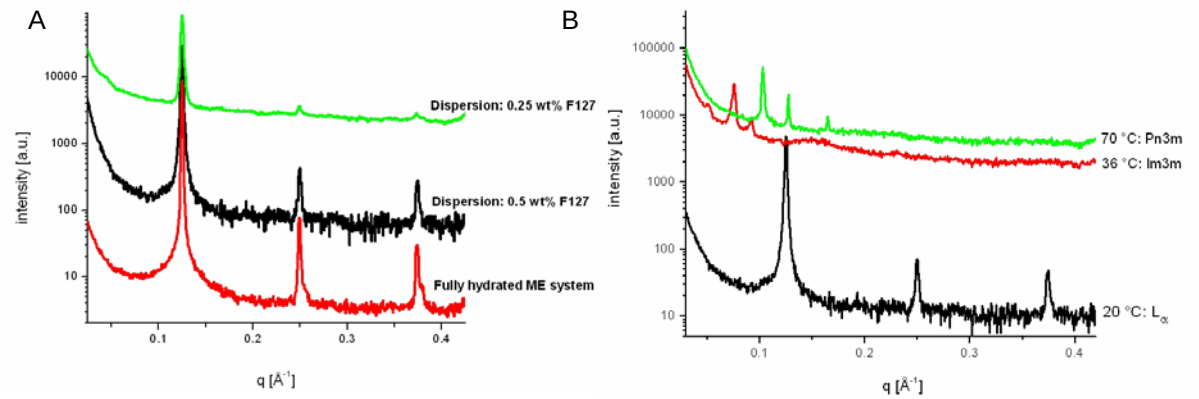

Figure 1. (A) SAXS scattering curves comparing the ME-based aqueous dispersion (black line) with the non-dispersed fully hydrated bulk system (red line) at 20 °C. (B) the scattering curves of the ME dispersions at three different temperatures

Figure 2 shows an example of the temperature induced internal structural L_α-Im3m-Pn3m phase transitions observed in ME-based dispersion consisting of 4.5 wt% ME, 0.50 wt% F127, and 95 wt% PBS buffer in a temperature range of 20-80 °C. It is important mentioning that F127 is not effective stabilizer for the ME dispersion. It is significantly less stable than MO-based cubosome and hexosome particles and thus looses its stability few days after preparation.

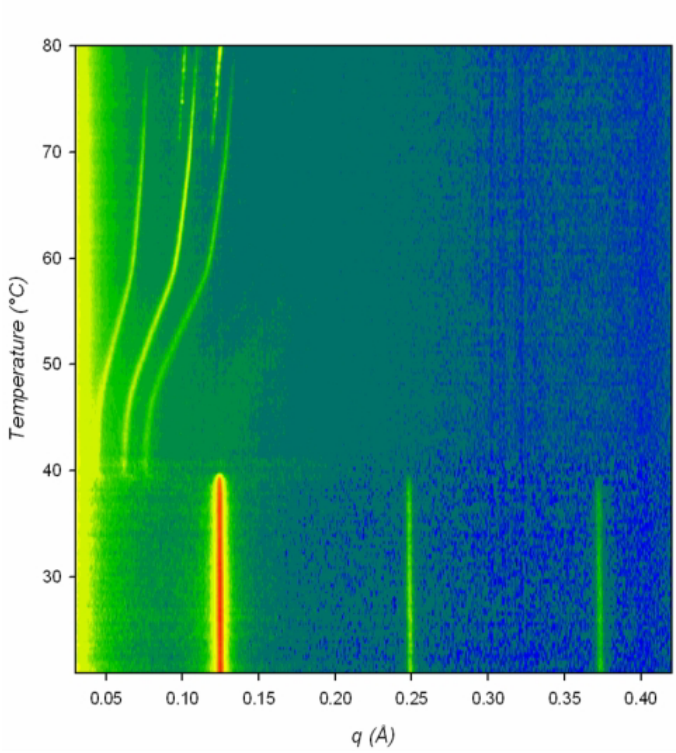

Figure 2. A representative contour plot for the ME aqueous dispersion: the internal Lα-Im3m-Pn3m transition is induced during heating the liposomal dispersion.

Acknowledgments We thank Dr. Manfred Kriechbaum for fruitful discussions on the behavior of ME/water system.

References:

[1] M. Malmsten; Soft drug delivery systems; Soft Matter 2, 760-769 (2006)
[2] K. Larsson; Aqueous dispersions of cubic lipid-water phases; Curr. Opin. Colloid Interface Sci. 5, 64-69 (2000)
[3] A. Yaghmur, L. de Campo, L. Sagalowicz, M.E. Leser and O. Glatter; Emulsified microemulsions and oil-containing liquid crystalline phases; Langmuir 21, 569-577 (2005)
[4] A. Angelova, B. Angelov, B. Papahadjopoulos-Sternberg, M. Ollivon and C. Bourgaux; Proteocubosomes: nanoporous vehicles with tertiary organized fluid interfaces; Langmuir 21, 4138-4143 (2005)
[5] C. Czeslik, R. Winter, G. Rapp and K. Bartels; Temperature- and pressure-dependent phase behavior of monoacylglycerides monoolein and monoelaidin; Biophys J. 68, 1423-1429 (1995)
[6] C.E. Conn, O. Ces, X. Mulet, S. Finet, R. Winter, J.M. Seddon and R.H. Templer; Dynamics of structural transformations between lamellar and inverse bicontinuous cubic lyotropic phases; PRL 96, 108102 (2006)
[7] H. Qiu and M. Caffrey; The phase diagram of the monoolein/water system: metastability and equilibrium aspects; Biomaterials 21, 223-234 (2000)
[8] L. de Campo, A. Yaghmur, L. Sagalowicz, M.E. Leser, H. Watzke and O. Glatter; Reversible phase transitions in emulsified nanostructured lipid systems; Langmuir 20, 5254-5261 (2004)

SELF-ASSEMBLED NANOSTRUCTURES OF MONOELAIDIN-ELAIDIC ACID AND MONOELAIDIN-OLEIC SYSTEMS: BULK VS. AQUEOUS DISPERSIONS

A. Yaghmur, M. Kriechbaum, P. Laggner, and M. Rappolt

Institute of Biophysics and Nanosystems Research (IBN), Austrian Academy of Sciences, Graz, Austria

The lipid composition plays a crucial role on modulating the lamellar-nonlamellar transition in biomembranes. The membrane structure is influenced by the presence of free fatty acids (FFAs) [1]. In general, the level of FFAs in biomembranes is low (less than 1 wt% of total lipid content) but it is high in certain membranes (such as the small intestine brush border membranes). Oleic acid (OA)-rich foods are important for providing this fatty acid to the plasma membranes [1]. It is important to understand how FFAs modulate the membrane structure and function.

In literature, monoelaidin (ME)/water system represents a good example on the lamellar-nonlamellar transition during membrane fusion analogue to that occurs in the biological cells under certain circumstances. As a continuation to our investigations on the dispersed and non-dispersed fully hydrated ME-water nanostructures [2], we are interested to understand the impact of loading oleic acid (OA) and its congener elaidic acid (EA) on these self-assembled nanostructures in both dispersed and non-dispersed states.
In the present study, we report on the structural characterization of different self-assembled nanostructures of the ternary ME/OA/water and ME/EA/water systems at different OA/ME and EA/ME weight ratios. OA and EA have the same molecular weight but with different molecular shape. EA has a *trans* double-bond located at the 9,10 position in its straight acyl chain (rod-shaped molecule). However, its counterpart OA has a different configuration (*cis* double-bond in the carbon atom backbone), which causes a "kink" in the middle of the molecule (wedge-shaped molecule) (Figure 1).

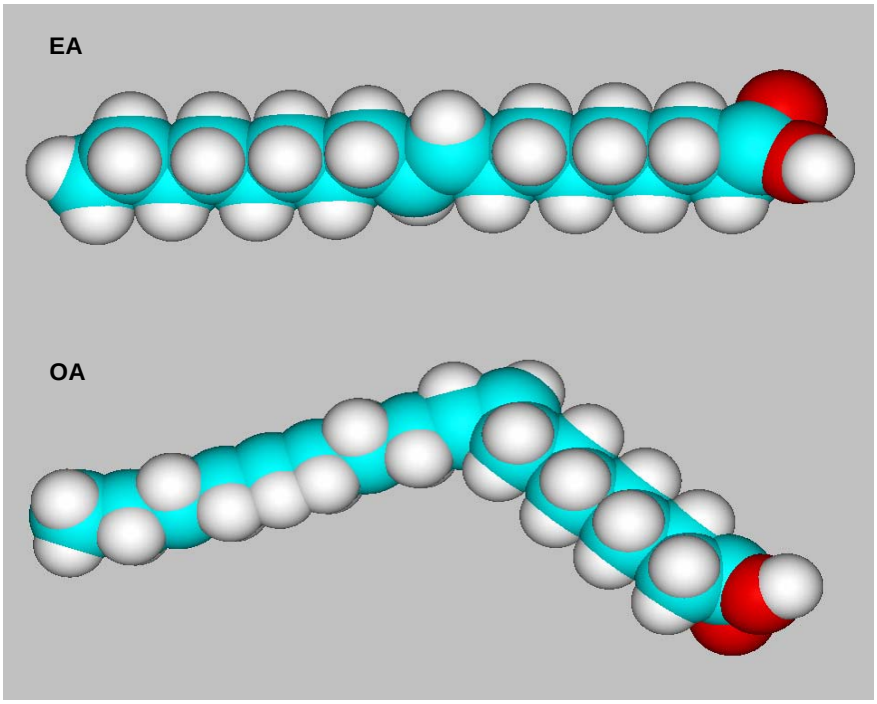

Figure 1. The molecular structure of EA and OA molecules

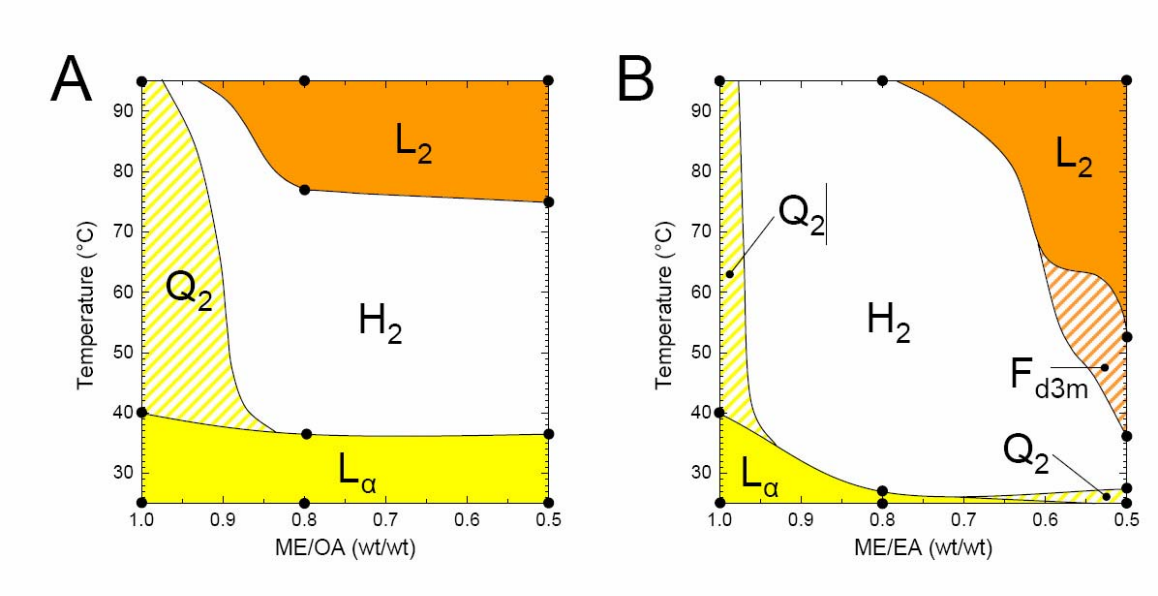

Figure 2. A partial temperature-water content phase diagrams for ME/OA/water and ME/EA/water ternary systems.

Figure 2 presents a partial phase diagrams of the ternary ME/OA/water (A) and ME/EA/water systems (B) as done by investigating different samples with synchrotron SAXS.

In addition, we were investigated the internal nanostructures of the EA- and (OA-) loaded ME aqueous dispersions stabilized by the polymeric stabilizer F127 (not shown in this contribution).

References

[1] S.S. Funari, F. Barcelo and P.V. Escriba; Effects of oleic acid and its congeners, elaidic and stearic acids, on the structural properties of phosphatidylethanolamine membranes; J Lipid Res. 44, 567-575 (2003)
[2] A. Yaghmur, M. Almgren, P. Laggner and M. Rappolt; Unpublished data

SWAX STUDIES ON FIBROUS COLLAGEN MEMBRANES UNDER THE INFLUENCE OF DIFFERENT ANTIBIOTICS

P. Zoumpoulakis[1], E. Siapi[1], M. Rappolt[2], and T. Mavromoustakos[1]

1.) Laboratory of Molecular Analysis, Institute of Organic and Pharmaceutical Chemistry, National Hellenic Research Foundation, Athens, Greece.
2.) Institute of Biophysics and Nanosystems Research, Austrian academy of Sciences, Schmiedlstr. 6, Graz, Austria

Our scope was to study the thermal changes caused by the antibiotic gentamycin and the antihypertensives losartan and captopril in different concentrations using two different fibrous membranes. In particular, in the first preparation used was 0.4% formaldehyde and the second 0.2% glutaraldehyde. Similarities but also significant differences in the thermal profiles between the two kinds of membranes were observed with previous experiments. More specifically, both membranes showed two distinct endothermic events located between 40−80 °C (T1 region) and 80−130 °C (T2 region). The first region at lower temperature range is attributed to the collapse of the triple helical domain, while the second to their dehydration.

Small angle X-ray experiments were performed on fibrous membranes prepared in formaldehyde and glutaraldehyde including drug gentamycin in concentrations of 0.5, 2 and 3%. None of them has shown any repeatability in structure even though they were tested in different beaming angles.

Fibrous membranes also prepared in formaldehyde were tested including the antihypertensive drug captopril in concentrations of 0.5 and 3% giving no diffraction orders as well.
Transparent collagen membranes including gentamycine in concentrations of 0.5 and 3% and in a temperature range of 30-130 °C using 3 °C/min step, have shown a transition at 58 and 88 °C respectively.

Fibrous membranes prepared in formaldehyde were tested using an image plate (25cm). Results have shown that fibrous membranes including the antihypertensive drug losartan and gentamycine at concentration of 0.5% show repeatability at 12.0 and 11.4 Å.
In case of 1.5 and 3% concentration values, we have noticed that 2 peaks appear left and right of the main peak at $d_1 \approx 15$ Å and $d_2 \approx 8.5$ Å. Moreover, hydration of the sample causes the disappearance of the peaks.

These results are being processed while other complementary techniques are applied to further examine the structural changes of collagens caused from the presence of drugs.

Chemistry

IN-SITU, TIME RESOLVED GI-SAXS STUDIES OF THE MESOSTRUCTURING PROCESS OF SILICA NANOFILAMENTS IN CONFINED ENVIRONMENTS UNDER VACUUM OR VARYING RELATIVE HUMIDITY

D. C. Arnold[1], J. M. O'Callaghan[1], N. Petkov[1], H. Amenitsch[2], Michael A. Morris[1], and J. D. Holmes[1]

1.) Materials and Supercritical Fluids Group, Department of Chemistry, University College Cork, Cork, Ireland
2.) Institute for Biophysics and Nanosystems Research, Austrian Academy of Sciences, Schmiedlstraße 6, 8042, Graz, Austria

In recent years considerable attention has focused on nanoporous materials primarily due to their potential application as building blocks for constructing nanoscale architectures. In particular surfactant templated mesostructured materials, with pore-sizes between 2 and 10 nm, have been utilised as catalyst supports, nano-reactors for a variety of chemical reactions and as hosts for nano-structured materials with appealing properties. [1-3] If these materials are to be truly utilized for the potential construction of nanoelectronic and optoelectronic device architectures, the synthesis of preferentially aligned ordered arrays of mesoporous materials with controllable dimensions is crucial. At UCC our research has centred on the synthesis of highly aligned mesoporous silica thin films (MTFs), grown on etched silicon substrates and periodic mesoporous organosilica (PMO) materials formed within the pores of anodic aluminium oxide (AAO) membranes, which act as hierarchical templates for the assembly of such highly ordered porous structures. [4]

Experiments conducted on the Austrian SAXS beamline at Elettra have focussed on investigating the mesostructuring process of PMO materials within the pores of AAO membranes within different drying environments. Previous experiments conducted on the SAXS beamline have shown that the structure of the PMO nanofibres is not only critically dependent on the confinement effects and the drying environment but also on the amount of organic material present in the framework as shown in figure 1.

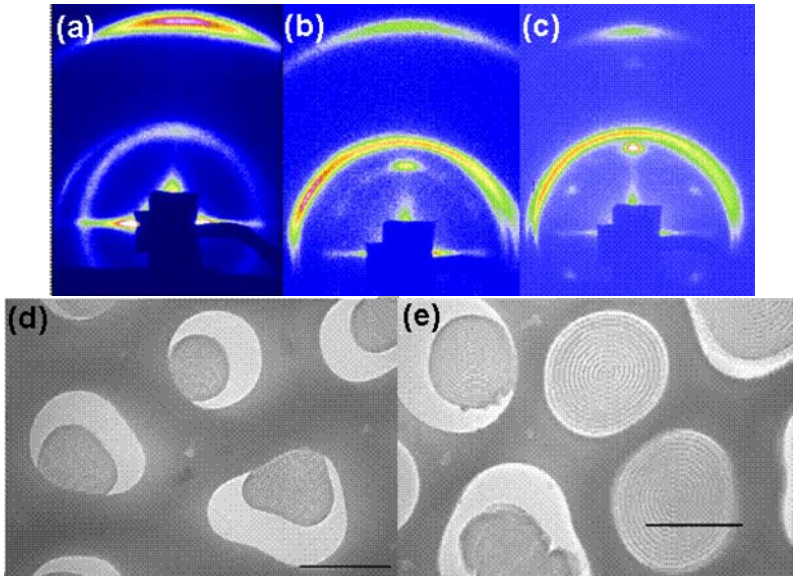

Figure 1. Typical SAXS patterns collected for (a) 75:25, (b) 50:50 and (c) 100:0 organic:silica ratio PMOs grown within the pores of an AAO membrane. (d) Transmission electron microscopy image showing the parallel pore arrangement of the mesopores and (e) Transmission electron microscopy image showing the perpendicular/lamellar pore arrangement of the mesopores. Scale bars represent 200 nm.

Understanding the effects that changes in the environment, such as relative humidity, have on the evaporation induced self assembly (EISA) mechanism is critical if the pore morphology is to be controlled. In order to elucidate these mechanisms in-situ, time resolved experiments were performed and SAXS patterns collected. Figure 2 shows a typical set of time resolved SAXS patterns collected for a PMO material drying in a 20 % humid atmosphere. It can be seen that initially there are no spots arising from any structure. As the gel begins to evaporate diffraction spots, readily assigned to the expected [100] reflections of the columnar structure, can be seen to occur. This structure then persists over the time frame of the experiment with no further structural changes. Changing the drying environment (not presented here) resulted in observable changes within the SAXS patterns collected and allowed us to further understand the EISA mechanisms involved.

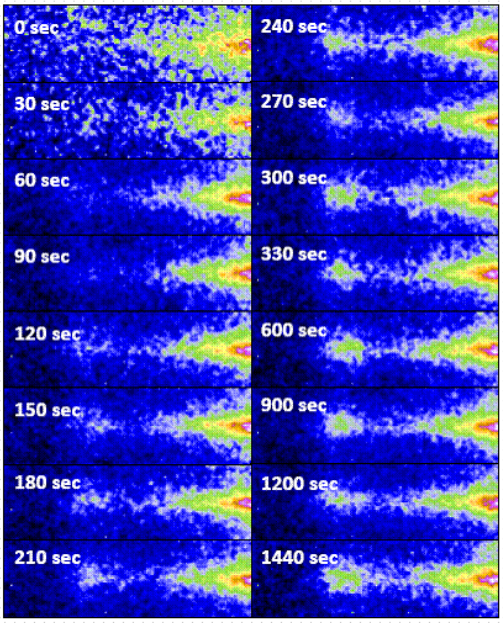

Figure 2. In-situ, time resolved SAXS measurements performed on a 50:50 organic:inorganic PMO material, left to dry in ambient conditions in a relative humidity of 20%.

In summary GI-SAXS has proved an essential tool for the analysis of mesoporous materials. Preliminary results collected for PMO thin films indicate that the use of confining architectures acts to promote the ordering of the mesopores providing highly ordered porous templates for possible future device applications. Furthermore, the mesostructuring/self assembly processes can be followed by conducting in-situ; time resolved GI-SAXS measurements. This has allowed us to probe the structural arrangement as a function of humidity and organic:inorganic ratio in ambient conditions and in the presence of a vacuum. These studies are essential if the mesoporous structure of these materials is to be controlled and ultimately exploited in applications.

References

[1] J. S. Beck, J. C. Vartuli, W. J. Roth, M. E. Leonowicz, C. T. Kresge, K. D. Schmitt, C. T. W. Chu, D. H. Olson, E. W. Sheppard, S. B. McCullen, J. B. Higgins and J. L. Schlenker; A New Family of Mesoporous Molecular Sieves Prepared with Liquid Crystal Templates; J. Am. Chem. Soc. 114, 10834-10843 (1992)
[2] A. P. Wright and M. E. Davis; Design and Preparation of Organic-Inorganic Hybrid Catalysts; Chem. Rev. 102, 3589-3614 (2002)
[3] B. J. Scott, G. Wirnsberger and G. D. Stucky; Mesoporous and Mesostrucured Materials for Optical applications; Chem. Mater. 13, 3140-3150 (2001)
[4] R. L. Rice, D. C. Arnold, M. T. Shaw, D. Iacopina, A. J. Quinn, H. Amenitsch, J. D. Holmes and M. A. Morris; Ordered Mesoporous Silicate Structures as Potential Templates for Nanowire Growth; Adv. Func. Mater. 17, 133-141 (2007)

STUDY OF BICELLAR SYSTEMS CONTAINING CERAMIDES USING SAXS

L. Barbosa-Barros[1], M. Rappolt[2], C.V. Texeira[3], H. Amenitsch[2], A. de la Maza[1], and O. López[1]

1.) Chemical and Environmental Research Institute of Barcelona (IIQAB-CSIC), Barcelona, Spain
2.) Institute for Biophysics and Nanosystems Research, Austrian Academy of Sciences c/o Sincrotrone Trieste, Italy
3.) Center of biophysical studies, Dept. Bioquímica i Biología Molecular, Universitat Autònoma de Barcelona, Spain

Bicelles are discoidal aggregates constituted in most cases by a flat dimyristoylphosphocholine (DMPC) bilayer, stabilized by a rim of dihexanoylphosphocholine (DHPC) in water [1]. In dependence on the molar ratio of both lipids, presence of other components, hydration and temperature, a number of different phases are present on the systems [1]. Nowadays bicelles are used as membrane models to orient proteins that can be inserted in their structure. For this reason, the inclusion in bicelles of specific cell membrane lipids such as ceramides (Cer) is a matter of interest. We previously studied the self assembly properties of various amphiphiles, the structural transitions involved in the interactions of surfactants with liposomes [2], and the influence of Cer in these interactions [3]. These works have demonstrated the important role of these lipids in the stability and permeability of bilayers. In recent studies, we have reported the inclusion of Cer in the DMPC/DHPC bicellar structure by using NMR, dynamic light scattering and freeze fracture electron microscopy, and some of the different structures formed in these systems have been characterized [4,5]. In addition, we have studied the behaviour of the bicellar systems when DMPC is replaced by dipalmitoylphosphocholine (DPPC) [6], which has higher gel-to-liquid transition temperature (Tm) than DMPC. Results obtained indicated that bicelles and, particularly, bicelles containing Cer are very sensitive to small changes on composition and temperature. Monitoring these changes is crucial to understand processes in which phospholipids and Cer are involved and requires a very sensitive and precise methodology. Small-angle X-ray scattering (SAXS) using Synchrotron radiation, which has proven to be a powerful technique for determining different phospholipid structures [2,7] seems to be one of the best options to study bicellar systems.

In this work the effect of the temperature (from 5ºC to 70ºC) on bicellar systems formed by different phospholipids and containing increasing amounts of Cer was evaluated. The following systems were studied in the mentioned temperature range: DMPC/DHPC molar ratio 2 containing 0%, 2.5% and 5% Cer (percentages in weight) and DPPC/DHPC molar ratio 3.5 also containing 0%, 2.5% and 5% Cer. SAXS measurements were performed at the Austrian SAXS station at the synchrotron light source ELETTRA (Trieste, Italy). The 2D scattering pattern was measured using a *mar345* image plate detector which covered the q range $q = 4\pi\sin\theta/\lambda$ between 0.03 and 0.6 $Å^{-1}$ at a photon energy of 8 keV. Heating rate at data collection times between 1 and 4 s. Samples were measured in quartz capillaries, which were placed in a sample holder block of brass. This sample holder block was in thermal contact with a water circuit, i.e., it was connected to a water bath with a freely programmable control unit (Unistat CC, Huber, Offenburg, Germany). The 2D data stored in TIFF format was treated with Fit2D software. Data analysis was performed using IGOR Pro 5 and reflections were plotted as a function of the scattering vector q.

Our results indicate that inclusion of Cer affects the termotropic behaviour of these systems. In samples containing 0% and 2.5% Cer, at least a phase transition was clearly detected at temperatures below the Tm of the long-chain phospholipid. In the systems with the highest

amount of Cer this transition was not so clearly visualized. The X-ray reflections detected at different conditions could be compatible with the presence of a variety of structures. In DMPC/DHPC samples, spherical objects could be transformed in large cylindrical aggregates by effect of the increasing temperature. The presence of Cer could promote the formation of bigger structures. For DPPC/DHPC samples, discoidal objects could be present at low temperatures. When temperature rises, systems could be formed by multilamellar vesicles and/or stacked bilayers. The presence of Cer in DPPC/DHPC seems to cause disorganization in these systems. Figure 1 plots the small angle X-ray diffraction patterns in a temperature range from 20ºC to 60ºC corresponding to DPPC/DHPC bicelles without Cer (A) and with 2.5% Cer (B) and 5% Cer (C). We are aware that in order to describe appropriately the behaviour and morphological features of these systems an accurate fitting work of the scattering curves is needed, this work is being currently performed.

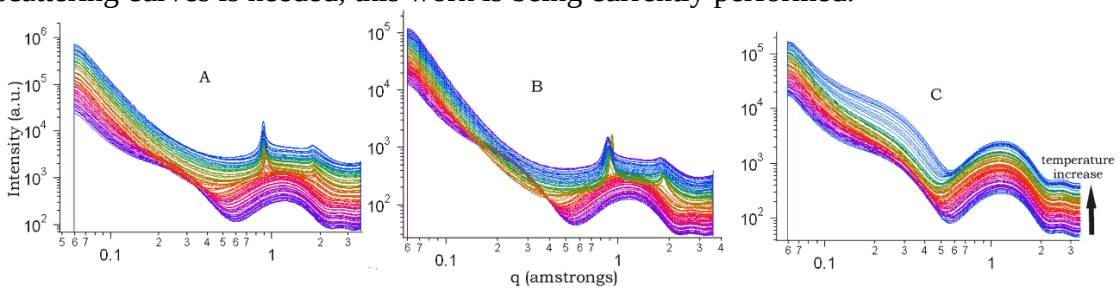

Figure 1. X-ray scattering patterns of DPPC/DHPC bicelles without Cer (A) and with 2.5% Cer (B) and 5% Cer (C) in a temperature range from 20ºC to 60ºC.

References

[1] M.P. Nieh, V.A. Raghunathan, C.J. Glinka, T.A. Harroun, G. Pabst, J. Katsaras; The magnetically alignable phase of phospholipid "bicelle" mixtures is a chiral nematic made up of worm-like micelles; Langmuir 20, 7893-7897 (2004)

[2] J. Pereira-Lachataignerais, R. Pons, H. Amenitsch, M. Rappolt, B. Sartori, O. López; Effect of sodium dodecyl sulfate at different hydration conditions on dioleoyl phosphatidylcholine bilayers studied by grazing incidence X-ray diffraction; Langmuir 22,5256-5260 (2006)

[3] O. López, M. Cócera, A. de la Maza, L. Coderch, J.L. Parra; Alterations in stratum corneum lipid liposomes due to the action of Triton X-100: influence of the level of ceramides on this process; J. Controlled Rel. 68, 387-396 (2000)

[4] L. Barbosa-Barros, A. de la Maza, C. López-Iglesias, O. López; Ceramide effects in the bicelle structure; Colloids Surf. A 317, 576-584 (2008)

[5] L. Barbosa-Barros, A. de la Maza, P. Walther, J. Estelrich, O. López; Morphological effects of ceramides on DMPC/DHPC bicelles; J. Microscopy 230, 16-26 (2008)

[6] L. Barbosa-Barros, A. de la Maza, J. Estelrich, A. M. Linares, M. Feliz, P. Walther, R. Pons, O. López; Penetration and growth of DPPC/DHPC bicelles inside the stratum corneum of the skin; Langmuir (*in press*)

[7] M. Cócera, O. López, R. Pons, H. Amenitsch, A. de la Maza; Effect of the electrostatic charge on the mechanism inducing liposome solubilization: a kinetic study by synchrotron radiation SAXS; Langmuir 20, 3074-3079 (2004)

THE EFFECT OF MESOPOROSITY ORDERING ON THE CRYSTALLISATION OF TiO_2 THIN FILM ASSESSED BY GISAXS AND THERMAL ELLIPSOMETRY ANALYSIS

J.D. Bass [1], C. Boissière[1], M. Kuemmel[1], and D. Grosso*[1]

1.) Laboratoire de Chimie de la Matière Condensée de Paris, Université Pierre et Marie Curie – Paris 6 and CNRS, 4 place Jussieu, 75252 Paris 05, France
*e-mail: grosso@ccr.jussieu.fr

In-situ thermal ellipsometric analysis is used to elucidate new and fine-scale details on the thermally driven densification, pyrolysis, crystallization, and sintering of ordered mesoporous titania thin films prepared by Evaporation-Induced-Self-Assembly.[1] The role of the degree of mesoporosity ordering deduced from GISAXS investigation is specifically examined. The ordering is shown to have unique and often substantial effects on the subsequent viscous sintering, crystallization and diffusive sintering phenomena taking place during thermal treatment. The evolution of both the porosity and the chemical processes occurring inside these materials are evaluated up to the final material. The latter is shown to be strongly dependent on the presence of meso-scale ordering, with ordered cubic films indicating a 1D diffusion limited crystallization process and dense films following a 3D diffusion limited process. Less well-ordered mesoporous films, despite similarities in pore volume and pore size distributions, are kinetically more reminiscent of dense films in terms of crystallization.

Thin mesoporous and dense titania films were prepared by dip-coating solutions made of $TiCl_4$ precursor and PEO-based bloc copolymers dispersed into a mixture of H_2O and Ethanol. After deposition, a humidity treatment was applied before thermal treatment.[2] In-situ ellipsometry measurements were performed with a continuous ramp rate of 30 °C per minute. Figure 1 displays the composite index of refraction and the thickness of the films as a function of temperature as prepared by fitting the ellipsometric data (WASE software) using the optical properties of the silicon substrate at both 65 and 630 °C. The two results were then linearized with respect to the temperature. This method provided excellent accuracy (<0.5% error) for the index of refraction and thickness data for both dense and templated films across all temperature ranges while reducing the computational burden of specifically imputing the optical properties of the substrate for each temperature. Long range periodicity and degree of mesoordering were assessed by Grazing-Incident Small-Angle X-ray Scattering (GI-SAXS) conducted at the Austrian SAXS beam line of Elettra synchrotron (Italy). Samples were placed under the beam at an incident angle of 0.2°. Scattering patterns were collected on an X-Ray-sensitive CCD camera (Energy: 8 KeV, beam size: 400 μm, sample-detector distance: 130cm, acquisition time: 10 s). Figure 1 displays the GISAXS patterns, taken at 400°C just before crystallization, of both a well ordered film exhibiting Im3m bbc mesoporosity and a less well ordered film exhibiting a 3D mesoporosity. Both films have the same porosity and have pores of the same dimension (≈ 7 nm). Only the well-ordered film exhibits mono-orientated domains with the [110] direction being perpendicular to the surface of the film. Lower ordering is obtained by exposing the film shorter time at high humidity.

The meso-scale organization of thin films is of great interest in terms of how such organization can be used to increase surface area, facilitate access to active sites, perturb physical and chemical process through confinement effects, and so on. For example, organizational effects have recently been investigated in the context of photocatalysis for titania films having 3D cubic mesostructure compared to transversally aligned 2D hexagonal mesostructure.[3,4,5] Here we compare the structural evolution during thermal treatment of ordered Im3m cubic films to less-ordered films. The latter prepared with the same starting solution but under low relative humidity dip-coating conditions. [2] The difference in

ordering is characterized by a lost of the preferential orientation of the ordered domains (diffraction ellipse on GISAXS patterns) and a slight deviation of the porous network corresponding d-spacing (slightly more diffused signal) for the less-ordered film. While there is virtually no difference between the two materials prior to template removal, significant deviations are observed just after the removal of the template. The less ordered structure shows a much larger relaxation event after template removal with a large increase in the index of refraction. This is followed by a significantly larger decrease in the index of refraction after crystallization due to sintering. The crystallization profile is also perturbed, with a sharper crystallization feature for the less ordered structure that is more reminiscent of dense films. *Ex-situ* GISAXS investigation (Elettra synchrotron SAXS line in Trieste, Italy) reveals the different degree of ordering for the two films at 400 °C and the slightly larger (14 nm versus 13.1 nm in the [1-10] direction), more narrowly distributed periodicity for the ordered film. The ordered film also shows a more well-defined cubic derived structure after stabilization at 130 °C, while after calcination to 630 °C peaks remain sharper (data not shown). Water adsorption-desorption using environmental ellipsometry porosimetry (EEP) [4,6] of films calcined to 630 °C, figure 2, show that the two materials have broadly similar accessible pore volumes, with the well-ordered material having slightly smaller, more narrow pore size distributions for the adsorption and desorption branches (inset). The sorption data also show the less-ordered film to be slightly unstable to the process of filling and emptying with water, with the desorption branch of the isotherm not returning to the same index of refraction value at the completion of the cycle. This, along with the greater relaxation of the structure after template removal, suggests that ordering provides a much more resilient matrix scaffold given a similar pore size distribution. The differences in sintering behavior also suggest that an ordered structure can more effectively maintain the stability of the network, reducing material displacement by providing a more internally balanced structure through a higher degree of meso-order symmetry in the direction normal to the surface. The integrity and balance of the interface is apparently also not sufficient to provide a check on crystal growth in the less ordered films, since the sharper crystallization peak suggests that the more collapsed porous structure is less efficient at restricting the dimensionality of crystal growth.

In-situ thermal ellipsometry combined with GISAXS, by detailing the evolution of the thermally driven chemistry and ceramization that dictate the final film properties, provides immensely important insight into the synthesis and optimization of advanced functional materials based on titania and other metal oxide thin films. Future investigations will be conducted simultaneously and *in situ* so as to record at the same time and on the same sample the mesoporosity evolution (GISAXS), the wall crystallization (WAXS) and the overall film density and thickness (Ellipsometry). We strongly believe that such study will conduct to the understanding of the latter thermally driven complex mechanisms and to the modeling of the sintering in ordered mesoporous materials.

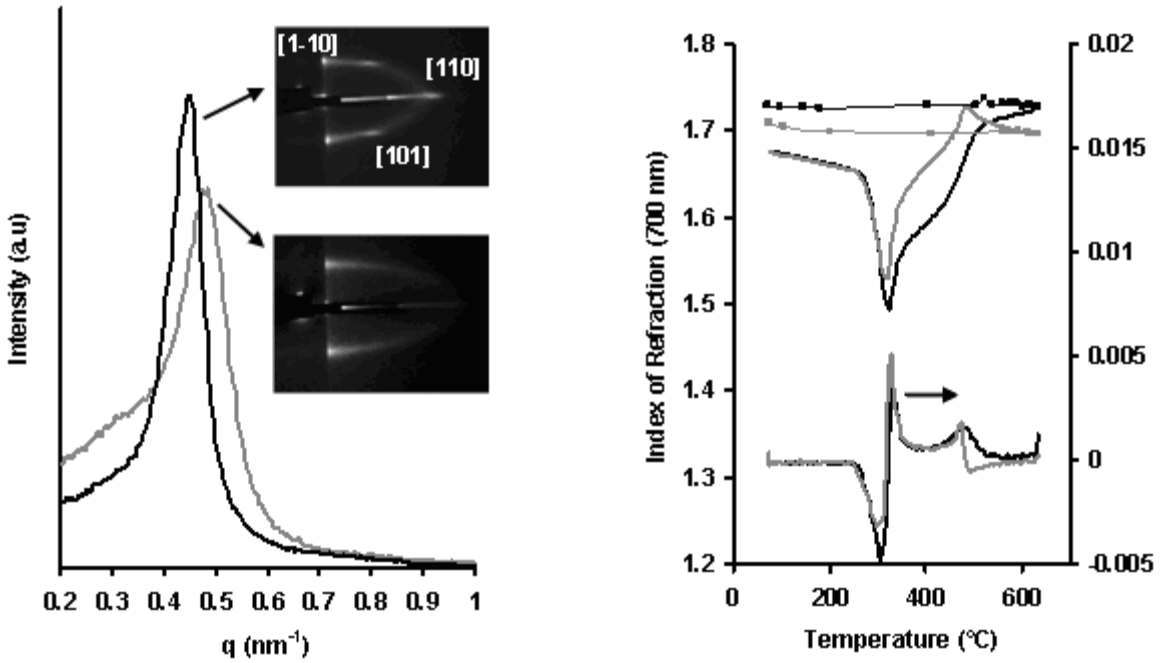

Figure 1. (Left) Index of refraction and its derivative with respect to temperature measured *in-situ* (**---**) an ordered pluronic film and (---) and a film synthesized under conditions leading to a disordered film. Cooling cycle traces are marked by (■). (Right) Intensity of GISAXS signal in the [1-10] direction for the (**---**) the ordered and (---) poorly ordered film calcined to 400 °C.

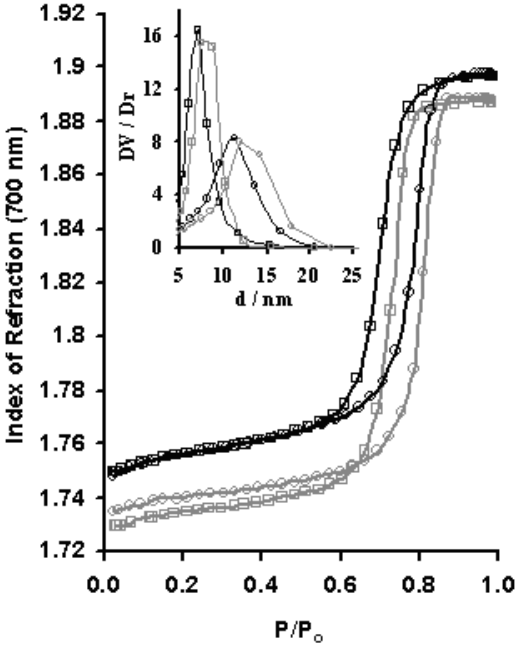

Figure 2. Water (○) adsorption and (□) desorption isotherms for (**---**) well ordered and (---) less ordered films calcined to 630 °C. (Inset) Pore size distributions determined using EEP with the adsorption branch showing the pore size distribution of the large axis parallel to the film surface and the desorption branch showing the size of pore interconnections.

References

[1] J. D. Bass, D. Grosso, C. Boissière, C. Sanchez J. Am. Chem. Soc. in press (2008)
[2] E. L. Crepaldi, G. J. D. A. Soler-Illia, D. Grosso, F. Cagnol, F. Ribot, C. Sanchez, J. Am. Chem. Soc. 125, 9770-9786 (2003)
[3] M. A. Carreon, S. Y. Choi, M. Mamak, N. Chopra, G. A. Ozin, J Mater Chem 17, 82-89 (2007)
[4] Y. Sakatani, D. Grosso, L. Nicole, C. Boissiere, G. J. D. A. Soler-Illia, C. Sanchez, J Mater Chem 16, 77-82 (2006)
[5] D. Grosso, F. Cagnol, G. J. D. A. Soler-Illia, E. L. Crepaldi, H. Amenitsch, A. Brunet-Bruneau, A. Bourgeois, C. Sanchez Adv Funct Mater 14, 309-322 (2004)
[6] C. Boissiere, D. Grosso, S. Lepoutre, L. Nicole, A. Bruneau, C. Sanchez, Langmuir 21, 12362-12371 (2005)

IN SITU STUDY OF NUCLEATION AND GROWTH OF ZINC OXIDE PARTICLES FROM NANO TO SUBMICROMETER SIZE

Z. Crnjak Orel[1], P. Podbrščček[1], M. Bitenc[1], B. Orel[2], P. Dubček[3], and S. Bernstorff[4]

1.) National Institute of Chemistry, Hajdrihova 19, SI-1000 Ljubljana, Slovenia
2.) Department of Mathematics and Mechanics, University of Ljubljana, Jadranska 19, SI-1000, Ljubljana, Slovenia
3.) Ruđer Bošković Institute, P.O. Box 180, 10002 Zagreb, Croatia
4.) Sincrotrone Trieste S.C.p.A., I-34012 Basovizza TS, Italy

We have investigated, by in situ small-angle X-ray scattering (SAXS), the formation of zinc oxide colloidal particles obtained after heating of aqueous or aqueous/polyol solution of zinc nitrate with urea. The preliminary experimental results demonstrate that the suspensions are composed of colloidal mostly spherical particles with wide size distribution. The average radius approximately in the range 5-7 nm was obtained after 120 min but the number of these basic particles continuously increases for increasing reaction time. The larger particles were probably formed by coagulation of the smaller.

Introduction

Nano- and submicrometer structured materials represent one of the fast growing fields in science, especially in the preparation of semiconductor materials. ZnO is one of the most attractive semiconductors and is becoming an important material in this field due to its unique properties of near-UV emission, electric conductivity and optical transparency. It shows potential applications in catalysis, optoelectronic devices, sensors, and photovoltaic uses.

The preparation of nano- and submicrometer-sized one-dimensional (1-D) zinc oxides (ZnO) from zinc nitrate was performed by precipitation with urea in different types of solvents (water and water/polyol mixtures). The influence of two different polyols (ethylene glycol and polyethy glycol) on the reaction kinetic was studied. In order to follow in-situ the formation process it was crucial to use a high-brilliance x-ray source at third generation synchrotron light sources like on the Austrian SAXS beamline at ELETTRA. Small-angle X-ray scattering (SAXS) is a well known technique to study structural features of colloidal particles at a nanometer scale and also the mechanisms of their aggregation. In order to follow the growth of particle sizes and forms, concentrations of starting reagents (0.01M-0.05M) were varied. We carried out in situ SAXS measurements, for increasing periods of time at a constant temperature, in order to better understand the phenomenon of colloidal particle formation and growth of ZnO particles.

The SAXS studies are expected to give additional insight in the mechanism of the formation of uniform nanodispersions, and advance the preparation (precipitation techniques) of materials of unique and reproducible properties. An understanding of the process can help us explain different properties of the matter in general. There are a number of parameters that have to be known when such a dispersion is produced, like the concentration of the starting reactants in the reacting solution, the internal composition of precipitate (obtained) materials, their homogeneity, aging conditions, pH, and temperature. The obtained results will be compared with results from TEM and SEM.

Experimental

All reagents were analytically pure. Solutions were prepared from $Zn(NO_3)_2 \times 6H_2O$ (Aldrich) and urea (Aldrich) in water. The experiments were carried out in 250 ml open reactors. As solvents water and a mixture of water and ethylene glycol (EG) and polyethylene glycol (PEG), were used respectively. A volume ratio 3/1, 1/1 and 1/3 of the water/polyol mixture were used in the experiments.

The reaction processes and the particle evolution were followed in situ by SAXS and WAXS using a flow-through capillary connected to the thermostated reaction vessel via a closed circle and a peristaltic pump. SAXS measurements were recorded using linear position-sensitive 1D Gabriel detectors. The beamline was set to a camera length of 2.55 m and a X-ray energy of 8 keV. Samples were also characterized by scanning field emission electron microscopy (FE-SEM, Zeiss Supra 35 VP with an EDS analyzer).

Result and discussion

Preliminary results of samples obtained in water/PEG mixture are presented in Figure 1 and Table 1. Figure 1a represents the changes of the SAXS intensity in dependence with S [nm^{-1}]. The graphs were fitted with a Porod function (Fig 1a). As the lines were linear, a spherical particle shape is predicted. The size was calculated with the Guinier equation. In Fig. 1b we represent the size distribution for particles obtained in water/PEG mixture after different times and concentration. The change of the SAXS signal in dependence of time of reaction is presented in Fig 1c. From that graph two reaction rates can be observed for each experiment. The reaction rate fits for graph 1 in Fig 1b are 58 in the first part and 85 in the second part of the reaction. We will analyze also experiments performed in water and in water/EG mixture (not presented in the report).

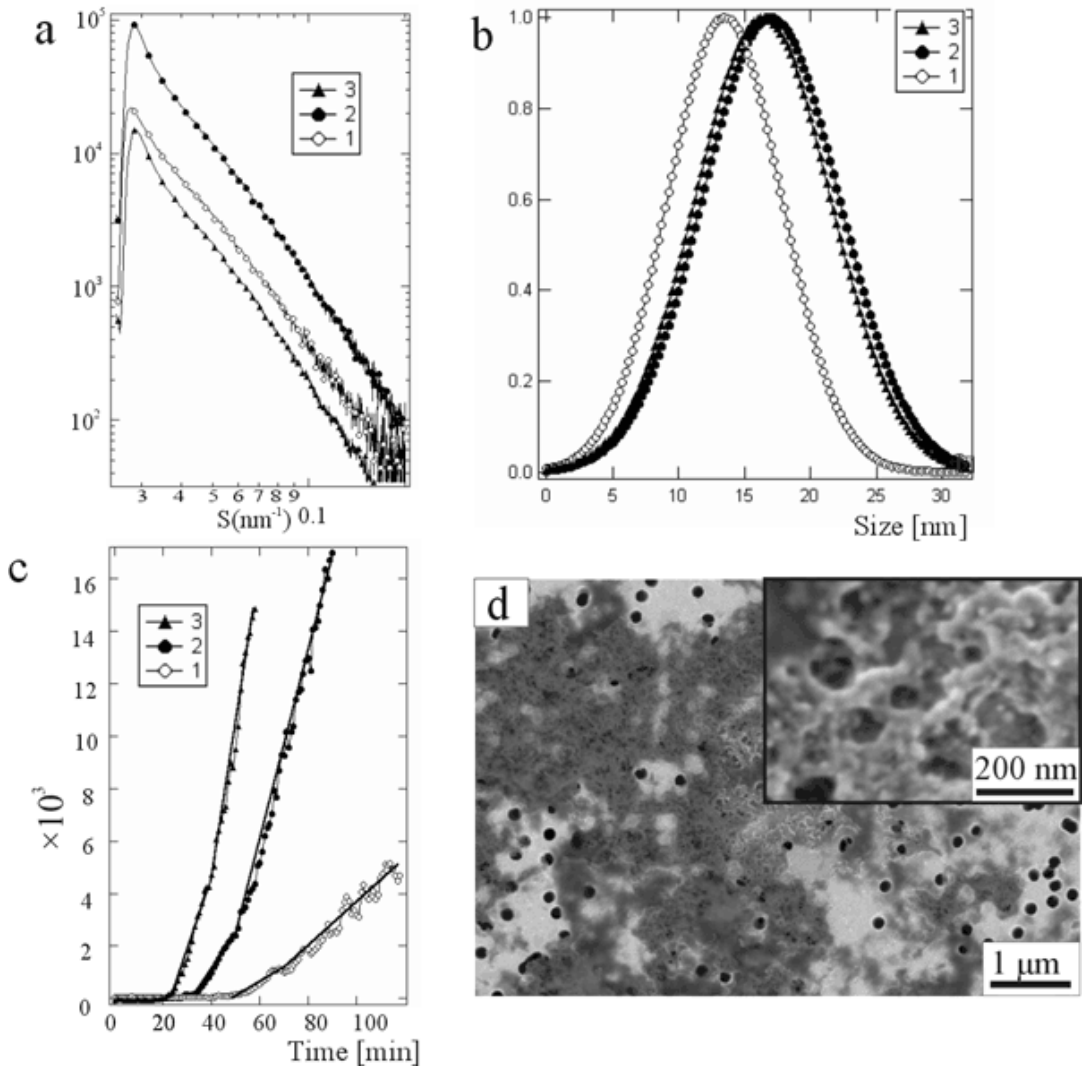

Figure 1. Samples obtained in water/PEG mixture (volume ratio 1/1). Graph of: a – changes of the SAXS intensity in dependence of S [nm^{-1}], b – size distribution, c – change of the SAXS signal in dependence of the reaction time: 1 – 118 minutes for [Zn^{2+}] = 0.025M and [Urea] = 0.125 M, 2 – 90 minutes for [Zn^{2+}] = 0.05 M and [Urea] = 0.25 M, and 3 – 119 minutes for [Zn^{2+}] = 0.1 and [Urea] = 0.5 M. d – FE-SEM micrograph of sample in water/PEG mixture (1/1) with 0.05 M Zn^{2+} and 0.25 M urea after 30 minutes of reaction.

No.	$[Zn^{2+}]$ (M)	[Urea] (M)	Time (min)	Size (nm)
1	0.025	0.125	50	6.4
			94	6.6
			118	7.6
2	0.05	0.25	28	5.7
			66	6.7
			90	7.3
3	0.1	0.5	42	5.8
			52	5.8
			118	7.5

Table 1. Size of particles prepared in water/PEG. The volume ratio of the water/PEG mixture was 1/1 in all experiments.

FABRICATION OF MESOPOROUS FUNCTIONALIZED ARRAYS BY INTEGRATING DEEP X-RAY LITHOGRAPHY WITH DIP-PEN WRITING

P. Falcaro[1], S. Costacurta[1,2], L. Malfatti[2], M. Takahashi[2], T. Kidchob[2], M. F. Casula[3], M. Piccinini[4], A. Marcelli[4], B. Marmiroli[5], H. Amenitsch[5], Piero Schiavuta[1], and P. Innocenzi[2]

1.) Associazione CIVEN – Nano Fabrication Facility, Via delle Industrie 5, 30175 Venezia Marghera, Italy
2.) Laboratorio di Scienza dei Materiali e Nanotecnologie (LMNT) Università di Sassari, Palazzo Pou Salid, Piazza Duomo 6, 07041 Alghero (SS), Italy
3.) Dipartimento di Scienze Chimiche, Università di Cagliari, S.S. 554 bivio per Sestu, 09042 Monserrato (CA), Italy
4.) Laboratori Nazionali di Frascati – INFN Via E. Fermi 40, 00044 Frascati (RM), Italy
5.) Institute of Biophysics and Nanosystems Structure Research Austrian Academy of Sciences Schmiedlstraße 6, 8042, Graz, Austria

Introduction

Research on mesostructured films has been focusing intensively on the control of geometric factors such as the symmetry and the degree of order of the mesostructure. However, much less effort has been directed to the tailoring of geometry in a larger (micron or millimetre) scale. For industrial applications, control on both factors is required in order to enable integration of mesoporous coatings in different objects and fabrication of devices. A possibility to pattern mesoporous films is offered by lithographic techniques [1] and dip-pen nanolithography or ink-jet printing using a "self-assembling ink" [2]. In the present work we have strived to develop a highly-integrated patterning technology based on this mesoporous response to X-ray radiation. We have employed the deep X-ray lithography (DXRL) beamline at Elettra [3] to pattern freshly-prepared mesostructured silica thin films [4]. In the present case, this lithographic approach is based on selective template removal and silica polycondensation induced by synchrotron radiation. As will be shown, the areas of the film that are not exposed to radiation can be selectively etched due to a lower crosslinking degree of the inorganic network.

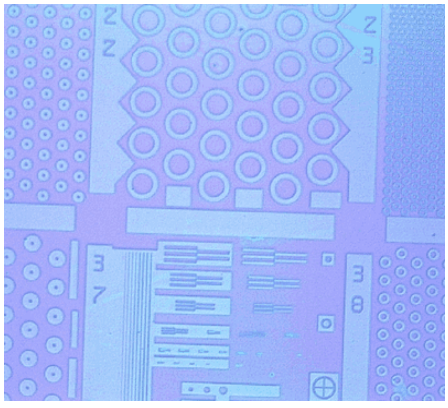

Figure 1. Optical micrograph of a patterned mesostructured silica film.

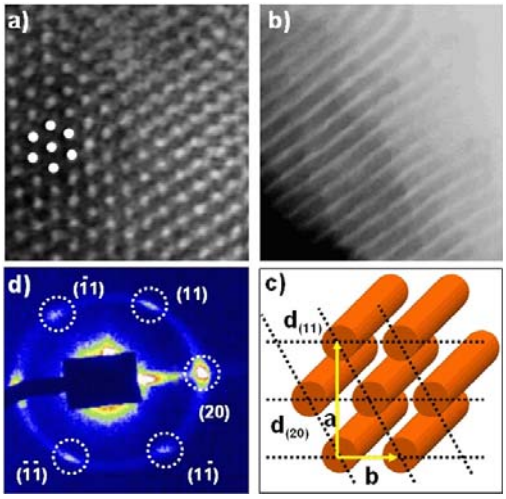

Figure 2. Transmission electron microscopy images showing the shape of the cylindrical mesopores (a and b), which are disposed according to a two-dimensional hexagonal cross section (c). The grazing incidence small-angle X-ray scattering pattern reveals a p6m symmetry group (d).

Results and discussion

The mesostructured films patterned by DXRL were first observed by optical microscopy to assess the quality of the lithographic process (Figure 1): patterned objects are discernible due

to the difference in refractive index between the masked and the unmasked regions. We have used grazing incidence small-angle X-ray scattering (GISAXS) and transmission electron microscopy (TEM) to detect mesophase variations in the films upon X-ray irradiation. GISAXS experiments showed that in both the irradiated and the masked regions, the mesostructure has two-dimensional hexagonal symmetry (space group *p*6*m*), which is composed of a stack of tubular micelles packed in structures with hexagonal cross section as confirmed by TEM measurements (Figure 2a, Figure 2b). A comparison between the GISAXS patterns with and without mask has shown that no substantial change in spot position and sharpness occurred. This indicates that the exposure of the films to X-rays did not cause any structural change in mesophase or damage such as cracking.

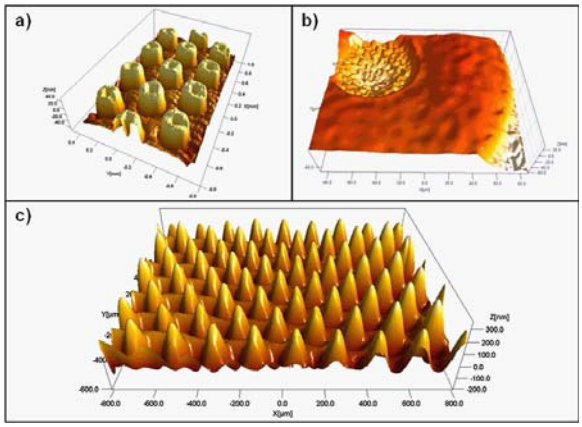

Figure 3. Optical profilometry of etched patterned mesoporous silica films relative to different objects: hollow pillars (a and b) and partial etching leading to low aspect ratio (c).

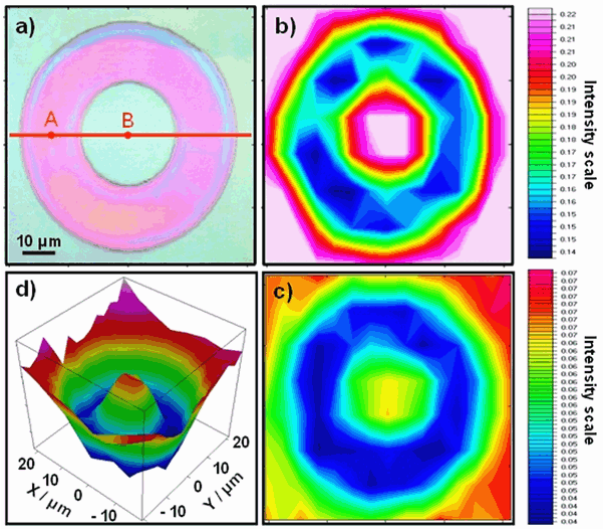

Figure 4. Visible image (a) and infrared microscopy images representing the integrated signal relative to the organic template (b and d) and silanols (c). These data indicate that both template removal and silica polycondensation occur upon X-ray exposure.

The regions that were not exposed to X-ray radiation could be easily etched as described in the Experimental section. Optical profilometry measurements have revealed that the masked areas of the samples were completely removed by etching. Figure 3a and 3b show portions of a mesoporous film patterned with circular pillars 50 µm in diameter and subsequently etched, whereas Figure 3c shows the results of a partial etching leading to low aspect ratio. An etched film presenting a large exposed area was investigated by GISAXS and no change in the diffraction patterns of the etched film could be detected, indicating that the mesostructure was retained upon etching.

Infrared microscopy was employed to track the chemical changes induced on the mesoporous materials induced by the patterning process. This imaging technique readily correlates the distribution of the chemical species by a three-dimensional mapping of the sample, substantially producing a "chemical picture" of a selected area. The visible image taken by the integrated optical microscope (Figure 4 a) refers to a $200 \times 200\ \mu m^2$ portion of a sample which was patterned but not etched, showing a purple-pink ring corresponding to the irradiated region, whereas the light-blue portion corresponds to the unirradiated region. The same area was observed by infrared microscopy, by which an image was obtained (Figure 4 b) by calculating the absorbance intensity of the FTIR spectrum at 2891 cm^{-1} (symmetric C-H stretching of CH_2 from Pluronic 127) A sharp decrease in intensity of the CH_2 stretching mode (2891 cm^{-1}) is observed in the ring area: this effect was induced by exposure to X-rays. The data referring to integration of the Si-OH stretching band at 930 cm^{-1} (Figure 4 c) indicates a strong decrease of silanols in the exposed area, which is associated with higher silica degree of polycondensation. The mechanism, supported by other works, is the decrease of pH upon X-ray irradiation due to radical photodecomposition of the photoacid, [5], leading to acid-catalyzed inorganic polycondensation [6]. De-polymerization in the organic phase is likely to be caused by the radicalic species generated upon irradiation from the photoacid molecules.

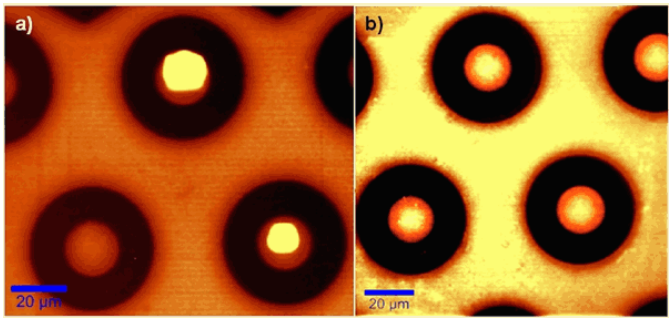

Figure 5. Confocal fluorescence image, in the spectral range 530–580 nm, of patterned mesoporous pillars functionalized by AFM with rhodamine 6G.

In a proof-of-concept experiment, an AFM cantilever tip was used as a dip pen using rhodamine 6G as the ink in order to functionalize selected mesoporous pillars (Figure 5 a is the result of confocal fluorescence microscopy). The two regions where the dip-pen functionalization was performed are characterized by a high fluorescence intensity and can be clearly distinguished on two separate pillars. This demonstrates that these mesoporous microstructures can be functionalized with different guest molecules (e.g., oligonucleotide strands in the fabrication of microarrays for DNA spotting), using small amounts of analytes. The patterned mesoporous support maximizes adsorption of guest molecules due to the high specific surface area of mesoporosity, which also allows accessibility of the material from the outside and diffusion of analytical species into the material, opening the route for efficient immobilization of biological species in analytical applications.

References

[1] D. A. Doshi, N. Huesing, M. Lu, H. Fan, Y. Lu, K. Simmons-Potter, B. G. Potter Jr., A. J. Hurd, C. J. Brinker; Science 290, 107 (2000)
[2] Y. Lu, Y. Yang, A. Sellinger, M. Lu, J. Huang, H. Fan, R. Haddad, G. Lopez, A. R. Burns, D. Y. Sasaki, J. Shelnutt, C. J. Brinker; Nature 410, 913 (2001)
[3] E. W. Becker, W. Ehrfeld, P. Hagmann, A. Maner; D. Munchmeyer, Microelectron. Eng. 4, 35 (1986)
[4] P. Falcaro, D. Grosso, H. Amenistch, P. Innocenzi; *J. Phys. Chem. B* 108, 10942 (2004)
[5] J. V. Crivello, J. H. W. Lam; *Macromolecules* 10, 1307 (1977)
[6] C. J. Brinker, G. W. Scherer; *Sol-gel Science*, Academic Press, San Diego (1992)

IN SITU GISAXS STUDY OF THE FORMATION AND PHASE TRANSFORMATION OF PURE SILICA AND PMO MESOSTRUCTURES WITHIN THE CONFINED SPACE OF ANODIC ALUMINA MEMBRANE PORES

R. Köhn[1], A. Keilbach[1], A. Zürner[1], H. Amenitsch[2], and T. Bein[1]

1.) University of Munich, Department of Chemistry & Biochemistry, Butenandtstr. 11, 81377 Munich, Germany
2.) Institute of Biophysics and Nanosystem Research, Austrian Academy of Sciences, Schmiedlstraße 6, Graz, Austria

The synthesis of mesostructured material within the confined tubular environment of anodic alumina membranes (AAM) has been established recently[1]. The unique combination of anisotropic spatial constraints and micellar interactions with the curved AAM channel walls leads to the formation of new and unusual mesophase morphologies with different pore orientations as depicted in the figure on top right.
The phase of the mesostructure formed during the evaporation induced self-assembly (EISA[2]) is strongly depending on the nature and concentration of the structure director and on the synthesis conditions, especially temperature and humidity. With respect to the latter the formation mechanism of the mesostructure within the confined environment of the AAM-channels was investigated by in situ small-angle X-ray scattering (SAXS) experiments.
Figure 1a) and b) show SAXS measurements of the periodic mesoporous silica at different stages of the drying process at a relative humidity of 20%. in 1a) after 30 minutes two structures are visible a hexagonal surface film represented by the 10 and 01 reflections designated as H_{10} and H_{01} and a circular hexagonal structure that we reported before [3] represented by the 10r and 01r reflections designated as C_iH_{10r} and C_iH_{01r}, respectively. While the surface film decreases due to mass transport into the pores of the anodisc the circular structure changes into the columnar hexagonal structure as depicted in figure 1b), showing only the C_oH_{0-1} and the C_oH_{01} reflections. In contrast, the formation of structure at 60% relative humidity starts with a delay of 10 minutes compared to the 20% r.h. sample. The formation of surface film is much less at the beginning and in the final material a pure circular lamellar phase is formed without any intermediate phases.
Special focus was drawn to a recently found new phase of a periodic mesoporous organosilica (PMO) which phase could not be elucidated by standard laboratory methods, e.g. TEM and in house SAXS. These correlations became only possible after corresponding GISAXS measurements allowed the correct determination of the Im-3m structure. The GISAXS data exhibit the 110, 101, and the 1-10 reflections of the cubic structure measured in transmission mode at an angle of -2.353° with respect to the incoming X-ray beam. The average d-spacing calculated from the scattering data is 6.5 nm correlating very well with the calculation from the TEM of ca. 6.8 nm.

In summary the in situ GISAXS experiments allowed to follow the phase formations and transformation in the AAM systems with respect to humidity. The phase formation starts when the material is almost dry after 30 minutes at 20% r.h. and 40 minutes at 60% r.h. and phase transformations were observed even in the “dry” mesostructure. Also GISAXS allowed to proof for the first time the existence of a cubic PMO structure within the pores of an AAM.

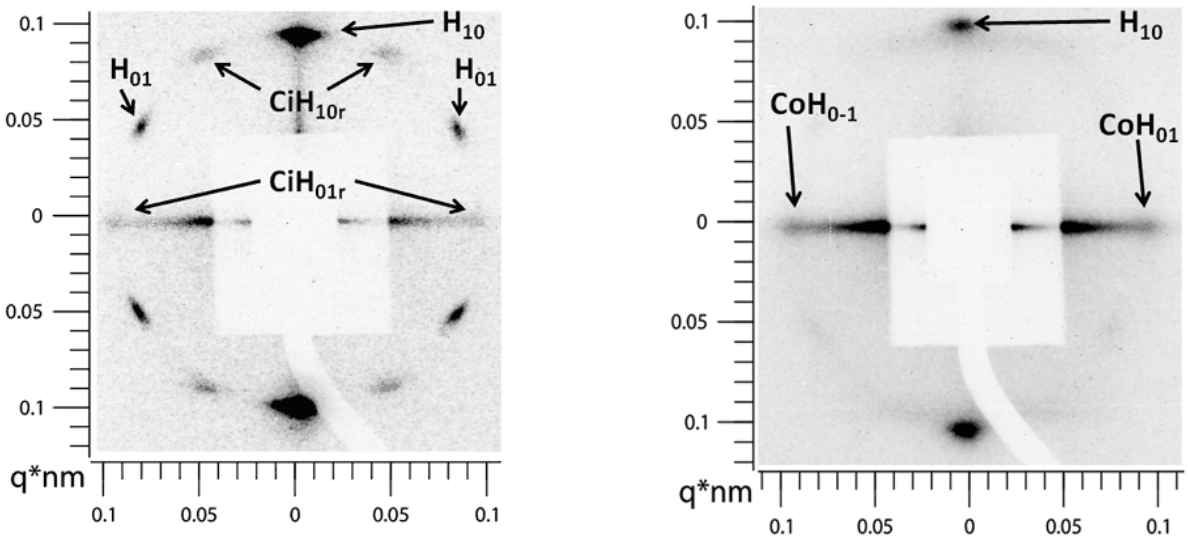

Figure 1. a) and b) depict the SAXS data at two different stages of drying. After 30 min (a) the first structures can be observed, a surface film (H_{10} & $_{01}$ reflections) and a circular hexagonal structure in the anopores (CiH_{10r} & $_{01r}$ reflections). After 100 minutes (b) the surface film has decreased and only its H_{10} reflection shows still significant intensity while the circular structure has completely transformed into the columnar hexagonal structure (C_oH_{0-1} & C_oH_{01} reflections).

References

[1] B. Platschek, N. Petkov, T. Bein, *Angewandte Chemie, International Edition* 2006, *45*, 1134.
[2] C. J. Brinker, Y. Lu, A. Sellinger, H. Fan, *Advanced Materials (Weinheim, Germany)* 1999, *11*, 579
[3] B. Platschek, R. Köhn, M. Döblinger, T. Bein *Langmuir* 2008, *24*, 5018

FORMATION OF NON-ORDERED AND HIGHLY ORDERED HELICAL NANOTUBES STUDIED IN-SITU BY SAXS

C.V. Teixeira[1], H. Amenitsch[2], T. Fukushima[3], W. Jin[3], and M. Lindén[4]

1.) Universitat Autónoma de Barcelona, Facultat de Medicina, Unitat de Biofísica, 08191, Bellaterra, Spain
2.) Institute of Biophysics and Nanosystems Research, Austrian Academy of Science, Schmiedlstrasse, 6, 8043, Graz, Austria
3.) Aida Nanospace Project, Exploratory Research for Advanced Technology Agency, National Museum for Emerging Science and Innovation, 2-41 Aomi, Koto-ku, Tokyo, 135-0064, Japan
4.) Department of Physical Chemistry, Åbo Akademi University, Porthansgatan, 3-5, 20500, Turku, Finland

The self-assembly of amphiphilic precursors is a highly promising route towards a rational design of nanotubes (NT)[1]. Typically, these nanotubes are formed upon cooling an isotropic precursor solution to a temperature which is below the gel-to-liquid crystalline phase transition temperature. Recently, Aida and collaborators reported the formation of helical arrays of a stacked graphene molecule, using the amphiphilic hexa-peri-hexabenzocoronene (HBC) as the precursor, by slowly cooling a solution of HBC in tetrahydrofurane (THF) followed by aging under ambient conditions[2]. A nanotubular graphitic structure was then formed, where the graphene sheets were stacked in axial direction. The wall thickness was 3 nm, which suggests that the wall consists of a bilayer of HBC. The overall structure consisted of a uniform, smooth, 14-nanometer-wide, open-ended hollow space with an aspect ratio greater than 1000. The radius is an order of magnitude larger than those of conventional carbon NTs.

In a previous beamtime we studied the assembly and disintegration of HBC nanotubes, confirming the hypothesis of Aida et al. that the HBC, soluble in THF at high temperatures, forms long bilayers, infinite in one-dimension when the temperature decreases, and that the nanotubes are formed by a rolling up of the bilayers. We also saw that although a rough aggregation occurs shortly just upon cooling, the nanotubes need a long time to form a well defined equilibrated structure. The curves obtained at intermediate temperatures exhibited asymmetric peaks.

In the present experiment we followed the nanotube formation up to 43 hours, with a slower cooling ratio (0.2 ˚C/min), to study the structure of the equilibrated nanotubes. The well equilibrated structure formed by the HBC was compared with the aggregates formed by a modified HBC molecule with a chirality point in its hydrophilic chain, dissolved in 2-methyltetrahydrofuran[3]. To the equilibrated structure obtained with the original HBC molecule we attempted to fit the form factor of an infinite cylinder, but the fitting result was not satisfactory. Thus we could successfully fit the form factor of a helix, shown in Figure 1. After heating up the same sample up to 70 ˚C, part of the solvent seems to have evaporated and a fiber-like diffraction pattern was obtained, and the reflections presented hexagonal order. The curves obtained for an intermediate temperature during the heating process of a sample equilibrating for only 10 hours, of the sample equilibrating for 43 hours at 20 ˚C and this last sample after being heated to 70 ˚C, are shown in Figure 2.

With the modified HBC with chirality point, the fiber-like structure was obtained after just 4 hours equilibrating at 20 ˚C (Figure 3). A fiber structure has been observed with the HBC with chirality point after aging for three weeks[3]. In this case, macroscopic bundles were formed. Our experiments show that the fiber-like structure forms much earlier than the resting time of three weeks and much faster then the original HBC. This suggests that the chiral feature of the molecule stimulates them to roll-up. It is also concluded the previous hypothesis that the nanotubes are formed by rolling-up the long bilayer, since the helical form factor fits better than the infinite cylinder.

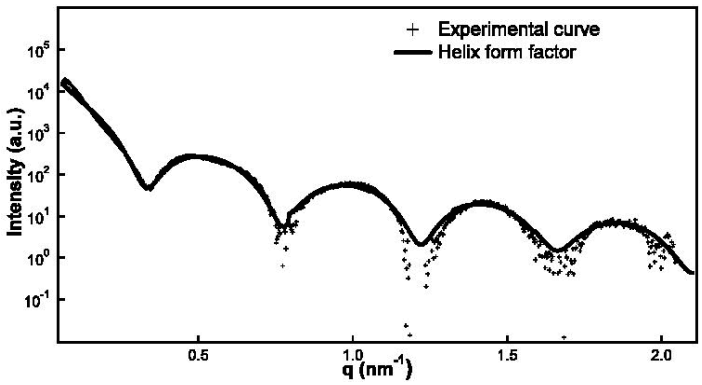

Figure 1. Scattering curve of an equilibrated sample of HBC (symbols) with the fitted helical form factor (solid line).

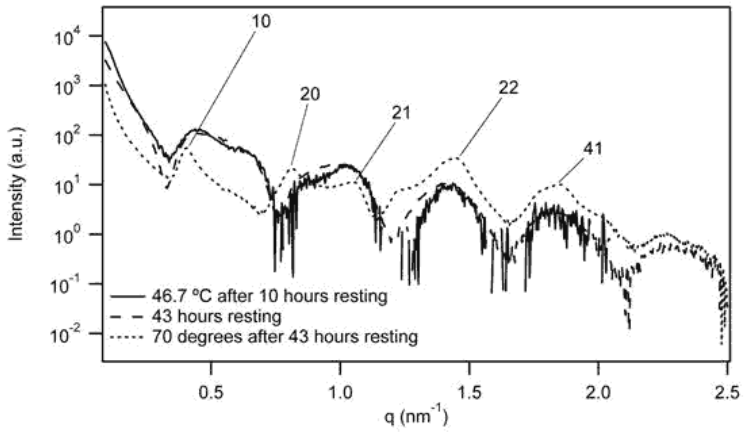

Figure 2. Scattering curve of HBC at different times during the process of formation of the nanotubes.

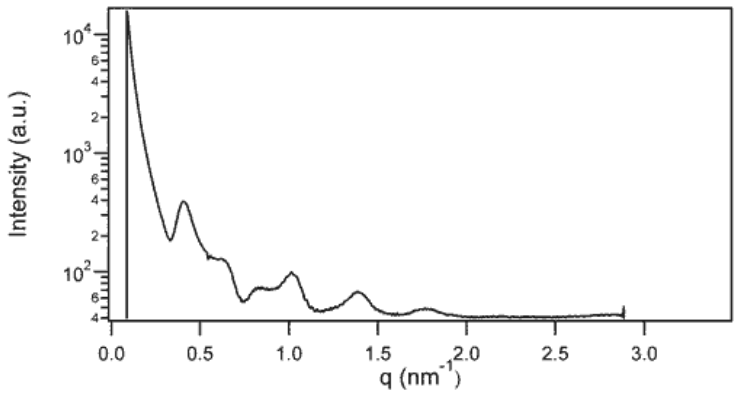

Figure 3. Scattering curve of the modified HBC with chirality point, after 4 hours equilibrating at 20 ˚C.

References

[1] T. Shimizu, M. Masuda, H. Minamikawa; Supramolecular Nanotube Architecture based on amphiphilic molecules; Chem. Rev. 105, 1401-1443 (2005) ; P. Terech, A. De Geyers and Y. Talmon; Self-assembled monodisperse steroid nanotubes in water; Adv. Mater 14, 495-498 (2002)

[2] J.P. Hill, W. Jin, A. Kosaka, T. Fukushima, H. Ichihara, T. Shimomura, K. Ito, T. Hashizume, N. Ishii and T. Aida; Self-assembled hexa-peri-hexabenzocoronene graphitic nanotube ; Science 304, 1481-1483 (2004)

[3] Y. Yamamoto, T. Fukushima, W. Jin, A. Kosaka, T. Hara, T. Nakamura, A. Saeki, S. Seki, S. Tagawa and T. Aida; A glass-hook allows fishing of hexa-peri-hexabenzocoronene graphitic nanotubes; fabrication of a macroscopic fiber with anisotropic electrical conduction; Adv. Mat. 18, 1297-1300 (2006)

STUDY OF THE GROWTH OF CdSe NANOCRYSTALS USING SAXS TECHNIQUE.

Ranjani Viswanatha[1], Angshuman Nag[1], Heinz Amenitsch[2], and D.D. Sarma[1,3]

1.) Solid State and Structural Chemistry Unit, Indian Institute of Science, Bangalore-560012, India
2.) Institute of Biophysics and X-ray Structure Research, Austrian Academy of Sciences, Schmiedlstr. 6, 8042 Graz, Austria
3) Centre for Advanced Materials, Indian Association for Cultivation of Science, Kolkata – 700032, India.

Green chemistry principles or environmentally benign chemistry, whose main goal is to minimize the damage to the environment by the human activities, have gradually obtained increasing importance in the development of the synthetic chemistry of high-quality semiconductor nanocrystals.[1,2] In comparison with the original organometallic approach, the resulting alternative routes are safe, simple, inexpensive, reproducible, versatile, "user friendly", and yield nanocrystals with well-controlled size, shape, and size/ shape distribution. Today, CdSe is one of the most well studied system using CdO as an alternative to the organometallic approach and nearly monodisperse CdSe nanocrystals have been synthesized in a large size range, from about 1.5 nm to 25 nm[3]. The nanocrystals as prepared are nearly monodisperse, with 5 ± 10% relative standard deviation, and the photoluminescence quantum efficiency of the as-prepared CdSe nanocrystals can reproducibly reach as high as 85%. The quality of the as-prepared CdSe nanocrystals synthesized by the alternative routes has long been considered to be a result of nucleation and growth path in the solution. However a detailed knowledge of growth of these nanocrystals does not exist and understanding the growth mechanism in these systems can promote an understanding of the exact role played by each of the precursors involved in the growth. Hence it allows us to understand the crystallization process in these nanocrystals in general at a fundamental level.

Recently we have synthesized very high quality CdSe nanocrystals[4] that have exhibited an extraordinary ordered arrangement over a micron range as shown by the STM picture in Figure 1(a). However there is hardly any explanation available as to why and how such ordered arrays are formed. The major drawbacks for studying these processes are the absence of in-situ techniques to study the growth and ordering in these nanocrystals which typically form in 10-15 minutes at temperatures of 200°C to 250°C. The inset to Fig. 1(a) shows an ex-situ small angle X-ray diffraction peak arising due to the ordered structures. Hence following the ordering of these nanocrystals by in situ monitoring of this peak in these structures would give us an insight into the mechanism of growth as well as the formation of these arrays.

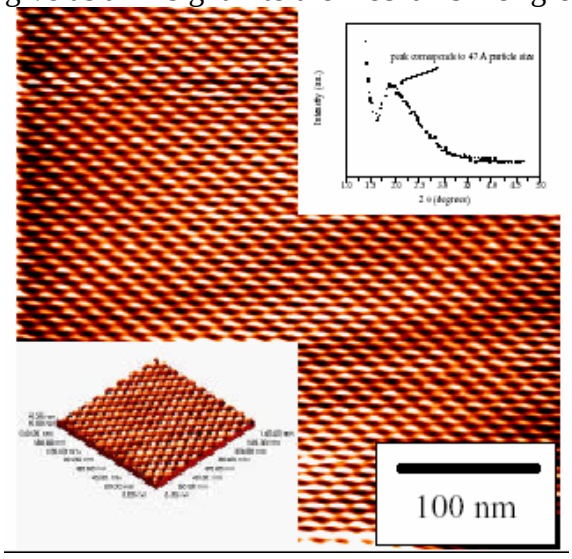

Figure 1: STM picture showing the ordered arrays of CdSe nanocrystals. The insets show the small angle X-ray diffraction peak corresponding to an ordering size of ~5 nm and a three dimensional close-up STM picture.

In this work, we have used in-situ Small Angle X-ray scattering (SAXS) technique to study the growth of CdSe nanocrystals at different temperatures using different precursor concentrations. Using the results obtained from these experiments, we try to model and understand the growth mechanism in these nanocrystals, thus being able to predict the growth mechanism in these nanocrystals.

A mixture of CdO (0.10 mmol), Oleic acid (0.30 mmol), and 4 ml 1-Octadecane (ODE) was heated in a three-necked 125 ml round-bottom flux under Argon flow; this formed a colourless solution at an elevated temperature. Then a solution of Se (0.05 mmol) in 0.5 ml Trioctylphosphine (TOP) prepared at room temperature was injected to the above solution and this solution was sealed in capillary glass tubes. These tubes were exposed to the beam at a temp between 200°C – 300°C and the evolution of the saxs patern was collected at a interval of 1 sec. The time resolved diffraction patterns of the CdSe nanocrystals obtained during a typical reaction were normalized and background subtracted and shown in Fig. 2a and the diameter of the particles obtained at a few typical times and temperatures are shown in Fig. 2b.

From the figure it can be seen that the temperature plays a major role in deciding the size of the CdSe nanocrystals. Also from the figure, we observe some interesting features like the initial rapid increase in the sizes of the nanocrystal suggesting the need to use SAXS with a high time resolution to understand the growth mechanism. Further analyses of the scattering plots to obtain a more quantitative measure of the size as well as the size distribution are underway. These analyses would provide conclusive evidence of the mechanism of growth as well as the role played by each precursor, thus giving predictive ability to the synthesis of high quality nanocrystals.

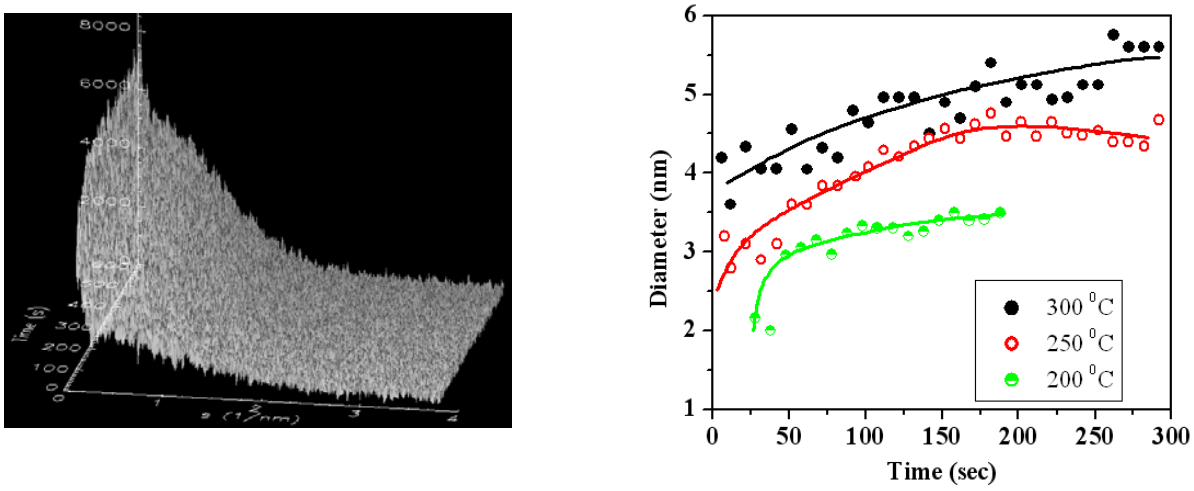

Figure 2: (a) Scattering patterns of CdSe nanocrystals as a function of time at 250°C. (b) Growth of the nanocrystals at different temperatures. The solid lines are a guide to the eye.

References:

[1.] Z. A. Peng, X. Peng, J. Am. Chem. Soc. 2001, 123, 183.
[2.] C. B. Murray, C. R. Kagan, M. G. Bawendi, Annu. Rev. Mater. Sci. 2000, 545.
[3.] L. Qu, Z. A. Peng, X. Peng, Nano Lett. 2001, 1, 333.
[4.] A. Nag, S. Sapra, S. Chakraborty, S. Basu and D. D. Sarma, J. Nanosci. Nanotech. 2007, 7, 1965.

Publications

Publications in Journals and Reviewed Proceedings 2007

H. Amenitsch, D. Cojoc, M. Rappolt, B. Sartori, P. Laggner, E. Ferrari, V. Garbin, M. Burghammer, Ch. Riekel, and E. Di Fabrizio
Optical Tweezers for Sample Fixing in Micro-Diffraction Experiments
AIPConfProc 879: 1287-1290 (2007)

M.A. Bagni, B. Colombini, G. Cecchi, S. Bernstorff, H. Amenitsch, P.J. Griffiths
Intensity changes of equatorial 1,1 1,0 and meridional 14.3 nm X-ray reflections during slow stretching of activated muscle fibre bundles
Journal of Muscle Research and Cell Motility 28, issue 7-8, 479 (Oct 2007, abstract)

S. Bernstorff, P. Dubček, I. Kovačević, N. Radić, B. Pivac
Si nanocrystals in SiO_2 films analyzed by small angle X-ray scattering
Thin Solid Films 515, 5637 – 5640 (2007)

I. Capan, B. Pivac, S. Duguay, A. Slaoui, P. Dubček, and S. Bernstorff
Structural Properties of Ge Nanocrystals Embeded in SiO_2
Proc. MIPRO 2007, edited by: P. Biljanović and K. Skala, Opatija 2007, pp. 50-52

G. Caracciolo, C. Marchini, D. Pozzi, R. Caminiti, H. Amenitsch, M. Montani, A. Amici
Structural stability against disintegration by anionic lipids rationalizes the efficiency of cationic liposome/DNA complexes
Langmuir 23 (8), 4498-4508 (2007)

G. Caracciolo, D. Pozzi, H. Amenitsch and R. Caminiti
Interaction of lipoplexes with anionic lipids resulting in DNA release is a two-stage process
Langmuir 23 (17), p. 8713-8717, Aug 2007

G. Caracciolo, D. Pozzi, G. Mancini and R. Caminiti
Role of the spacer stereochemistry on the structure of solid-supported gemini surfactants aggregates
Langmuir 23, 10040-10043 (2007)

G. Caracciolo, D. Pozzi and R. Caminiti
Hydration effect on the structure of dioleoylphosphatidylcholine bilayers
Applied Physics Letters 90, 183901 (2007)

G. Caracciolo, D. Pozzi, R. Caminiti, C. Marchini, M. Montani, A. Amici, H. Amenitsch
On the correlation between phase evolution of lipoplexes/anionic lipid mixtures and DNA release
Applied Physics Letters 91, 1439031-1439033 (2007) (3 pages)

G. Caracciolo, D. Pozzi, R. Caminiti, C. Marchini, M. Montani, A. Amici, H. Amenitsch
Transfection efficiency boost by designer multicomponent lipoplexes
Biochimica et biophysica acta (BBA), 1768 (9), p.2280-2292 (2007)

G. Caracciolo, D. Pozzi, R. Caminiti, G. Mancini, P. Luciani, H. Amenitsch
Observation of a rectangular DNA superlattice in the liquid-crystalline phase of cationic lipid/DNA complexes
Journal of the American Chemical Society, 129 (33), p.10092-10093 (2007)

Y. Castro, B. Julian-Lopez, C. Boissière, B. Viana, H. Amenitsch, D. Grosso, and C. Sanchez
Synthesis, characterization and optical properties of Eu_2O_3 mesoporous thin films
Nanotechnology 18 (5), p.055705 1-7 (2007)

D. Cojoc, E. Ferrari, V. Garbin, E. Di Fabrizio, H. Amenitsch, M. Rappolt, B. Sartori, P. Laggner, M. Burghammer and C. Riekel
Scanning x-ray microdiffraction of optically manipulated liposomes
Applied Physics Letters, Appl. Phys. Lett. 91, 234107 (2007)

Barbara Colombini, Maria Angela Bagni, Giovanni Cecchi and Peter John Griffiths
Effects of solution tonicity on crossbridge properties and myosin lever arm disposition in intact frog muscle fibres
J Physiol 578.1 (2007) pp 337–346 337

S. Costacurta, L. Biasetto, E. Pippel, J. Woltersdorf, P. Colombo
Hierarchical Porosity Components by Infiltration of a Ceramic Foam
J. Amer. Ceram. Soc. **2007**, 90, 2172-2177

G. Croce, D. Viterbo, M. Milanesio, H. Amenitsch
Mesoporous pattern created by nature in spicules from Thetya Aurantium sponge
Biophysical Journal 92 (1), 2007, 288-292

D. Erdemir, S. Chattopadhyay, L. Guo, J. Ilavsky, H. Amenitsch, C.U. Segre, A.S. Myerson
Relationship between Self-Association of Glycine Molecules in Supersaturated Solutions and Solid State Outcome
Physical Review Letters, 99 (11), p.115702, Sep 2007

P. Dubcek, B. Pivac, I. Capan, S. Bernstorff, R. Mu, B. Vlahovic
Evolution of nanoparticles in gold-implanted glass
Vacuum, 82 (2), p.130-133, Oct 2007

R. A. Farrell, K. Cherkaoui, N. Petkov, H. Amenitsch, J. D. Holmes, P. K. Hurley and M. A. Morris
Physical and Electrical Properties of Low Dielectric Constant Self Assembled Mesoporous Silica Thin Films
Microelectronics Reliability 47 (4), 759-763 (Apr. 2007)

D. Gracin, S. Bernstorff, P. Dubcek, A. Gajovic and K. Juraic
Study of amorphous nanocrystalline thin silicon films by grazing-incidence small-angle X-ray scattering
J. Appl. Cryst. 40 (2007) s373–s376

D. Gracin, S. Bernstorff, P. Dubcek, A. Gajovic, K. Juraic
The influence of substrate morphology on the growth of thin silicon films: a GISAXS study
Thin Solid Films 515, 5615 – 5619 (May 2007)

D. Gracin, K. Juraic, A. Gajovic, P. Dubcek, I. Djerdj, N. Tomasic, S. Krajinovic, M. Milun and S. Bernstorff
The influence of post deposition plasma treatment on SnOx structural properties
Vacuum, 82 (2), p.266-269, Oct 2007

D. Gracin, B. Etlinger, K. Juraic, A. Gajovic, P. Dubcek, S. Bernstorff
The DC conductivity and structural ordering of thin silicon films at the amorphous to nano-crystalline phase transition
Vacuum, 82 (2), p.205-208, Oct 2007

D. Grozdanić, B. Rakvin, B. Pivac, P. Dubček, N. Radić, S. Bernstorff
Structural characterization of thin amorphous Si films
Thin Solid Films 515, 5620 – 5623 (2007)

P. Gupta, A. Gupta, G. Principi, A. Maddalena, S. Bernstorff, and H. Amenitsch
Effect of annealing current density on the microstructure of nanocrystalline FeCuNbSiB alloy
J. Appl. Phys. 101 (5), 053907 (2007) (5 pages 0539071-5)

J.P. Hanrahan, M.P. Copley, T.R. Spalding, J.D. Holmes, D.C. Steytler, H. Amenitsch, M. Steinhart and M.A. Morris
In situ studies of order-disorder phenomena in the synthesis of mesoporous silica Journal of Non-Crystalline Solids, Bd. 353, S. 4823-4829 (2007)

P. Innocenzi, L. Malfatti, T. Kidchob, P. Falcaro, S. Costacurta, M. Piccinini, A. Marcelli, P. Morini, D. Sali, H. Amenitsch
Time-Resolved Simultaneous Detection of Structural and Chemical Changes during Self-Assembly of Mesostructured Films
Journal of Physical Chemistry C 111, 5345-5350, 2007

T. Koch, S. Seidler, E. Halwax, S. Bernstorff
Microhardness of quenched and annealed isotactic polypropylene
Journal of Materials Science 42 (14), pp. 5318-5326 July 2007

I. Kovačević, B. Pivac, P. Dubček, H. Zorc, N. Radić, S. Bernstorff, M. Campione, and A. Sassella
Formation of Ge islands from a Ge layer on Si substrate during post-growth annealing
Applied Surface Science 253 (6), 3034-3040 (Jan 2007)

I. Kovačević, P. Dubček, S. Duguay, H. Zorc, N. Radić, B. Pivac, A. Slaoui, S. Bernstorff
Silicon nanoparticles formation in annealed SiO/SiO_2 multilayers
Physica E38 (1), p.50-53 (Apr 2007)

S. Kralj, G. Cordoyiannis, A. Zidansek, G. Lahajnar, H. Amenitsch, S. Zumer, Z. Kutnjak
Presmectic wetting and supercritical-like phase behavior of octylcyanobiphenyl liquid crystal confined to controlled-pore glass matrices.
The Journal of Chemical Physics, 127 (15), p.154905, Oct 2007

M. Kuemmel, J. Allouche, L. Nicole, C. Re, C. Laberty, H. Amenitsch, C. Sanchez, D. Grosso
A chemical solution deposition route to nanopatterned inorganic material surfaces
Chemistry of Materials, Bd. 19, S. 3717-372 (2007)

M. Lučić-Lavčević, P. Dubček, A. Turković, Z. Crnjak Orel, S. Bernstorff
Nanostructural Depth-Profile of Vanadium/Cerium Oxide Film as a Host for Lithium Ions
Solar Energy Materials & Solar Cells. 91 (7), 616-620 (2007)

M. Lučić Lavčević, A. Turković, P. Dubček, S. Bernstorff
Nanostructured CeO_2 thin films: a SAXS study of the interface between grains and pores
Thin Solid Films 515 (14), pp. 5624 – 5626 (May 2007)

G. A. Maier, G. M. Wallner, R. W. Lang, J. Keckes, H. Amenitsch and P. Fratzl
Fracture of poly(vinylidene fluoride): a combined synchrotron and laboratory in-situ X-ray scattering study
J. Appl. Cryst. **40**, s564-s567 (2007)

L. Malfatti, T. Kidchob, P. Falcaro, S. Costacurta, M. Piccinini, M. Cestelli Guidi, A. Marcelli, A. Corrias, M. F. Casula, H. Amenitsch, P. Innocenzi
Highly ordered self-assembled mesostructured membranes: Porous structure and pore surface coverage
Microporous and Mesoporous Materials 103, 113-122 (2007)

A.G. Marangoni, S.H.J. Idziak, C. Vega, H. Batte, M. Ollivon, P.S. Jantzi, J.W.E. Rush
Encapsulation-stucturing of edible oil attenuates acute elevation of blood lipids and insulin in humans
Soft Matter 3, 183-187 (2007)

G. Pabst, A. Hodzic, J. Strancar, S. Danner, M. Rappolt and P. Laggner
Rigidification of neutral lipid bilayers in the presence of salts.
Biophysical journal, 93 (8), p.2688-2696, Oct 2007

H.Peterlik, H.Rennhofer, V.Torma, U.Bauer, M.Puchberger, N.Hüsing, S.Bernstorff, and U.Schubert:
Structural investigation of alumina silica mixed oxide gels prepared from organically modified precursors
Journal of Non-Crystalline Solids 353 (16), 1635–1644 (Jun 2007)

B. Pivac, P. Dubcek, I. Capan, N. Radic, S. Bernstorff
GISAXS study of Si nanoclusters in SiO/SiO_2 layers
Vacuum, 82 (2), p.189-192, Oct 2007

S. Puchegger, H. Rennhofer, F.R. Kogler, D. Loidl, S. Bernstorff, U. Schubert, H. Peterlik
Suppression of Crazing in Polystyrene Crosslinked with a Multifunctional Zirconium Oxo Cluster Observed In Situ During Tensile Tests
Macromol. Rapid Commun. 2007, 28, 2145–2150

N. Radić, P. Dubček, S. Bernstorff, I. Djerdj and A. M. Tonejc
Structural study of nanocrystalline nickel thin films
J.Appl. Cryst. 40, 377–382 (2007)

M. Rappolt
The biologically relevant lipid mesophases as "seen" by X-rays
Elsevier book series "Advances in Planar Lipid Bilayers and Liposomes", Vol. 5, chapter 9, page 253-284 (2007) by A. Leitmannova Liu (Editor), Monte Carlo, New York, Elsevier Inc, Academic Press, USA

M. Rappolt, P, Laggner, S. Zhan and A. Yaghmur
Tuning curvature and stability of monoolein bilayers by amphiphilic designer peptides
Chemistry and Physics of Lipids, 149, p.S41-S41, Sep 2007 (abstract)

R. L. Rice, D. C. Arnold, M. T. Shaw, D. Iacopina, A. J. Quinn, H. Amenitsch, J. D. Holmes and M. A. Morris
Ordered Mesoporous Silicate Structures as Potential Templates for Nanowire Growth Adv. Func. Mater. **17**, 133-141 (2007)

C. Sinturel, M. Vayer, R. Erre and H. Amenitsch
Nanostructured Polymers Obtained from Polyethylene-block-poly(ethylene oxide) Block Copolymer in Unsaturated Polyester
Macromolecules 40 - 7, 2532-2537 (2007)

F. Spinozzi, P. Mariani, L. Saturni, F. Carsughi, S. Bernstorff, S. Cinelli, and G. Onori
Met-myoglobin association in dilute solution during pressure-induced denaturation: an analysis at pH 4.5 by high-pressure small-angle X-ray scattering
Journal Physical Chemistry B111, 3822-3830 (2007)

Ralf Supplit, Nicola Hüsing, Silvia Gross, Sigrid Bernstorff and Michael Puchberger
Hafnium Oxide Doped Mesostructured Silica Films
European Journal of Inorganic Chemistry 2007, 2797-2802

M. Tiemann, C. V. Teixeira, M. Cornelius, J. Morell, H. Amenitsch, M. Lindén, and M. Fröba
In-situ X-ray diffraction study on the formation of a periodic mesoporous organosilica material
Stud. Surf. Sci. Catal. 165, S. 9-12 (15.06.2007)

A. Turković, M. Pavlović, P. Dubček, M. Lučić-Lavčević, B. Etlinger, and S. Bernstorff
SAXS/DSC Study of Polymer Electrolyte for Zn Rechargeable Nanostructured Galvanic Cells
ECS Transactions, 2 (20) 11-23 (2007)

A. Turković, M. Pavlović, P. Dubček, M. Lučić-Lavčević, B. Etlinger, and S. Bernstorff
SAXS/DSC Study of Polymer Electrolyte for Zn Rechargeable Nanostructured Galvanic Cells
Journal of The Electrochemical Society 154, A554-A560 (2007)
and also:
Virtual Journal of Nanoscale Science & Technology, Vol. 15, Issue 17, April 30, 2007

A. Turković, B. Orel, M. Lučić-Lavčević, P. Dubček, Z. Crnjak Orel, S. Bernstorff

GISAXS study of temperature evolution in nanostructured CeVO4 films
Solar Energy Materials & Solar Cells 91 (14) 1299–1304 (2007)
Tusar, N.N. / Ristic, A. / Cecowski, S. / Arcon, I. / Lazar, K. / Amenitsch, H. / Kaucic, V.
Local environment of isolated iron in mesoporous silicate catalyst FeTUD-1
Microporous and Mesoporous Materials, 104 (1), p.289-295, Aug 2007

T. Ungár, E. Schafler, P. Hanák, S. Bernstorff, M. Zehetbauer
Vacancy Production During Plastic Deformation in Copper Determined by In-situ X-ray Diffraction
Materials Science & Engineering A 462 (1), 398-401 (Jul 2007)

R. Viswanatha, H. Amenitsch and D.D. Sarma
Growth Kinetics of ZnO Nanocrystals: A Few Surprises
Journal of the American Chemical Society 129(14), 4470-4475 (Apr. 2007)

R. Viswanatha, S. Sapra, H. Amenitsch, B. Sartori and D.D. Sarma
Growth of semiconducting nanocrystals of CdS and ZnS
Journal of Nanoscience and Nanotechnology 7(6), pp. 1726-1729 (2007)

A. Yaghmur, P. Laggner, S. Zhang and M. Rappolt
Tuning Curvature and Stability of Monoolein Bilayers by Designer Lipid-Like Peptide Surfactants
PLoS ONE, 2 (5), e479, May 2007

A. Yaghmur, P. Laggner, S. Zhang and M. Rappolt
Combined SAXS and rapid mixing studies on Ca2+ induced structural transitions in lipid systems
Chemistry and Physics of Lipids, 149, p.S48-S48, Sep 2007 (Abstract)

Publications during January to June 2008

D. Gracin, K.Juraic, A. Gajovic, P. Dubcek, C. Devilee, H.J. Muffler, W.J. Soppe, S. Bernstorff
The structural ordering of thin silicon films at the amorphous to nano-crystalline phase transition by GISAXS and Raman spectroscopy
Renewable Energy 33 (2008) 326–330

N. Baccile, C.V. Teixeira, H. Amenitsch, F. Villain, M. Lindén and F. Babonneau
Time-resolved in situ Raman and small-angle X-ray diffraction experiments: from silica precursor hydrolysis to development of mesoscopic order in SBA-3 surfactant-templated silica
Chem. Mater. 20, pp. 1161-1172 (2008)

P.Couvreur, L.H. Reddy, S.Mangenot, J.H.Poupaert, D.Desmaele, S.Lepetre Mouelhi, B.Pili, C.Bourgaux, H.Amenitsch and M.Ollivon
Discovery of new hexagonal supramolecular nanostructures formed by squalenoylation of an anticancer nucleoside analogue
Small 4(2), 247-253 (2008)

A. W. Dong, C. Pascual-Izarra, Y.-D. Dong, S. J. Pas, A.J. Hill, B. J. Boyd, C. J. Drummond
Positron annihilation lifetime spectroscopy (PALS) and small angle x-ray scattering (SAXS) of self-assembled amphiphiles
Proceedings of SPIE, 2008, 6800 (Device and process technologies for microelectronics, MEMS photonics and nanotechnology IV), 680001C/1-68001C/6

P. Falcaro, S. Costacurta, L. Malfatti, T. Kidchob, M. Casula, M. Piccinini, A. Marcelli, B. Marmiroli, H. Amenitsch, P. Schiavuta, P. Innocenzi
Fabrication of mesoporous functionalized arrays by integrating deep X-ray lithography with dip-pen writing
Adv. Mater. 2008, 9999, 1–6 (2008)

R. A. Farrell, N. Petkov, H. Amenitsch, J. D. Holmes and M. A. Morris
Thin and Continuous Films with Controlled Bi- and Tri-Modal Porosities by Embedment of Zeolite Nanoparticles in a Mesoporous Matrix
J. Mater. Chem. **18**, 2213-2220 (2008)

A. Hodzic, M. Rappolt, H. Amenitsch, P. Laggner and G. Pabst,
Differential modulation of membrane structure and fluctuations by plant sterols and cholesterol
Biophs. J. 94, 3935-3944 (2008)

I. Shyjumon, M. Rappolt, B. Sartori, H. Amenitsch and P. Laggner
Novel in situ setup to study the formation of nanoparticles in the gas phase by small angle x-ray scattering
Rev. Sci. Instrum. 79: 043905 (1-5) (2008)

Anan Yaghmur, Peter Laggner, Barbara Sartori, Michael Rappolt
Calcium Triggered Lα-H2 Phase Transition Monitored by Combined Rapid Mixing and Time-Resolved Synchrotron SAXS
PLoS ONE, www.plosone.org, April 2008, Volume 3, Issue 4, e2072, 11 pages

International Conferences and Workshops in 2007

W.B. Amara-Dali, P. Lesieur, H. Attia, M. Ollivon
Crystallization behavior of anhydrous goat milk fat as studied by coupled time-resolved Synchrotron X-RAY diffraction and DSC
5th International Symposium on the Challenge to Sheep and Goats Milk Sectors, 18-20 April 2007, Alghero/Sardinia, Italy (poster)

H. Amenitsch
Time-resolved scattering and GISAXS
5th European Winter School (NESY 2007), Planneralm, Austria, 6.3.2007 (invited lecture)

H. Amenitsch
SAXS in solution and under extreme conditions
II Scuola "applicazioni della radiazione di sincrotrone allo studio dei materiali nanostrutturati e dei film sottili (ARS2)" Trieste, Italy, 22-26 Aprile 2007 (invited lecture)

H. Amenitsch
SAXIER: Small-angle X-ray scattering at high brilliance European synchrotrons for bio- and nano-technology
SAXIER workshop, France, 5.2.2007 (talk)

H. Amenitsch
The Austrian-SAXS-Beamline at ELETTRA
Workshop on laboratory synchrotrons (TU-Graz, Nanonet Styria, Karl-Franzens Universität), Graz, Austria, 4.7.2007 (talk)

H. Amenitsch
Compact light sources: perspectives and applications
57. Jahrestagung der Österreichischen Physikalischen Gesellschaft (ÖPG), Vienna, Austria, 26.09.2007 (talk)

H. Amenitsch
Introduction to SAXS and WAXS
Master program in nano biotecnologie, Porto Conte, Italy, 25.05.2007 (talk)

H. Amenitsch
Practical aspects of SAXS and WAXS measurements
Master program in nano biotecnologie, Porto Conte, Italy, 25.05.2007 (talk)

H. Amenitsch
Time-resolved scattering and grazing incidence small angle scattering (GISAXS)
Master program in nano biotecnologie, Porto Conte, Italy, 26.5.2007 (talk)

H. Amenitsch
The Austrian SAXS beamline at ELETTRA: Ist Application from Biology to Materials Sciences
Seminar, Taiwan, 22.10.2007 (talk)

H. Amenitsch, S. Bernstorff, F. Cacho Nerin, S. Ibrahimkutty, B. Marmiroli, M. Rappolt, B. Sartori, F. Schmid
Small Angle X-ray Scattering.
Scientific advisory council meeting, Trieste, Italy, 05.06.2007 (talk)

H. Amenitsch, D. Cojoc, M. Rappolt, B. Sartori, B. Marmiroli et al.
Combing Laser Tweezer and Micro-diffraction: New Possibilities for In Situ Manipulation
24th European Crystallography Meeting (ECM24), Marrakech 22-27 August 2007, Morocco (talk)

H. Amenitsch, P. Laggner, D.E. Moncton
Compact high brilliance - hard X-ray source and ist potential from material science to biology
Compact Light Sources (TU-Graz), Austria, 8.2.2007 (talk)

H. Amenitsch, M. Rappolt, M. Kriechbaum, B. Sartori, P. Laggner et al.
Self assembly and high pressure behavior of non-lamellar lipidphases on solid supports studied with GISAXD
Denver X-ray Conference, Denver, USA, 2.8.2007 (talk)

H. Amenitsch, M. Rappolt, B. Sartori, M. Kriechbaum, M. Steinhart et al.
In situ self assembly and high pressure behavior of solid supported non-lamellar phospholipid phases investigated with Grazing Incidence small angle diffraction
International Conference on Materials for Advanced Technologies 2007 ICMAT 2007, Synchrotron Radiation for Making and Measureing Materials, Suntec City Singapore, Singapore, 04.07.2007 (talk)

D. C. Arnold, R. L. Rice, M. A. Morris and J. D. Holmes
Structural Studies of Ordered Mesoporous Silica in Channelled Substrates
British Crystallography Association (BCA) Spring Meeting, Canterbury, UK, 16^{th} – 19^{th} April 2007 (Oral Presentation)

M.A.Bagni, B.Colombini, G.Cecchi, S.Bernstorff, H. Amenitsch, P.J. Griffiths
Intensity changes of equatorial 1,1 1,0 and meridional 14.3 nm X-ray reflections during slow stretching of activated muscle fibre bundles
XXXVIth European Muscle Conference (EMC) of the European Society for Muscle Research, Stockholm, Sweden, September 8-12, 2007

S. Bernstorff
Synchrotron Radiation: Sources and Instrumentation
NESY Winter School 2007, Planneralm, Austria, 5.3.2007 (invited lecture)

S. Bernstorff
GISAXS in materials science
II Scuola "applicazioni della radiazione di sincrotrone allo studio dei materiali nanostrutturati e dei film sottili (ARS2)"
Trieste, 22-26 Aprile 2007 (invited lecture)

S. Bernstorff
Study of Nanostructures in the fields of Materials Science and Chemistry
Ruđer Bošković Institute, Zagreb, Croatia, 11 June 2007 (invited lecture)

S. Bernstorff
Medical and biological applications at the SAXS beamline for fast time resolved structural studies on the nanometer-scale
Ruđer Bošković Institute, Zagreb, Croatia, 12 June 2007 (invited lecture)

S. Bernstorff
Study of Nanostructures in the fields of Materials Science and Chemistry
University of Split, Croatia, 15 June 2007 (invited lecture)

S. Bernstorff
SAXS
1st Croatian Summer School on Synchrotron Radiation – SynCro'07, Hotel Bonavia, Rijeka, Croatia, September 3rd - 7th, 2007 (invited lecture)

S. Bernstorff
Study of Nanostructures in the fields of Materials Science, Biology and Chemistry
University of Nova Gorica, Slovenia, 13 December 2007 (invited lecture)

S. Bernstorff, P. Dubcek and N. Radić
Nanocrystalline nickel thin film growth on various substrates
IVC-17/ICSS-13 & ICN+T2007, Stockholm, Sweden, July 2-6, 2007 (poster)

S. Bernstorff, B. Pivac, I. Capan, P. Dubcek, V. Janicki, H. Zorc, N. Radic, I. Zulim, T. Betti
Preparation of SiO/SiO2 superlattice
IVC-17/ICSS-13 & ICN+T2007, Stockholm, Sweden, July 2-6, 2007 (poster)

B. Boulgaropoulus, P. Laggner, G. Pabst
Effects of ceramide on structure and fluctuations in ternary lipid model systems
48th International Conference on the Bioscience of Lipids, Turku/FINLAND, 05.09.2007 (poster)

M. Buljan, U.V. Desnica, G. Dražić, M. Ivanda, N. Radić, P. Dubček, K. Salamon, S. Bernstorff
Quantum dot superlattices in amorphous systems
E-MRS Fall Meeting 2007, Warsaw, Poland (Oral)

F. Cacho-Nerin
From micro to macro: a model to explain complexity in biomaterials
Elettra sit and relax session, Trieste, Italy, 29.03.2007 (talk)

F. Cacho Nerin
From micro to macro: explaining the mechanical behavior of fibrous tissues through their structure
9th US National Congress on Computational Mechanics, San Francisco, USA, 25.07.2007 (talk)

I. Capan, B. Pivac, S. Duguay, A. Slaoui, P. Dubcek, S. Bernstorff
Structural properties of Ge nanocrystals embedded in SiO_2
30th Jubilee international convention MIPRO
Conference on microelectronics, electronics, and electronic technologies (MEET), Opatija, Adriatic Coast, Croatia, May 21-25, 2007 (talk)

I. Capan, P. Dubček, H. Zorc, N. Radić, B. Pivac, S. Bernstorff
Characterization of Ge islands on Si(100) substrates
2nd Workshop "GISAXS - An Advanced Scattering Method", HASYLAB / DESY, Hamburg, Germany, May 9-11, 2007 (poster)

I.Capan, B. Pivac, P.Dubček, S.Bernstorff, A.Misiuk, M.Prujszczyk
GISAXS study of defects induced by helium implantation in silicon
Symposium on Nanotechnology Approaches, Nanomaterials and Thin Films for Energy Technologies, 9-11 July, 2007, Algarve, Portugal

I. Capan, B. Pivac, P. Dubcek, S. Bernstorff, A. Misiuk, M. Prujszczyk
Effect of high pressure annealing on defects induced by helium implantation in silicon
IVC-17/ICSS-13 & ICN+T2007, Stockholm, Sweden, July 2-6, 2007 (poster)

G. Caracciolo, D. Pozzi, R. Caminiti, C. Marchini, M. Montani, A. Amici, H. Amenitsch
Structural Stability Against Disintegration by Anionic Lipids Rationalizes the Efficiency of Cationic Liposome/DNA Complexes
XXXVI Congresso Nazionale Società Chimica Italiana–Sezione di Chimica-Fisica, Gallipoli (Lecce), 17-22 Giugno 2007 (oral)

G. Caracciolo, D. Pozzi, R. Caminiti, C. Marchini, M. Montani, A. Amici, H. Amenitsch
Multicomponent cationic liposome/DNA complexes: efficient vectors for gene delivery
XXXVI Congresso Nazionale Società Chimica Italiana–Sezione di Chimica-Fisica., Gallipoli (Lecce), 17-22 Giugno 2007 (poster)

I.D. Desnica-Frankovic, K. Furic, U.V. Desnica, P. Dubcek, M. Buljan, S. Bernstorff, H. Kar, I. Großhans, and B. Stritzker
Complementary application of Raman scattering and GISAXS in characterization of embedded semiconductor QDs
E-MRS Spring Meeting, Strasbourg, France, 28.5.2007 - 1.6.2007 (Poster)

I.D. Desnica-Frankovic, P. Dubcek, M. Buljan, V. Desnica, S Bernstorff, M.C. Ridgway and C.J. Glover
Quantitative analysis of vacancy clusters induced by ion-beam processing
24th International Conference on Defects in Semiconductors, Albuquerque, NM, USA, July 22 - 27, 2007 (Poster)

Dunja Desnica-Frankovic, Pavo Dubcek, Maja Buljan, Uros Desnica, Sigrid Bernstorff,
Klasteriranje vakancija u germaniju izazvano ionskom implantacijom
5th Meeting of Croatian Physical Society, Primosten, Croatia, 05-08. 10. 2007
Poster (in Croatian)

U.V. Desnica, M. Buljan, P. Dubcek, I.D. Desnica-Frankovic, N. Radic, M. Ivanda, Z. Siketic, I. Bogdanovic-Radovic, K. Salamon, S. Bernstorff,
Formation of Ge- nanocrystals in SiO_2 substrate by magnetron sputtering and post-deposition thermal treatment
E-MRS (European Material Research Society) - Spring Meeting, Symposium K, Strasbourg, France; 28. May 2007 - 01. June 2007 (Oral)

U.V. Desnica, M. Buljan, I.D. Desnica-Frankovic, N. Radic, P. Dubcek, S. Bernstorff
Ge quantum dots: from amorphous to crystalline three-dimensional superlattices in glass silica matrix
24th International Conference on Defects in Semiconductors, Albuquerque, NM, USA, July 22 - 27, 2007 (Poster)

Uroš Desnica, Maja Buljan, Ida Dunja Desnica Frankovic, Nikola Radic, Pavo Dubcek, Krešimir Salamon, Zdravko Sikatic, Iva Bogdanovic Radovic, Mile Ivanda, Sigrid Bernstorff
Ge kvantne točke: od amorfnih do kristaliničnih, od slučajano raspoređenih u u amorfnoj SiO2 matrici do organiziranih u 3D super-rešetku
5th Meeting of Croatian Physical Society, Primosten, Croatia, 05-08. 10. 2007
Poster (in Croatian)

Y. D. Dong, T. Hanley, I. Larson, H. Amenitsch, M. Rappolt, B. J. Boyd
Structure of liquid crystalline nanostructured drug delivery particles by synchrotron DSC-SAXS
Australian Colloid and Interface Symposium, Sydney, Australia, 4-8 February 2007

P. Dubček, B. Pivac, I. Capan, S. Bernstorff, B. Vlahovic
Evolution of nanoparticles in gold implanted glass
2nd Workshop "GISAXS - An Advanced Scattering Method", HASYLAB / DESY, Hamburg, Germany, May 9-11, 2007

P. Dubcek, N. Radic, S. Bernstorff,
GISAXS study of Ge-refractory metals (Nb, Mo, Ta, W) thin films
IVC-17/ICSS-13 & ICN+T2007, Stockholm, Sweden, July 2-6, 2007 (poster)

P. Dubcek, B. Pivac, I. Capan, N. Radic and S. Bernstorff
Effective film thickness influence on self-organization of Ge islands on Si(100) substrates
IVC-17/ICSS-13 & ICN+T2007, Stockholm, Sweden, July 2-6, 2007 (poster)

C. Fritscher
In situ Synchrotron SAXS/XRD Study on the Formation of Ordered Mesoscopic Hybrid Materials
Seminar, Department of Inorganic Chemistry I, University Ulm, Germany, 1st February 2007 (oral)

D. Gracin, A. Gajović, M. Čeh, K. Juraić, P. Dubček, S. Bernstorff
Structural ordering of thin amorphous-nano-crystalline films studied by HRTEM, GISAXS and Raman spectroscopy
E-MRS 2007 Fall MeetingWarsaw, Poland, 17-21.09.2007 (oral)

A. Hodzic, M. Rappolt, P. Laggner, G. Pabst
Effects of plant sterols on structure and fluctuations of lipid membranes
51st Annual Meeting, Biophysical Society, Baltimore, USA, 07.03.2007 (poster)

A. Hodzic, M. Rappolt, H. Amenitsch, P. Laggner, G. Pabst
Effects of plant sterols on structure and fluctuations of lipid membranes
6th European Biophysics Congress, London, UK, 15.06.2007 (poster)

A. Hodzic, M. Rappolt, P. Laggner, G. Pabst
Effects of plant sterols on structure and fluctuations of lipid membranes.
Regional Biophysics Conference, Balatonfüred, Hungary, 21.08.2007 (poster)

A. Hodzic, M. Rappolt, P. Laggner, G. Pabst
Effects of plant sterols on structure and fluctuations of lipid membranes
51st Annual Meeting of the Biophysical Society, 15.06.2007 (poster)

A. Hodzic, P. Zoumpoulakis, T. Mavromoustakos, M. Rappolt, P. Laggner et al.
The role of membrane hydrocarbon chain composition in interactions with antihypertensive drugs
52nd Annual Meeting of the Biophysical Society. 15.02.2008 (poster)

S. Ibrahimkutty, M.Rappolt, P. Laggner, H. Amenitsch
SAXS study of aerosol particles in gas phase
SAXIER Workshop, Grenoble, France, 05.02.2007 (poster)

Plinio Innocenzi
Time Resolved Infrared Analysis and Simultaneous Detection of Structural and Chemical Changes During Self-assembly of Mesostructured Films by in-situ SAXS and FTIR
MRS Spring Meeting, San Francisco, USA, 9 – 13 April 2007 (oral)

P. Innocenzi, L. Malfatti, T. Kidchob, S. Costacurta, P. Falcaro, M. Piccinini, A. Marcelli, P. Morini, D.Sali and H. Amenitsch
In-Situ Study of Self-Assembling Films by Simultaneous and Time Resolved Analytical Techniques
XIVth international Sol-Gel conference, Montpellier- France September 2-7, 2007)talk)

M.B. Kerber, E. Schafler, A.K. Wieczorek, G. Ribarik, S. Bernstorff, M.J. Zehetbauer
In-situ Bragg Profile Analysis during deformation of SPD Nanometals
Int. Symp. on Bulk Nanostructured Materials: from fundamentals to innovations, Ufa, Russia, August 2007 (poster)

K. Juraić, D. Gracin, P. Dubček, A. Gajović, S. Bernstorff
2D GISAXS of nano-crystalline silicon thin films: analysis and modelling
14th International meeting vacuum science and technology, 01 June 2007 (poster)

K. Juraić, D. Gracin, P. Dubček, A. Gajović, M. Čeh, S. Bernstorff
Modeling of 2D GISAXS of nano-crystalline silicon thin films
E-MRS 2007 Fall Meeting Warsaw, Poland, 17-21.09.2007 (poster)

K. Juraić, D. Gracin, P. Dubček, A. Gajović, M. Čeh, S. Bernstorff
GISAXS analysis of amorphous and nano-crystalline silicon thin films
5th Scientific Meeting Croatian Physical Society, Primošten, Croatia, 05-08. 10. 2007 (poster)

Ralf Köhn, Andreas Keilbach, Andreas Zürner, Barbara Platschek, Markus Döblinger, Thomas Bein
In situ GISAXS Study of the Formation and Phase Transformation of Mesostructures within the Confined Space of Anodic Alumina Membrane Pores
Advanced Micro- and Mesoporous Materials, Varna, Bulgaria, 6.-9.9.2007

P. Laggner
Overview on synchrotron and neutron applications
5th European Winter School (NESY 2007), 05.03.2007, Planneralm/AUSTRIA, invited lecture

T. Lebold, C. Jung, J. Kirstein, B. Platschek, K. Müllen, J. Michaelis, T. Bein C. Bräuchle
Investigation of the structural properties of mesoporous silica nanostructures
20. Deutsche Zeolith Tagung, Halle, Germany, 5.-7.3.2008

M. Lucic Lavcevic, P. Dubcek, A. Sreder, A. Turkovic, B. Orel, Z. Crnjak Orel, S. Bernstorff
A study of 2D GISAXS patterns of nanostructured cerium/vanadium oxide thin films
IVC-17/ICSS-13 & ICN+T2007, Stockholm, Sweden, July 2-6, 2007 (poster)

Paolo Mariani, Francesco Spinozzi, Flavio Carsughi, Maria Grazia Ortore, Raffaele Sinibaldi, Leandro Barbosa
Protein in solution: an analysis of hydrational properties and stability by neutron and X-ray scattering techniques
MISCA 2007 (1st Meeting of the Italian and Spanish Crystallographic Associations), 24-28.9.2007, Copanello di Staletti, Italy (oral)

B. Marmiroli, G. Grenci, L. Businaro, B. Sartori, A. Gosparini, P. Laggner and H. Amenitsch
Jet micromixer for studying ultrafast chemical reactions by SAXS
High Aspect Ratio Micro-Structure Technology Workshop (HARMST), Besancon, France, 08.06.2007 (poster)

B. Marmiroli
Microfluidics for SAXS experiments
Seminar talk, Berlin, Germany, 19.10.2007

B. Marmiroli
Microfluidics for SAXS experiments
Elettra sit and relax session, Trieste/, Italy, 24.04.2007 (talk)

M. Ollivon, C. Bourgaux, G. Keller, D. Kalnin
Coupling of DSC and SWAX-Ray diffraction for the design and characterisation of lipidic nanostructures
38emes Journées de Calorimétrie et d'Analyse Thermique, Montpellier, 6, 7 et 8 juin 2007 (invited lecture)

M. Ollivon
Nanoencapsulation by lipidic structures for food applications, Qualità degli alimenti: Percorsi Compiuti, Recenti Acquisizioni, Problematiche Future, Scienze e Tecnologie Alimentari
Università degli Studi di Udine, June, 13th, 2007, Udine, Italy (invited lecture)

Pabst, G.; Danner, S.; Hickel, A.; Raghunathan, V.A.
On the propensity of phosphatidylglycerols to form interdigitated phases
6th European Biophysics Congress, London, UK, 15.06.2007 (poster)

G. Pabst
Coupling of local and global properties in biomimetic membranes
2nd Christmas Biophysics Workshop, Bled, Slovenia, 19.12.2007 (talk)

G. Pabst
Increase of order in fluid lipid bilayers by salts
15th International Symposion "Spectroscopy in Theory and Practice", Nova Gorica, Slovenia, 21.04.2007 (talk)

G. Pabst
Small-Angle Diffraction in Biomembranes
International School "Scattering for Biologists", Villingen, Switzerland, 24.10.2007 (talk)

G. Pabst
Biological model membranes - From cells to vesicles and solid supported bilayers
Seminar, Leoben, Austria, 14.03.2007 (talk)

G. Pabst
How interdigitated phase formation may couple to lipid/peptide interactions
Seminar, Bangalore, India, 08.02.2007 (talk)

G. Pabst
On the connection of interdigitated phases and lipid/peptide interactions
Seminar, Golm, Germany, 08.01.2007 (talk)

G. Pabst
SAXS and SANS on biomaterials.
5th European Winter School (NESY 2007), Planneralm, Austria, 06.03.2007 (invited talk)

A. J. Perez-Berna, J.G. Casas, M. Moreno, A.I. Gomez Sanchez, A. Gonzalez-Alvarez et al. [..] ()
The membrane-active regions of the hepatitis C virus E1 and E2 envelope glycoproteins. Structural and biophysical characterization of the fusogenic region
52nd Annual Meeting, Biophysical Society, 15.02.2008 (poster)

B. Pivac, I. Capan, P. Dubcek, N. Radić, S. Bernstorff
Substrate temperature dependence of Si nanostructures formation in SiO/SiO_2 superlattice
2nd Workshop "GISAXS - An Advanced Scattering Method", HASYLAB / DESY, Hamburg, Germany, May 9-11, 2007 (poster)

B. Pivac, P. Dubcek, I. Capan, N. Radic, S. Bernstorff, S. Duguay, A. Slaoui
Study of Ge islands growth on Si substrates
EMRS Spring Meeting, Strasbourg, France, May 28 – June 1, 2007

B. Pivac, I. Capan, P. Dubcek, N. Radic, S. Bernstorff, S. Duguay, A. Slaoui
Substrate temperature dependence of Si nanostructures formation in SiO/SiO_2 superlattice
EMRS Spring Meeting, Strasbourg, France, May 28 – June 1, 2007 (talk)

B. Pivac, I. Capan, P. Dubcek, N. Radic, S. Bernstorff, S. Duguay, A. Slaoui
Si nanostructures formation in SiO/SiO_2 superlattice for next generation solar cells
EMRS Spring Meeting, Strasbourg, France, May 28 – June 1, 2007

B. Pivac, P. Dubček, I. Capan, H. Zorc, S. Bernstorff, S. Duguay, A. Slaoui
Structural analysis of annealed amorphous SiO/SiO_2 superlattice
EMRS Spring Meeting, Strasbourg, France, May 28 – June 1, 2007

B. Pivac, I. Capan, I. Zulim, T. Betti, V. Janicki, H. Zorc, P. Dubcek, S. Bernstorff
Silicon nanostructures for memory devices
2nd International Conference on Surfaces, Coatings and Nanostructured Materials (NanoSMat 2007), Alvor, Portugal, 9-11 July 2007

B. Pivac, I. Capan, I. Zulim, T. Betti, V. Janicki, H. Zorc, P. Dubček, S. Bernstorff
Nano Si Superlattices for the next generation solar cells
2nd International Conference on Surfaces, Coatings and Nanostructured Materials (NanoSMat 2007), Alvor, Portugal, 9-11 July 2007 (talk)

B. Pivac, I. Capan, P. Dubcek, V. Janicki, H. Zorc, S. Bernstorff
Formation of silicon nanostructures in SiO2
IVC-17/ICSS-13 & ICN+T2007, Stockholm, Sweden, July 2-6, 2007 (poster)

B. Platschek, R. Köhn, T. Bein
Salt-induced phase-transformation of mesostructures confined within the channels of porous anodic alumina
20. Deutsche Zeolith Tagung, Halle, Germany, 5.-7.3.2008

N. Radić, P. Dubček, M. Ristić, S. Musić, Ž. Skoko, S. Bernstorff and R. Grötzschel
Thin films of immiscible Ag-W system
IVC-17/ICSS-13 & ICN+T2007, Stockholm, Sweden, July 2-6, 2007 (poster)

N. Radić, P. Dubcek, M. Ristic, S. Music, R. Grötzschel, Z. Skoko, S. Bernstorff
Struktura tankih filmova slitina srebra i volframa
14. Mednarodni znanstveni sestanek Vakuumska znanost in tehnika, Bled, Slovenia, 2007

M. Rappolt
Curved Membranes: From Models to Applications
"Progress Report Seminar of Sincrotrone Trieste", Trieste, Italy, 19.4.2007

M. Rappolt, P. Laggner, S. Zhang, A. Yaghmur
Tuning curvature and stability of monoolein bilayers by designer lipid-like peptide surfactants
48th International Conference on the Bioscience of Lipids, Turku, Finland, 05.09.2007 (poster)

M. Rappolt
The power of SAXS: exploration of the magic world of biomaterials
Excursion to Sincrotrone Trieste (Elettra), Trieste, Italy, 27.01.2007(talk)

M. Rappolt
Curved membranes: from models to applications
Seminar talk, Ljubljana, Slovenia, 13.11.2007

H. Rennhofer, S. Puchegger, FR. Kogler, D. Loidl, S. Bernstorff, U. Schubert and H. Peterlik
In-situ tensile tests on polystyrene crosslinked with a multifunctional Zirconium Oxo-cluster
57. Jahrestagung der Österreichischen Physikalischen Gesellschaft (ÖPG), Vienna, Austria, 26.09.2007 (talk)

K. Salamon, O. Milat, M. Buljan, U. Desnica, N. Radic, P. Dubcek, S. Bernstorff
X-ray study of Ge nanocrystals formation in Ge:SiO2/SiO2 multilayers
IVC-17/ICSS-13 & ICN+T2007, Stockholm, Sweden, July 2-6, 2007 (poster)

Kresimir Salamon, Ognjen Milat, Maja Buljan, Uros Desnica, Nikola Radic
Istrazivanje strukture i morfologije tankih filmova povrsinski osjetljivim rendgenskim tehnikama
5th Meeting of Croatian Physical Society, Primosten, Croatia, 05-08. 10. 2007
Poster (in Croatian)

K. Salamon, O. Milat, M. Buljan, U.V. Desnica, N. Radić, P. Dubček, S. Bernstorff
X-ray study of Ge nanoparticle formation in Ge:SiO2/SiO2 multilayers
E-MRS Fall Meeting 2007, Warsaw, Poland (poster)

E. Schafler
Application of X-ray line profile analysis to polymers
Workshop " Diffraction Peak Broadening and Peak Shape Analysis"
56th Annual Conference on Applications of X-ray Analysis – Denver X-ray Conference, Colorado Springs, USA, July 2007 (invited lecture)

E. Schafler, M. Zehetbauer, T. Ungár
X-ray diffraction analysis of planar faulting in SPD-metals
Int. Symp. on Bulk Nanostructured Materials: from fundamentals to innovations, Ufa, Russia, August 2007 (lecture)

C. Sinturel, M. Vayer, R. Erre, H. Amenitsch
Dispersion of crystallized nano-platelets of PE in thermoset matrix obtained by blending and curing PE-b-PEO copolymer and unsaturated polyester
Polymer Blends, 9th European Symposium, Palermo, Italy, 9-12 september 2007

C.V.Teixeira, H.Amenitsch, T.Fukushima, T.Aida, W.Jin, M-Hotokka, M.Lindén
A helical intermediate during the formation of hexa-peri-hexabenzocoronene (HBC) graphitic nanotubes
II Workshop on Applications of Synchrotron Light to Non-Crystalline Diffraction in Materials and Life Sciences, Madrid (Spain), 15th -17th October, 2007

Aleksandra Turković
SAXS Characterization of Mesoporous Thin Films: A Brief Review
E-MRS Fall Meeting 2007, Symposium A (Invited talk)

Aleksandra Turković, Magdy Lučić-Lavčević, Bojan Orel, Aljoška Šreder, Pavo Dubček, Zorica Crnjak Orel, Mladen Pavlović, Sigrid Bernstorff
2D GISAXS Analysis of Morphology in Nanostructured Cerium/Vanadium Oxide Thin Films
EMRS 2007 Fall Meeting, Symposium A (poster)

A. Yaghmur, P. Laggner, S. Zhang, M. Rappolt
Modulation of monoolein (MO) nanostructures by designer lipid-like peptide surfactants
Pharma Day (TU Graz), Graz, Austria, 01.06.2007 (poster)

A. Yaghmur, P. Laggner, S. Zhang, M. Rappolt
Modulation of lipidic nanostructures by designer lipid-like peptide surfactants
9th Conference on Colloid Chemistry (Hungarian Chemical Society), Siofok, Hungary, 04.10.2007 (talk)

A. Yaghmur, P. Laggner, M. Rappolt
Combined SAXS and Rapid Mixing Studies on Ca2+ Induced Structural Transitions in Lipid Systems
48th International Conference on the Biosciences of Lipids, Turku, Finland, 05.09.2007 (poster)

A. Yaghmur, M. Rappolt, P. Laggner, S. Zhang
Tuning curvature and stability of monoolein bilayers by designer lipid-like peptide surfactants
Austrian-Croatian Science Days (FFG - Austrian Research Promotion Agency), Graz, Austria, 19.10.2007 (poster)

A. Yaghmur, B. Sartori, P. Laggner, M. Rappolt
Tuning curvature and stability of monoolein bilayers by designer lipid-like peptide surfactants
21st Conference of the European Colloid and Interface Society (ECIS), Geneva, Switzerland, 10.09.2007 (poster)

A. Yaghmur, B. Sartori, P. Laggner, M. Rappolt
Combination rapid mixing and SAXS detects fast structural transitions in lipid systems induced by low concentrations of Ca+2
9th Conference on Colloid Chemistry (Hungarian Chemical Society), Siofok, Hungary, 03.10.2007 (poster)

M. J. Zehetbauer, M. Kerber, E. Schafler, T. Ungar
New Applications of the X-ray Line Profile Analysis for Investigation of Structural Parameters of Nanocrystalline Materials
2nd Symposium on Texture and Microstructure Analysis – SOTAMA'2007,
Cracow, Poland, September 2007 (invited lecture)

ELETTRA Highlights 2006-2007

G. Croce, D. Viterbo, M. Milanesio, H. Amenitsch
A mesoporous pattern created by nature in spicules from Thetya aurantium sponge
Elettra Research Highlight, pp. 22-23 (2007)

P. K. Nayak, R. S. Srinivasa, S. S. Major, S. Bernstorff
Study of intralayer structure and molecular packing in LB multilayers and related nanostructures
Elettra Research Highlight, pp. 24-25 (2007)

B. Gehl, M. Bäumer, Th. Schmidt, J. Falta, S. Bernstorff
In-situ characterization of self-assembled nanoparticles films under harsh conditions
Elettra Research Highlight, pp. 42-43 (2007)

T. Brezesinski, B. M. Smarsly, H. Amenitsch
"Soft epitaxy": Surfactant-mediated generation of iso-oriented crystalline, mesoprous metal oxide layers
Elettra Research Highlight, pp. 80-81 (2007)

R. Viswanatha, D. D. Sarma, H. Amenitsch
Growth kinetics of ZnO nanocrystals: a few surprises
Elettra Research Highlight, pp. 82-83 (2007)

SAXS training courses

The SAXS group participated in the school ARS2 (Applicazioni della Radiazione di Sincrotrone allo studio dei materiali nanostrutturati e dei film sottili) in Trieste, Italy. During 26.4.2007, they gave two lectures (S. Bernstorff, "GISAXS in materials science", and H. Amenitsch, "SAXS in solution and under extreme conditions"), and 1 half-day tutorial "Computer Session - Analisi dei dati SAXS e interpretazione" (S. Bernstorff, M. Rappolt, B. Sartori)

PhD Thesis 2007

Stefano Costacurta
Mesoporous films obtained by supramolecular self-assembly and their characterisation by advanced techniques
University of Padova and University of Sassari, Italy

Richard A. Farrell
Ultra Low Dielectric Constant Self-Assembled Nanostructured Porous Oxide Films
University College Cork, Ireland

Aden Hodzic
Coupling of Local and Global Features in Phospholipid Model Membranes: Effects of Sterols, Drugs and Salts
Technische Universität, Institut für Materialphysik, Graz, Austria.

Barbara Platschek
Ordered Mesoporous Silica: Control of Morphology and Exploration with Single Molecules
Ludwig-Maximilians-University, Munich, Germany

Master Thesis (Tesi di Laurea, Diplomarbeit) 2007

Moritz Speckmann
Adsorbat-induzierte Facettierung und Ge-Wachstum auf vicinalen Si-Oberflächen
Universität Bremen, Germany

Authors Index